

Local Temperatures Out of Equilibrium

Daochi Zhang^a, Xiao Zheng^a, Massimiliano Di Ventra^b

^a*Hefei National Laboratory for Physical Sciences at the Microscale & Synergetic Innovation Center of Quantum Information and Quantum Physics & CAS Center for Excellence in Nanoscience, University of Science and Technology of China, Hefei, Anhui 230026, China*

^b*Department of Physics, University of California, San Diego, 9500 Gilman Drive, La Jolla, CA 92093-0319*

Abstract

The temperature of a physical system is operationally defined in physics as “that quantity which is measured by a thermometer” weakly coupled to, and at equilibrium with the system. This definition is unique only at global equilibrium in view of the zeroth law of thermodynamics: when the system and the thermometer have reached equilibrium, the “thermometer degrees of freedom” can be traced out and the temperature read by the thermometer can be uniquely assigned to the system. Unfortunately, such a procedure cannot be straightforwardly extended to a system out of equilibrium, where local excitations may be spatially inhomogeneous and the zeroth law of thermodynamics does not hold. With the advent of several experimental techniques that attempt to extract a single parameter characterizing the degree of local excitations of a (mesoscopic or nanoscale) system out of equilibrium, this issue is making a strong comeback to the forefront of research. In this paper, we will review the difficulties to define a unique temperature out of equilibrium, the majority of definitions that have been proposed so far, and discuss both their advantages and limitations. We will then examine a variety of experimental techniques developed for measuring the non-equilibrium local temperatures under various conditions. Finally we will discuss the physical implications of the notion of local temperature, and present the practical applications of such a concept in a variety of nanosystems out of equilibrium.

Keywords:

local temperature; nanosystem; non-equilibrium; thermodynamics

Contents

1	Introduction	2
1.1	Plan of the review	2
1.1.1	Scope of the review	2
1.1.2	Organization of the review	6
1.2	Temperature at equilibrium	7
1.2.1	The measurement of temperature	7
1.2.2	Finite-size effects	8
1.2.3	Influence of the environment	10
1.2.4	Local equilibrium conditions	11
1.3	Physical motivations to extend the concept of temperature out of equilibrium	14
2	Theoretical definitions of local temperature out of equilibrium	15
2.1	General Remarks	15
2.2	Definitions of non-equilibrium local temperatures	18
2.2.1	Definitions based on zero-current condition	18

*Corresponding author at: Hefei National Laboratory for Physical Sciences at the Microscale, University of Science and Technology of China, Hefei, Anhui 230026, China

Email address: xz58@ustc.edu.cn (Xiao Zheng)

2.2.2	Definitions based on balance of local heat generation and dissipation	19
2.2.3	Definitions based on thermodynamic relations	21
2.2.4	Definitions based on statistical relations	23
2.2.5	Definitions based on minimal perturbation condition	26
2.3	Uniqueness/non-uniqueness of local temperature out of equilibrium	27
3	Experimental measurement of non-equilibrium local temperatures	30
3.1	Experimental strategies to measure the local temperature	30
3.2	Measurement of heat current at the nanoscale	31
3.2.1	General principle of nanocalorimetric techniques	31
3.2.2	Bimaterial cantilever-based calorimeters	31
3.2.3	Resistance thermometry-based calorimeters	33
3.2.4	Advantages and limitations of nanocalorimetric techniques	35
3.3	Measurement of local temperatures of non-equilibrium nanosystems	35
3.3.1	Mechanically-controlled break junction techniques	35
3.3.2	Spectroscopic techniques	39
3.3.3	Scanning thermal microscope	43
3.3.4	Relation between experiments and theories	46
4	Implications and applications of non-equilibrium local temperatures	47
4.1	Physical Implications	47
4.1.1	Generalization of the thermodynamic laws	47
4.1.2	A scale of local thermal fluctuations and excitations	49
4.1.3	Local properties of nanosystems	50
4.2	Practical applications	52
4.2.1	Quantum oscillations of local temperature in nanostructures	52
4.2.2	Recovering Fourier's law at the nanoscale	53
4.2.3	Laser-induced ultrafast adsorption dynamics of molecules on metal surfaces	56
4.2.4	Local temperature of Kondo systems	56
4.2.5	Local electrochemical potential of two-dimensional networks	57
4.2.6	Local chemical potential of non-equilibrium magnons	59
5	Summary and perspectives	61
	Acknowledgments	61
	References	61

1. Introduction

1.1. Plan of the review

1.1.1. Scope of the review

Temperature is one of the most fundamental properties of physical systems. In fact, the concept of temperature reaches far beyond the realm of physics, and profoundly influences our daily life in many aspects. The importance of temperature for living systems (such as the human body) is self-evident. For example, studies on biological processes at the molecular level have demonstrated sensitive dependence of protein function on temperature [1, 2]. A small fluctuation in temperature may then significantly affect the protein structure, causing it to lose its normal bioactivity.

Biosystems and living organisms are certainly interesting. However, what really motivates this review is the tremendous advancements, we have witnessed in the past decade or so, in the experimental techniques for fabricating [3–5], measuring [6], and manipulating [7–9] objects at the nanometer scale. These techniques allow nanoscale systems to be probed out of equilibrium, often far from equilibrium, and attempt to characterize the state of non-equilibrium with one or a few parameters. One such parameter is the “local temperature” of the system. However,

unlike its equilibrium counterpart, it is clear that the notion of temperature in nanoscale systems, hence its local definition, and in contexts in which this concept is not so solidly grounded, requires further investigation and a critical assessment.

The scope of this review is precisely to provide an overview of this concept, its various experimental incarnations, its strengths and limitations. Although many of the ideas discussed in this review apply to general systems out of equilibrium, for the sake of definiteness we will mostly consider nanoscale systems as test beds. Therefore, to complete this introduction, let us provide a bird’s-eye view of typical physical situations in which the notion of a temperature out of equilibrium may emerge in these systems.

Let us first recall that one of the main goals of nanotechnology is to design and manufacture devices at the nanoscale with desirable properties and functions [10]. Typically, the specific function of a nano-device is realized via the response of a certain local physical property to an external field, which drives the nanosystem out of equilibrium. Therefore, the action of the external field on the nanosystem results in a certain form of work that serves a practical purpose. However, besides the “desired” response, other internal degrees of freedom (DOF) may also be excited by the external field or through the coupling between the internal DOF, which inevitably leads to accumulation of heat within the system. If the locally produced heat cannot be dissipated efficiently into the surrounding environment, the “undesired” local motion may hamper the function of the nanosystem or even imperil its structural stability.

In order to provide the reader with a practical example where these effects are particularly pressing we consider the important case of our modern computers built out of a collection of transistors [11]. The increasing demand for computational performance has spurred the development and proposal of novel materials and techniques to increase the switch frequency of transistors in computer processors. Nowadays, the miniaturization of transistors has reached the size of a few nanometers. Under such a small scale, the local physical properties of a material may differ drastically from those of its bulk counterpart [12], and quantum effects may be prominent as the size of the transistor is comparable to the mean free path of conduction electrons. Moreover, the construction of novel types of transistors has gone beyond silicon-based materials [13, 14]. For instance, electronic devices based on single molecules have also been proposed [15, 16]. Related experiments can be traced back to the conductivity measurements on monolayers of cadmium salts of fatty acids conducted by Kuhn and coworkers in the 1970s [17]. A nanoelectronic or molecular electronic device usually has the geometry of a nanojunction, which consists of a nano-sized material that provides the electron conduction channel, and two or more macroscopic leads that play the role of electron reservoir and heat bath. Figure 1 depicts various types of nanoelectronic devices, including a metal-oxide-semiconductor field-effect transistor (MOSFET) [18], a carbon-nanotube-based transistor [19], a graphene-sheet-based transistor [20–22], and a molecular transistor [23–26].

Although these devices vary in size and structure, one expects that due to the large current densities that flow in the device, local heating may develop [27]. Physically, local heating arises due to the electron-electron and electron-phonon scattering processes both within the nano-sized conduction channel and at the contact interfaces between the channel and the leads. In particular, when a nanoelectronic device is operating under an applied voltage, the local phonon modes are excited by the conduction electrons via electron-phonon scattering. Consequently, the device experiences local Joule heating. For a computer chip that integrates billions of nanoscale transistors, the local Joule heating becomes a major bottleneck that limits the performance and efficiency of the device. Moreover, the intensive current-induced heating also threatens the stability of the device, and may even lead to breakdown of the nanostructure if the local heating is too severe [28].

A current-carrying nanoelectronic device is a typical non-equilibrium nanosystem, yet the concept of “local temperature” has been adopted, in an intuitive sense, to describe or characterize the local heating effect. For instance, it has been argued that a smaller external force is needed to break a nanojunction with a higher local temperature. Based on this idea, experimental measurements on the local heating in nanojunctions have been conducted [29–31]. For instance, Huang *et al.* have investigated the local heating in a single molecule covalently bonded to two electrodes by a mechanically controlled break junction (MCBJ) [28]. By measuring the average breakdown force of the MCBJ, the local temperature was estimated. These authors found that at a bias voltage of about 1 V, the temperature could be raised to ~ 30 K above the ambient room temperature. Moreover, the development of scanning tunneling microscope (STM) and atomic force microscope (AFM) techniques has greatly enriched the experimental means of probing the local temperature. In an AFM, an atomically sharp tip mounted at the free end of a cantilever can sense the thermal expansion of a sample, which provides the technical basis for a scanning Joule expansion microscope [32]. Thermal imaging has also been realized by measuring the variation of Joule expansion signal with the cantilever position. Us-

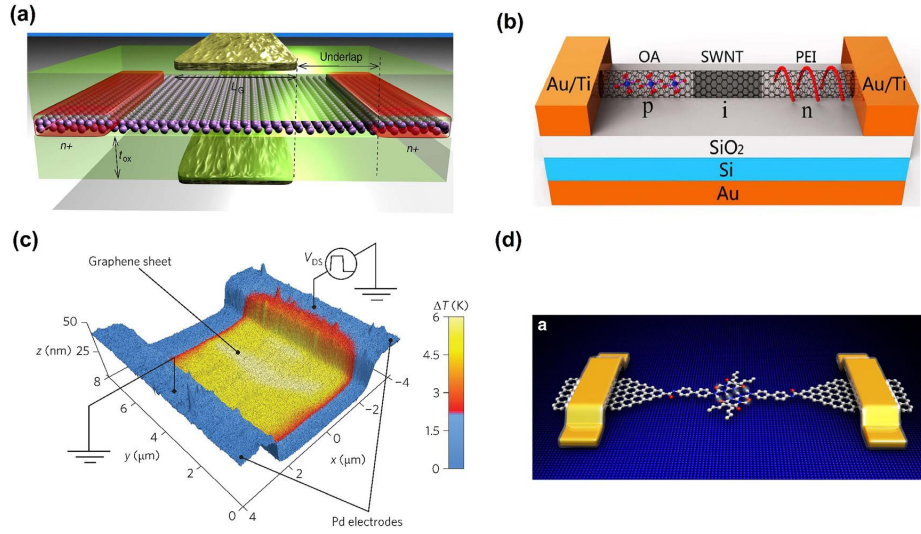


Figure 1: Schematic representation of various types of nanoelectronic devices with different nano-sized materials as the electron conduction channel. (a) A MOSFET. Reprinted with permission from [18]. Copyright 2016 Springer Nature. (b) A carbon-nanotube-based transistor. Reprinted with permission from [19]. Copyright 2017 Elsevier. (c) A graphene-sheet-based transistor. Reprinted with permission from [22]. Copyright 2011 Springer Nature. (d) A molecular transistor. Reprinted with permission from [26]. Copyright 2018 Springer Nature.

ing an AFM-based instrument and techniques, Grosse *et al.* have been able to measure the spatial distribution of local temperature in a graphene-sheet-based transistor [22]. More experimental works will be introduced in Section 3 of this review.

Local heating is also important for other types of nanosystems. The 2016's Nobel Prize in chemistry was awarded to Sauvage, Stoddart and Feringa, for the design and synthesis of molecular machines [33]. Like a traditional electric motor, a molecular motor operates in an out-of-equilibrium state and converts a certain form of energy into mechanical work. However, because of the small size of molecules and limited energy relaxation channels, it may be rather challenging to efficiently dissipate the heat generated during the operation of the motor into the environment, so as to sustain the functionality of the molecular machine.

Besides local heating, external sources (voltage, temperature gradient, electromagnetic fields, mechanical force, etc.) may affect the physical properties and functions of a nanosystem in many other aspects. Being out of equilibrium, the local properties of a nanosystem may deviate significantly from their equilibrium values, which are likely manifested by a change in local temperature. In particular, the quantum features of a nanosystem, including quantum coherence, quantum entanglement and quantum correlation, are profoundly influenced by the local thermal excitations in the system. Therefore, local temperature, which by intuition measures the degree of local thermal excitations, would also be an ideal quantity for characterizing the local properties of quantum origin.

In the past decade, there have been enormous experimental efforts on realizing the precise control and manipulation of local quantum states in nanoscopic materials. These efforts have opened new horizons for nanotechnology, which may lead to important applications in spintronics [34–37], quantum storage [38, 39], quantum information processing [40–42], and quantum computation [40].

Take the quantum dot (QD) as an example. A QD is an artificial object that has discretized energy levels, and which is typically coupled to macroscopic leads which serve as electron reservoirs. Experimentally, a QD can be realized by a magnetic atom [43], an organometallic molecule with transition metal centers [44], and a two-dimensional electron gas at the interface of semiconductors [45] (see Figure 2). The local charge or spin state in a QD can be utilized as a quantum bit (qubit) [46], a fundamental element of quantum computers. Because of the finite size of a QD, the on-dot electrons are subjected to strong Coulomb repulsion. The electron-electron interaction and the dot-lead coupling give rise to diversified exotic phenomena, such as Coulomb blockade [47], spin excitations [48], quantum memristive effect [49], and Kondo effect [50]. Some of these phenomena, like the Kondo effect, occur only at sufficiently low temperatures.

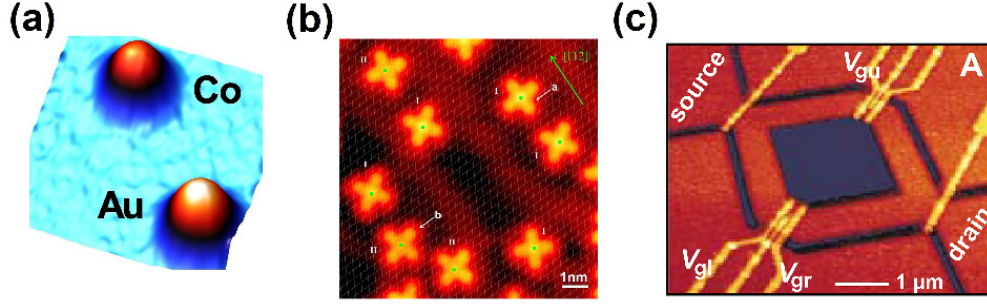


Figure 2: Various forms of QDs: (a) Au and Co atoms adsorbed on a Cu(100) surface. Reprinted with permission from [43]. Copyright 2012 American Physical Society. (b) FePc molecules adsorbed on an Au(111) surface. Reprinted with permission from [44]. Copyright 2007 American Physical Society. (c) Two-dimensional electron gas formed at the interface of an AlGaAs/GaAs heterostructure. Reprinted with permission from [51]. Copyright 2000 AAAS.

Kondo phenomena are a characteristic signature of strong electron correlations. Theoretically, the Kondo state in a QD can be described by a quantum impurity model introduced by Anderson [52], in which the QD is represented by a number of discretized energy levels and the metallic leads are approximated by reservoirs of free electrons. When the background temperature is lower than the Kondo temperature ($T < T_K$), the spectral function of the QD exhibits a sharp resonant peak at the Fermi energy of the leads, corresponding to the Kondo state that originates from the screening of the local spin by the spins of the surrounding free electrons; see Figure 3(a). In contrast, at a high temperature ($T > T_K$) the central resonant peak is absent, because the Kondo screening is destroyed by the enhanced thermal fluctuations; see Figure 3(b). It has been found both experimentally [53] and theoretically [54] that the relation between the zero-bias conductance of a Kondo QD, G , and the equilibrium temperature T obeys the following scaling relation:

$$G(T) = G_0 \left[1 + \left(\frac{T}{T_K} \right)^2 (2^{1/s} - 1) \right]^{-s}, \quad (1)$$

where G_0 is the conductance at $T = 0$ K, and s is a parameter depending only on the total spin of the QD.

For both practical and fundamental reasons, it is important to learn how the quantum features of nanosystems vary in response to external perturbations. For instance, for a QD, it has been observed in experiments that the Kondo correlation is suppressed by an applied magnetic field [55] or a bias voltage [56, 57], leading to broadening or splitting of the Kondo peak in the measured differential conductance spectra. It has also been proposed that the non-equilibrium properties of a Kondo QD can be described by universal scaling relations [58]. For instance, Rosch *et al.* [59] have discovered that for a QD under a high bias voltage V , the Kondo physics is governed by the scales V and γ , where $\gamma \sim V / \ln^2(V/T_K)$ is the non-equilibrium decoherence rate induced by the voltage-driven current. In view of the simple form of Eq. (1), it is intriguing to ask whether it is possible to define a local temperature (denoted as T^*) for a non-equilibrium QD, so that it can be used in lieu of the equilibrium temperature T in Eq. (1), to achieve a unified and preferably more convenient description of non-equilibrium properties.

From a statistical perspective, a properly defined local temperature T^* should be able to characterize the magnitude of local excitations and the local distribution of particles inside a non-equilibrium nanosystem, and thus quantify its deviation from equilibrium. This is particularly important for the studies on precise control or fine-tuning of local quantum states in nanostructures. For instance, in the past few years, the competition between Kondo resonance and local spin excitations in magnetic molecular QDs has become a focus of experimental efforts [60]. Parks *et al.* have demonstrated that, by stretching a molecular QD embedded in an MCBJ, the Kondo conductance peak is gradually split by enhancing the spin-orbit coupling [61]. Hiraoka *et al.* have used an STM tip as a probe to tune the local quantum states in an adsorbed FePc molecule [62]. By varying the position of the tip, they have realized a crossover between the Kondo-dominant regime and the spin-excitation-dominant regime. These studies have paved the way for the realization and design of more sophisticated quantum-state control techniques.

Quantum thermodynamics is expected to be a useful method to explore the underlying relations between different response functions. However, it is still a developing field with a considerable gap between theoretical predictions and

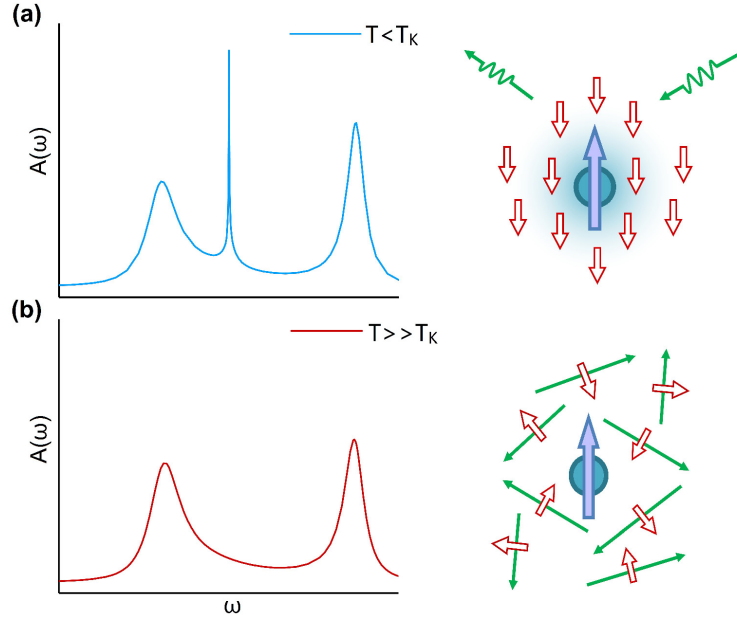


Figure 3: (a) Impurity spectral function $A(\omega)$ of a single-level Anderson impurity model (sketched on the left panel) at a temperature lower than the characteristic Kondo temperature ($T < T_K$). The sharp peak centered at the Fermi energy of the leads is the Kondo resonance peak. Schematic illustration on the right shows that the Kondo state is formed with the local spin moment at the impurity, screened by the spins of conduction electrons in the leads. (b) $A(\omega)$ of the same model (left panel) at a temperature that is much higher than the Kondo temperature ($T \gg T_K$), and the Kondo resonance peak is absent. As illustrated in the right panel, the enhanced thermal motion of conduction electrons destroys the Kondo state.

experiments [63]. The concept of local temperature is thus of critical importance for bridging this gap, provided that such a quantity can be measured reliably in experiments.

The above examples, which represent only a small fraction of a large body of studies, clearly show that it would be highly desirable to extend the notion of temperature from thermal equilibrium to out of equilibrium. However, such an extension is not at all trivial, because the zeroth law of thermodynamics that defines the temperature for equilibrium systems cannot be applied directly to non-equilibrium situations. Moreover, the “unique” aspects of nanosystems, such as their small sizes, inhomogeneous structures, quantum features, and the embedded environment, all add to the challenge of defining a local temperature.

The goal of this review is thus to survey the existing theoretical and experimental efforts to do just so, with the focus on the following basic questions:

1. How do we define a local temperature for systems out of equilibrium?
2. How do we measure it?
3. What is its physical meaning?

Logically speaking, a question 0 before the above three should be addressed: does a local temperature even exist for a non-equilibrium system?

1.1.2. Organization of the review

In the remainder of Section 1 we shall give a historical account on the measurement of temperature for systems in thermal equilibrium, which will be followed by addressing the challenges in the definition and measurement of local temperature in non-equilibrium systems. We will finish this section by further elaborating on the physical motivations to extend the concept of local temperature out of equilibrium.

In Section 2, we will review the existing theoretical definitions of local temperatures for nanoscopic systems out of equilibrium. We will begin by describing the basic ideas and physical considerations behind these definitions, which generally fall into several categories. We will then elaborate on a number of theoretical definitions by discussing

their advantages and limitations, particularly focusing on the practical feasibility of the experimental realization of these definitions. We will finish this section by discussing the uniqueness/non-uniqueness of the local temperature in non-equilibrium situations, as well as the underlying connections, if they exist, among the different definitions.

In Section 3, we will review the experimental techniques that have been proposed or implemented to determine the local temperatures of non-equilibrium systems. We will start with the general principles of the experimental strategies. In particular, we will discuss the difficulties in realizing a nano-sized thermometer via measuring the heat current flow. Then we will review a number of representative experimental works that have been carried out on measuring the local temperature of different types of systems and for various non-equilibrium situations. The strengths and limitations of these works will be analyzed.

In Section 4, we will focus on the practicality and usefulness of the concept of local temperature. We will first discuss the physical interpretations of the measured local temperatures, along with their implications on the extension of the thermodynamic laws to non-equilibrium scenarios, and on the quantitative correspondence between the equilibrium and non-equilibrium systems. We will then review the applications of local temperature in various emerging fields.

In Section 5, we will conclude the review by summarizing the contents presented in the previous sections. Finally, we will provide future perspectives by discussing the ongoing activities in related fields, addressing the remaining open questions, and suggesting possible directions for future research.

1.2. Temperature at equilibrium

1.2.1. The measurement of temperature

In early times the standard of temperature was simply our bodily sensation of “hot” and “cold” [64]. In the 16th and 17th centuries, a more quantitative way of measuring this sensation was established. It is believed that Galileo Galilei invented the first “thermoscope”, a tubular device in which a liquid rises and falls as the temperature changes due to the variation in liquid density [64, 65]. Using the thermoscope, scientists were then able to understand basic thermal phenomena, such as the distinction between physiological senses and physical properties [65]. The thermoscope then gradually evolved into the modern thermometer, with the addition of a scale in the early 17th century, and its standardization through the 17th and 18th centuries [66].

The early temperature measurements depended on various empirical physical phenomena, and different temperature scales had been introduced to determine the quantitative value of temperature [64]. The second law of thermodynamics selects the definition of an absolute thermodynamic temperature, unique up to an arbitrary scale factor [67]. Until 2018, the kelvin, the base unit of thermodynamic temperature in the International System of Units (SI), was defined as the fraction $1/273.16$ of the thermodynamic temperature of the triple point of water. On November 16, 2018, a new definition was adopted, by which the Boltzmann’s constant is fixed to the exact value of $k_B = 1.380\,649 \times 10^{-23} \text{ J} \cdot \text{K}^{-1}$. The advantage of the new definition is obvious: it is independent of any particular substance, and thus provides a universal standard for any measurement method [68].

The thermodynamical meaning of temperature is given by the zeroth law of thermodynamics proposed by Fowler and Guggenheim [69] in 1939, as follows:

If two assemblies are each in thermal equilibrium with a third assembly, they are in thermal equilibrium with each other.

The zeroth law states the transitivity of thermal equilibrium and hence provides a solid physical basis for a thermometer. From an operational point of view, *temperature is defined as that quantity measured by a thermometer coupled to the system with which it reaches thermal equilibrium*. Precisely because the thermometer plus the system reach a state of global equilibrium when coupled, the quantity that is measured by the thermometer is then attributed to the system in the limit of weak coupling and negligible heat capacity of the thermometer.

Because of the inextricable connection between the concept of temperature and that of heat in thermodynamics, the measurement of the two quantities is closely related to each other. In practice, the heat production Q is usually determined by counting the amount of latent heat released during a phase transition process, or by tracing the temperature change ΔT of a substance with known heat capacity C , *i.e.*,

$$C = \frac{Q}{\Delta T}, \quad (2)$$

where C is assumed to be constant if the temperature change ΔT is sufficiently small [67]. However, this assumption must be used with caution for nanosystems with a small number of DOF, because the heat capacity may depend rather sensitively to the microscopic details (such as the electronic structure) of the system and may thus vary significantly upon the small change in temperature [70].

In the conventional experiments carried out on bulk materials it is reasonable to assume that the measurement is conducted in an adiabatic manner, *i.e.*, the heat dissipated into the surrounding environment is negligibly small as compared to the heat collected by the thermometer or calorimeter. However, the situation can be quite different for nanosystems. This is because the number of energy transfer channels diminishes with the reduced size or dimension of the system, while the energy dissipation between the system and the environment may be enhanced by quantum coherence. In this sense, energy dissipation has been regarded as a main characteristic that distinguishes quantum from classical phenomena [71]. Such a distinct difference should be carefully taken into account in the definition and actual measurement of a local temperature.

More detailed discussions on thermometers at the nanoscale and experimental measurement of local temperature will be given in Sec. 3.3.

1.2.2. Finite-size effects

Small is different [72]. In fact, because of the finite DOF of nanosystems, a careful definition of local thermodynamical quantities is important, to preserve as much as possible their original thermodynamical meaning in macroscopic bulk systems, and to retain a correct asymptotic behavior as the system approaches the thermodynamical limit. Experiments also face new challenges. The thermal probe or, in general, the detector of local observables should be made comparable in size to the target object to ensure the measurement is truly local, and the coupling between the probe and the system should be kept sufficiently weak, to avoid any significant perturbation to the system's intrinsic structure or thermal state. Moreover, as the system size diminishes, the fluctuations of the local observables increase as $1/\sqrt{N}$ [73], with N being the number of DOF. Thus, an appropriate time average or ensemble average is needed to minimize the uncertainty of the measured quantity.

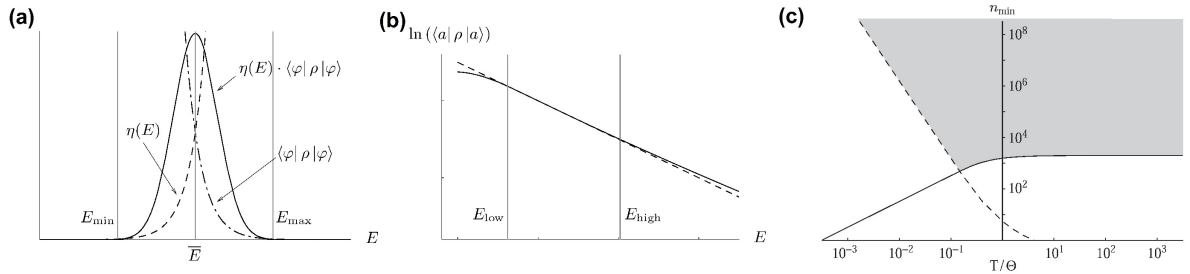


Figure 4: (a) The product of the density of states $\eta(E)$ times the global distribution function $\langle \varphi | \rho | \varphi \rangle$ forms a strongly pronounced peak at the expectation value of the global system energy \bar{E} . (b) The logarithm of the local distribution function $\langle a | \rho | a \rangle$ (solid line) and the logarithm of a canonical distribution (dashed line) with the same local temperature for a harmonic chain. (a) and (b) are reprinted with permission from [74]. Copyright 2004 American Physical Society; (c) Minimal scale n_{\min} as a function of temperature T for a harmonic chain. Local temperature exists in the shaded regions in (c). Θ is the Debye temperature, a characteristic constant of the respective material. Reprinted with permission from [75]. Copyright 2005 Elsevier.

So, can a system be too small to even define a local temperature? To address this question, from the perspective of statistical mechanics, Hartmann *et al.* have investigated the minimal length scales for the existence of a local temperature in a periodic lattice involving short-range interactions [74, 76–79]. They divided a large quantum system in global thermal equilibrium into a group of equivalent subsystems, and analyzed at what size a local temperature exists in each individual subsystem. In the global system, the density of states (DOS) exponentially grows as a function of energy [79], while the canonical distribution function $\langle \varphi | \rho | \varphi \rangle$ (with $|\varphi\rangle$ being an eigenstate of the global Hamiltonian and the global equilibrium state ρ) is an exponentially decaying function of energy. The product of these two functions forms a strongly pronounced peak at the expectation value of the global energy \bar{E} ; see Figure 4(a).

According to Hartmann *et al.*, the only requirement for the existence of local temperature is that the local distribution function $\langle a | \rho | a \rangle$ (with $|a\rangle$ being a tensor product of eigenstates of the individual subsystems) is canonically

distributed in an appropriate energy range around \bar{E} ; see Figure 4(b). In other words, the local distribution function should reproduce the line shape of the global distribution function, so that any local observable that can be evaluated from the former will agree with the true value extracted from the latter. Using this criterion, these authors have estimated the minimal length scale over which a local temperature exists in a harmonic chain. Multiplying n_{\min} by a lattice constant a_0 , namely the distance between the neighboring atoms, the minimal length scale on which temperature can exist in real materials is given by $l_{\min} = n_{\min}a_0$. The results of two representative examples, crystalline silicon and carbon nanotubes, have been shown in Figures (8) and (9) of [79]. From their estimation the minimal length can be quite large at a somewhat low global temperature. Clearly, Hartmann *et al.*'s definition of local temperature relies on the existence of a local Boltzmann distribution. It is applicable to systems in a global thermal equilibrium state, with possible extension to situations in which temperature gradients are small.

From the perspective of thermodynamics, Kliesch *et al.* have attempted to determine the minimal length scales for the existence of a local temperature in a spin- and fermionic-lattice with short-range interactions [80]. For a large system in a global equilibrium state divided into a group of subsystems with various length scales, the zeroth law shows that [81]: (1) there exists a thermal equilibrium state which is characterized by a single parameter called temperature; (2) the temperature is local, namely, each subsystem of the global system is in a thermal state with its own local temperature; (3) the temperature is an intensive quantity, meaning that if the global system is in equilibrium, all the subsystems have the same temperature. Nevertheless, when the interactions present in a global system are non-negligible, the state of a subsystem will be strongly perturbed by its environment, namely, the rest of the global system, and will deviate from its equilibrium thermal state with a specific value of the global temperature. Thus, temperature is not intensive for a global system with strong interactions.

To address under what scale temperature is an intensive property, Kliesch *et al.* focused on a subsystem with a specific length scale. According to Kliesch *et al.*'s work, temperature is an intensive quantity in the subsystem with a given length scale, if and only if the interactions are negligible compared to $k_B T^*$ with T^* being the local temperature of the subsystem. In other word, the minimal scale of local temperatures is related to the decay of the interactions. When the interactions between the subsystem and its environment become vanishingly weak, the subsystem is homogenous inside, and is nearly independent of the rest of the global system. Kliesch *et al.*'s condition for the existence of local temperature is applicable to systems with sufficiently weak interactions.

De Pasquale *et al.* have defined a size-dependent quantity, the local quantum thermal susceptibility, to quantify the accuracy of local temperature measurement on quantum systems [82, 83]. The local quantum thermal susceptibility increases with the size of the measured subsystem. When the subsystem coincides with the whole system, it reaches the maximum value and thus corresponds to the highest achievable accuracy for the local temperature measurement.

If the size of a system is comparable to or even smaller than the wavelength or mean free path of its constituent particles, quantum coherence effects will come into play, and the motion of a particle is more appropriately described by the propagation of its wave-function. This gives rise to important consequences.

First, the wave-function of a particle in the system may extend into the surrounding environment. Because of the system-environment entanglement, the local distribution function of the particles often deviates significantly from the global distribution function, *i.e.*, the equilibrium state of the system may not be described by a local Boltzmann distribution. In such cases, a rigorous treatment of the system-environment entanglement is essential for defining a local temperature and understanding the thermodynamic behavior of the system.

Second, as already mentioned in Sec. 1.2.1, energy dissipation is one important characteristic that distinguishes quantum from classical phenomena. In classical systems, energy dissipation is always one-way and irreversible; whereas in the quantum regime, the system-environment entanglement may greatly prolong the time scale of energy dissipation, and occasionally even results in temporary revival of dissipated energy back into the system. Further remarks on the influence of the environment will be given in Sec. 1.2.3.

Third, the microscopic mechanism of energy exchange largely determines how the energy is distributed over the constituent particles or internal DOF of the system. It is well-known that, for a classical system in the linear response regime, the electric current density i through the system driven by an electric field E obeys Ohm's law [84],

$$i = \sigma E, \quad (3)$$

with σ being the electrical conductivity. Similarly, the heat current density j driven by a temperature gradient ∇T

follows the Fourier's law [85],

$$j = -\lambda \nabla T, \quad (4)$$

with λ being the thermal conductivity.

The physical mechanism behind Ohm's law is the incoherent or phase-breaking scattering processes between the conduction electrons and the local phonons [27]. The same incoherent scattering events also lead to Joule heating in a conductor [27]. Moreover, the conventional mechanisms that lead to the Fourier's law, such as collisions between particles and vibrational motions of atoms, are also incoherent.

However, in the case of a nano- or molecular conductor whose size is smaller than the electron coherence length (mean free path for the quantum phase), the electron transport process can be fully coherent due to the absence of phase-breaking scattering events inside the conductor [86, 87]. In the coherent limit, both the Ohm's law and Fourier's law are no longer valid. Interestingly, it has been found that Fourier's law can be reconstructed by introducing disorders in the conductor, because disorder leads to dephasing [88]. The crossover from the fully coherent regime (invalid Fourier's law) to incoherent (valid Fourier's law) regime is characterized by a thermal length scale, which is directly related to the profile of the local temperature [89].

1.2.3. Influence of the environment

When a nanosystem is embedded in or adsorbed onto a macroscopic bulk material, the latter serves as an environment of the former. For instance, in the case of a QD coupled to a metal lead, the lead plays the role of heat bath and electron reservoir of the QD. The environment usually possesses a much larger number of DOF than the system. Therefore, when the two are put into contact and form a composite system, the thermalization process will ultimately lead to a global thermal equilibrium state, with the global temperature T and global chemical potential μ determined largely by those of the environment. The spontaneous thermal fluctuations within the environment always exist and they have crucial influence on the dynamics of the system [90]. Such influence can be understood by considering the classical Brownian motion of pollen grains in solution [91]. The thermal fluctuations of the surrounding solvent molecules result in random impacts on a pollen grain. These random impacts generally cause two kinds of effects at the same time: firstly, they act as a random driving force to maintain the irregular motion of the pollen grain; and secondly, they give rise to a frictional force to dissipate away the energy of the pollen grain and thus slow down its motion. In thermal equilibrium, these two opposite effects of environmental fluctuations reach a certain form of balance, which is usually described by a quantitative relation, the fluctuation-dissipation theorem (FDT) [90], we will discuss in the following.

Similar effects are also generally found in open quantum systems, in which the environmental fluctuations govern the system's dissipative dynamics [92, 93]. Besides the exchange of particles and energy, the environmental fluctuations also cause decoherence through the phase-breaking system-environment interactions, which makes the quantum system behave more classical-like.

For a general system-plus-environment composite, the total Hamiltonian H_T consists of three parts:

$$H_T = H_S + H_B + H_{SB}, \quad (5)$$

where H_S , H_B and H_{SB} are the Hamiltonian of the system, the Hamiltonian of the environment (heat bath or particle reservoir), and the system-environment coupling Hamiltonian, respectively. The specific formulation of H_S , H_B and H_{SB} depends on the details of the composite system under study.

The dynamics of the system in the presence of the environment is generally characterized by the reduced density matrix $\rho_s(t) \equiv \text{tr}_B[\rho_T(t)]$. The time evolution of ρ_s generally follows the Nakajima-Zwanzig quantum master equation (QME) as follows [94–96] (hereafter, we adopt the atomic units, *i.e.*, $\hbar \equiv 1$ and $k_B \equiv 1$):

$$\dot{\rho}_s(t) = -i[H_S, \rho_s(t)] - \int_{t_0}^t d\tau \tilde{C}(t - \tau) \rho_s(\tau). \quad (6)$$

Here, the first term on the right-hand side describes the intrinsic system dynamics, while the second term accounts for the influence of the environment on the system dynamics. Clearly, the second term has the form of a convolution integral. Consequently, ρ_s at the present time t depends explicitly on $\rho_s(\tau < t)$, namely the whole history of its evolution.

The two-time environment correlation function $\tilde{C}(t - \tau) \equiv \langle \hat{F}^\dagger(t) \hat{F}(\tau) \rangle_{\text{B}}$ serves as the non-Markovian memory kernel. Here, $\langle \hat{O} \rangle_{\text{B}} \equiv \text{tr}_{\text{B}}(\hat{O} \rho_{\text{B}}^{\text{eq}})$ represents expectation value taken for the equilibrium bath, with tr_{B} denoting the trace over all the environment's DOF, and $\hat{F}(t) \equiv e^{iH_{\text{B}}t} \hat{F} e^{-iH_{\text{B}}t}$ with \hat{F} being a bath operator. For bath environments that satisfy Gaussian statistics, such as harmonic oscillator baths, non-interacting phonon baths or non-interacting electron reservoirs, the two-time correlation function $\tilde{C}(t - \tau)$ completely characterizes the influence of the environment [97].

If the longest correlation time scale of the bath dynamics τ_{B} is shorter than the characteristic time scale of the system Hamiltonian τ_{S} *i.e.*, $\tau_{\text{B}} \ll \tau_{\text{S}}$, the influence of the environment fluctuations on the reduced system dynamics is almost instantaneous. This is referred to as the Markovian limit, in which the memory effect of the environment is negligible [98]. On the contrary, if $\tau_{\text{B}} > \tau_{\text{S}}$ holds, the system's state at the present time will depend strongly on the history of the dynamics, and such a situation is called non-Markovian [99]. In the non-Markovian regime, the memory effect of the environment is important and quantum coherence effects become prominent. The non-Markovian memory affects both the transient behavior and the asymptotic long-time limit of the reduced system dynamics [99].

Traditionally, the derivation of a QME often involves various approximations to the dissipative process between the system and the environment. For instance, the Born approximation gives a perturbative treatment of H_{SB} , while the Markovian approximation neglects any long-time component of $\tilde{C}(t - \tau)$ [93, 97]. These approximations have led to simplified QMEs, such as the Redfield theory [100, 101]. Another frequently used QME is the Lindblad equation [102, 103], which has the advantage that the resulting ρ_{S} is positive semidefinite [104].

In the past two decades, formally exact quantum dissipative theories have been developed. These include the deterministic hierarchical equations of motion (HEOM) [105–109] and the stochastic theories such as the quantum state diffusion theory [110–113] and the stochastic equation of motion theory [114–117]. Interested readers may refer to review articles, such as Refs. [99, 109, 118].

The memory kernel is of central importance to the influence of the environment, as it directly reflects the FDT. For a boson bath at thermal equilibrium, the memory kernel satisfies the following relationship [97]:

$$\tilde{C}(t - \tau) = \frac{1}{\pi} \int_{-\infty}^{\infty} d\omega e^{-i\omega(t-\tau)} f(\omega) J(\omega). \quad (7)$$

Here, $f(\omega) \equiv 1 + f^{\text{BE}}(\omega)$, with $f^{\text{BE}}(\omega) = 1/[e^{\beta(\omega-\mu)} - 1]$ being the Bose–Einstein distribution function, $\beta = 1/T$ is the inverse temperature, μ is the chemical potential of the environment, and $J(\omega)$ is the bath linewidth or hybridization function.

Equation (7) is a manifestation of the FDT, because $\tilde{C}(t - \tau)$ on the left-hand side quantifies the statistical features of the random fluctuations in the bath [115, 117, 119], while the linewidth function on the right-hand side characterizes the rate of energy dissipation between the system and the bath for any energy ω . If the environment is a fermionic bath, such as a reservoir of free electrons, an FDT that is formally analogous to Eq. (7) can be derived [97].

The memory time of the environment τ_{B} as well as the non-Markovianity of the reduced system dynamics depend substantially on the background temperature T . For a fermionic environment such as a metal lead, it is the imaginary part of $\tilde{C}(t)$ that varies with T . Figure 5 depicts $\text{Im}[\tilde{C}(t)]$ of a free-electron reservoir. As it is evident, the reservoir correlation function exhibits a much slower decay at low temperatures. From the Fourier transform relation of Eq. (7), the long-time behavior of $\tilde{C}(t)$ is closely related to the line shape of the Fermi–Dirac distribution function in the low-energy range. Recently, Cui *et al.* have shown that $\tau_{\text{B}} \propto 1/T$ at low temperatures [120]. In the zero-temperature limit, $\tau_{\text{B}} \rightarrow \infty$, and overall $\tilde{C}(t)$ decays as $1/t$ in the long-time regime. This implies that the non-Markovian memory is crucially important for many exotic quantum phenomena in nanosystems, such as the Kondo resonance and spin excitations in systems, which are prominent only at sufficiently low temperatures.

1.2.4. Local equilibrium conditions

The concept of local equilibrium can be traced back to non-equilibrium bulk materials. For a nanosystem coupled to a macroscopic environment, the definition of local temperature is usually based on the assumption that the nanosystem is in some form of local equilibrium state, even when the whole composite is out of equilibrium [121]. For a macroscopic system in a global thermal equilibrium state, there is no net flow of energy or particles anywhere inside the system, and so the temperature and chemical potential are uniform in any subregion of the total system.

For near-equilibrium systems, a useful assumption is that in each sufficiently small region of space the gradients of intensive thermodynamic functions are small and their local values vary relatively slowly compared with those of

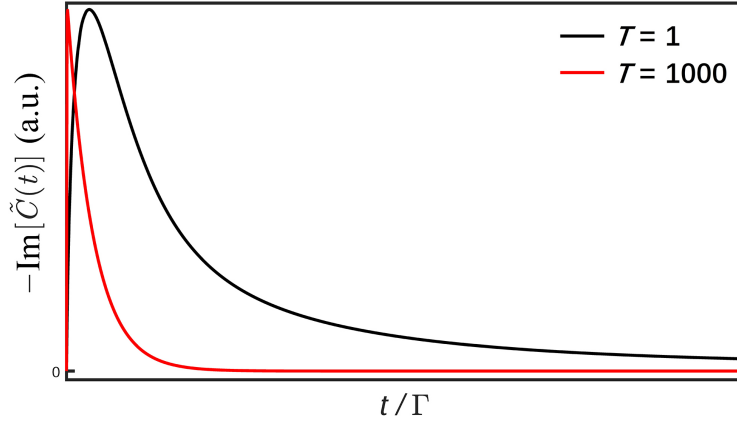


Figure 5: The imaginary part of $\tilde{C}(t)$ of a free-electron bath at high (red) and low (black) temperatures. The two lines are scaled to have the same maximum. The bath hybridization function assumes a Lorentzian form of $J(\omega) = \Gamma W^2/(\omega^2 + W^2)$ with $W = 20$. Γ is the strength of system-bath coupling, and W is the bandwidth of the electron bath. All energies are in units of Γ .

the global system [122]. This idea leads to a local equilibrium condition, which conceptually states that a large system can be spatially and temporally divided into subsystems of small sizes, and within a subsystem the net flow of energy or particles is negligibly small. Consequently, a common local temperature and a common local chemical potential can be defined for each subsystem.

It should be emphasized that if the local subsystem is allowed to exchange particles with its surrounding, it requires both the local temperature and local electrochemical potential to characterize the local equilibrium state as well as the associated local thermodynamics functions. In 1981 Engquist and Anderson [121] have proposed a local equilibrium condition from the perspective of the zeroth law of thermodynamics, by putting forward a definition of ideal potentiometer and thermometer. They considered a local subregion of a current-carrying system that is weakly coupled to a macroscopic probe. The local temperature and local electrochemical potential of the subsystem are well-defined only when the net electrical and heat currents flowing through the probe are zero:

$$I_p = 0, \quad (8)$$

$$J_p = 0, \quad (9)$$

where I_p and J_p are the net electrical current and heat current through the macroscopic probe, respectively. Therefore, the probe serves as an ideal potentiometer/thermometer. Equations (8) and (9) emphasize that in local equilibrium there is no net energy and particle flow between the local subsystem and its environment. The zero-current conditions have been extensively used to determine the local temperatures and local electrochemical potentials of various types of non-equilibrium systems. We will provide a more extensive discussion in Sec. 2.2.1.

From the statistical point of view, the local equilibrium condition for a classical system means that the statistical distribution of canonical states inside a subsystem closely approaches the Boltzmann distribution and hence classical thermodynamic functions and equations remain valid [123, 124].

In Sec. 1.2.2, we have given an example on the minimal size of a subsystem required for the existence of a local Boltzmann distribution; see Figure 4. However, we should point out that there exist a vast amount of nanosystems, such as molecules, nanotubes and few-electron QDs, whose sizes are distinctly smaller than that required to establish a local Boltzmann distribution. So, what are the theoretical criteria and experimental means that can be used to confirm the existence of local equilibrium in such “ultrasmall” systems?

The canonical density matrix of a system-plus-environment composite in its global equilibrium state is

$$\rho_{\tau}^{\text{eq}}(\beta) = \frac{e^{-\beta H_{\tau}}}{Z}, \quad (10)$$

where $Z = \text{tr}_{\tau}(e^{-\beta H_{\tau}})$ is the partition function of the composite, and tr_{τ} denotes the trace over all the system-plus-bath

DOF. In general, the system reduced density matrix does not follow the local Boltzmann distribution [125],

$$\rho_s^{\text{eq}} = \frac{\text{tr}_b(e^{-\beta H_T})}{Z} \neq \frac{e^{-\beta H_s}}{\text{tr}_s(e^{-\beta H_s})}, \quad (11)$$

even at the weak system-environment coupling limit. The same inequity in Eq. (11) also holds for a grand-canonical total density matrix $\rho_s^{\text{eq}}(\beta, \mu)$. This is because the system and environment Hamiltonians, H_s and H_b , usually do not commute, and ρ_T cannot be described as a product of independent system and environment states due to the system-environment entanglement. For instance, Moix *et al.* [126] have applied a stochastic quantum dissipation theory approach to compute ρ_s^{eq} of several exciton-transfer-related complexes, including the Fenna–Matthews–Olson protein and the light harvesting complex of purple bacteria, LH2. They have found that the reduced density matrix, ρ_s^{eq} , of an LH2 complex at 100 K is almost completely delocalized, whereas the coherence length of the exact ρ_s^{eq} is drastically reduced due to the coupling to the thermal bath. The difference becomes more important when either the temperature is lowered or the system-bath coupling increases.

Although local equilibrium cannot be verified by ρ_s , its existence can still be revealed by examining the detailed balance relation via the system's dynamical variables [127–130]. In practice, this idea has been adopted in some high-energy physics experiments to measure the temperature of a plasma by using x-ray Thomson scattering [131, 132], and it may be potentially useful for nanosystems of our primary interest as well.

Let us consider a fundamental question for non-equilibrium systems: how does an external field affect the dynamical variables of the systems? In the linear-response regime, the response of a system observable \hat{A} at time t to an external perturbation \hat{B} at prior time τ is generally characterized by the response function

$$\tilde{\chi}_{AB}(t - \tau) \equiv i\langle [\hat{A}(t), \hat{B}(\tau)] \rangle_T = i\{\langle \hat{A}(t)\hat{B}(\tau) \rangle_T - \langle \hat{B}(\tau)\hat{A}(t) \rangle_T\} = i\{\tilde{C}_{AB}(t - \tau) - \tilde{C}_{BA}(\tau - t)\}. \quad (12)$$

Here, $\hat{O}(t) \equiv e^{iH_T t} \hat{O} e^{-iH_T t}$, and $\tilde{C}_{AB}(t - \tau) \equiv \langle \hat{A}(t)\hat{B}(\tau) \rangle_T = \text{tr}_T[\hat{A}(t)\hat{B}(\tau)\rho_T^{\text{eq}}]$ is the two-time correlation function of the unperturbed system at thermal equilibrium.

Response and correlation functions are of great importance to spectroscopy [133] and many-body physics [134]. For instance, the emission and absorption of light and the transport of charge carriers are often described in terms of Green's functions, which are essentially correlation functions between particle creation and annihilation operators.

Let $C_{AB}(\omega) \equiv \frac{1}{2} \int_{-\infty}^{\infty} dt e^{i\omega t} \tilde{C}_{AB}(t)$. This quantity satisfies the detailed-balance relation as follows [97]:

$$\frac{C_{BA}(-\omega)}{C_{AB}(\omega)} = e^{-\beta\omega}. \quad (13)$$

Equation (13) can be interpreted as a characterization of the statistical relation between two dynamical processes of an equilibrium system. Here, $C_{AB}(\omega)$ is regarded as the rate of particle excitation by absorbing an energy ω , and $C_{BA}(-\omega)$ is the rate of the de-excitation process by releasing the energy ω . The ratio of these two rates is precisely controlled by the temperature of the system. For systems out of equilibrium, Eq. (13) provides a criterion for the existence of local equilibrium within a small subsystem.

For equilibrium systems, $C_{AB}(\omega)$ and the anti-Hermitian response function [97] $\chi_{AB}^{(-)}(\omega) \equiv \frac{1}{2i} \int_{-\infty}^{\infty} dt e^{i\omega t} \tilde{\chi}_{AB}(t)$ satisfy the FDT:

$$\tilde{C}_{AB}(t) = \frac{1}{\pi} \int_{-\infty}^{\infty} d\omega e^{-i\omega t} f(\omega) \chi_{AB}^{(-)}(\omega). \quad (14)$$

Equation (14) is formally analogous to Eq. (7). It is possible to acquire $C_{AB}(\omega)$ experimentally by measuring the response property $\chi_{AB}^{(-)}(\omega)$, and then check the validity of Eq. (13) to confirm the existence of local equilibrium. Furthermore, in equilibrium systems, the occupations of bosonic and fermionic particles on microstates obey the Bose-Einstein and Fermi-Dirac distributions, respectively. If the distribution is preserved approximately within a small subregion of a non-equilibrium system, a local equilibrium state is considered to exist for the small subsystem. Note that the particle distribution function involves both the local temperature and local electrochemical potential. For instance, Yan *et al.* have shown that the local chemical potential is essential for describing the non-equilibrium magnon density distribution in a Heisenberg spin chain [135].

1.3. Physical motivations to extend the concept of temperature out of equilibrium

Generally speaking, extension of thermodynamic and statistical approaches for equilibrium systems to non-equilibrium situations faces fundamental difficulties. For systems out of equilibrium, the local equilibrium conditions are in principle approximate, and some important relations such as the detailed-balance relation and the FDT may no longer hold true, though their non-equilibrium versions are being investigated [136, 137].

For macroscopic and classical systems out of equilibrium, the concept of local temperature has been adopted. Casas and Jou have provided a general overview of the definitions of temperature in non-equilibrium systems, as well as a wide range of applications of these definitions to different systems [138]. They have concluded that under the local equilibrium condition, different definitions give the same temperature, while in a non-equilibrium state beyond local equilibrium, the values of temperature defined by different approaches may deviate from one another. Puglisi *et al.* have reviewed different definitions of temperature in classical systems and discussed their relevance to energy fluctuations [139]. Particularly, a generalized fluctuation-dissipation relation (FDR) was introduced, which provides a statistical basis for extending the definition of temperature to far-from-equilibrium classical systems.

For non-equilibrium nanosystems, the quantum coherence effects and influence of the environment can be conspicuous. For instance, temperature oscillations may appear in nanosystems under bias voltages or temperature gradients [140–143], which clearly contradict the conventional Fourier’s law for classical systems [144]. For the case of a nanowire coupled to two metal leads at different temperatures, it was indeed predicted that the local temperature of the wire may exhibit spatial oscillations at certain lead-wire coupling strengths [140]. Similar oscillations have also been predicted to occur in a thermally-driven armchair graphene sheet [143]. Further calculations have revealed the relation between the wavelength of temperature oscillations and that of the Friedel oscillations [145], a ubiquitous oscillation of charge density in electronic systems. These works indicate that the temperature oscillation is a non-classical property and reflects the quantum coherent nature of the system [144].

From thermodynamic relations, we have the following definition of temperature at fixed volume V and number of particles N :

$$T = \left(\frac{\partial E}{\partial S} \right)_{V,N}, \quad (15)$$

where E and S are the system’s internal energy and entropy, respectively. The direct application of Eq. (15) to open quantum systems is difficult [139, 146], because different definitions of entropy do not lead to a consistent value even at the same temperature [147, 148]. For example, the von Neumann entropy of the reduced system, $S_{VN} \equiv -\text{tr}_s(\rho_s \ln \rho_s)$, has been used to define the local temperature via Eq. (15) [149–151]. However, unlike the thermodynamical entropy, S_{VN} remains finite even at zero background temperature [148].

For systems out of equilibrium, the definition of basic thermodynamic quantities, such as entropy and free energy, is still under debate [152–154]. In addition, the equipartition theorem of energy among the system’s different DOF has to be applied carefully [155, 156]. For instance, in a nanoelectronic device driven by a constant bias, the electron-electron interactions and electron-phonon interactions are expected to induce electronic and ionic temperatures that are different from each other [20, 27, 157, 158]. Such difference is particularly significant in elastic electron transport, because the motion of electrons and ions is completely decoupled [159].

Enormous efforts have been made to combine thermodynamics and quantum theory [160–164], leading to the development of *quantum thermodynamics* [165], which closely relates the laws of thermodynamics to their quantum origin. In 1959, Scovil *et al.* have established the equivalence between a three-level maser and a Carnot heat engine [166, 167]. Later, the Lindblad–Gorini–Kossakowski–Kossakowski semi-group master equation [102, 103] has been employed to address quantum thermodynamics from a dynamic perspective [160, 168] and to explore non-equilibrium thermodynamic processes such as heat flow and entropy production [154, 165, 169]. Despite this progress, there are still many unsolved or controversial problems in quantum thermodynamics, and experimental verifications of theoretical predictions are far from adequate [170–172]. At any rate, the problem of defining a local temperature stands again at the heart of quantum thermodynamics.

Summarizing the above, we see that extending the notion of temperature from equilibrium to non-equilibrium situations should at least have the following implications:

1. Existence of a local temperature indicates the local equilibrium approximation is valid. In view of the zeroth law of thermodynamics, this means that the net flow of particle or energy between the system and its environment should reduce to a minimal extent.

2. Local temperature offers a characteristic energy scale for the magnitude of local excitations and fluctuations, and it also determines the distribution of particles among the relevant microscopic states. Comparing the local temperature to the background temperature provides a quantitative description of how far the system is away from a global equilibrium state.
3. Local temperature is also useful for characterizing the variation of the system's intrinsic dynamical and thermodynamic properties under an external bias. This is particularly important for investigating systems involving strong electron correlations.

In addition, an ideal definition of local temperature should also be universal (so that it may be applied to as many non-equilibrium situations as possible), unique (so that it predicts one and only one parameter), feasible (so that it can be measured by experimental means), and asymptotically correct (so that it can retrieve the correct thermodynamic temperature in a global equilibrium state).

We end this section by some remarks on a pertinent concept that shows up frequently in the literature: the “effective temperature” T_{eff} [28, 141, 142, 173–176]. The physical meaning of effective temperature varies according to the different contexts in which it is employed. Sometimes it is used simply as an alias of local temperature [141, 142, 173, 174, 177]; whereas in certain circumstances, effective temperature merely provides an equivalent expression for a specific value of energy, such as Fermi temperature and Kondo temperature [178, 179]. In the latter scenario, T_{eff} is just an energy scale, and it hardly conveys any thermodynamic or statistical meaning. In the experimental works, the term “effective temperature T_{eff} ” is often adopted (see Sec. 3), and it usually provides a quantitative characterization of the magnitude of local heating or local excitation in a nanosystem. Therefore, in the rest of this review, we shall distinguish the two concepts only when T_{eff} refers to an energy scale rather than a physical temperature.

2. Theoretical definitions of local temperature out of equilibrium

2.1. General Remarks

Numerous theoretical approaches have been proposed to define local temperature of non-equilibrium nanosystems. In light of their different underlying physical assumptions, most of the existing theoretical approaches can be ascribed to three general categories, by making connection to the physical implications of local temperature as described in Sec. 1.3. In the following, we shall begin by giving a brief overview on the three categories of theoretical definitions, and then provide an in-depth review of these definitions at a more detailed level in Sec. 2.2.

First, from the thermodynamic point of view, the global thermal equilibration provides the conceptual and practical basis for the definition of a thermometer. In nanosystems out of equilibrium, the local equilibration of energy and particles has been taken by many authors as “local equilibrium condition” for determining the local temperature [79, 180–183]. However, in this review the above condition will be termed as “zero-current condition”, since the latter more precisely describes the consequence of local equilibration processes — vanishing of particle and heat currents in a local subregion of a system. Moreover, thermodynamic relations connect different intrinsic system properties. For instance, Eq. (15) links the system energy E to the entropy S via the temperature T . Extending thermodynamic relations such as Eq. (15) to non-equilibrium situations under the local equilibrium approximation also gives rise to quantitative definitions of local temperature out of equilibrium.

Second, from the statistical perspective, temperature determines the distribution of particles among microscopic states. The concept of particle distribution function has been extended to non-equilibrium situations, and determination of local temperature from a non-equilibrium distribution function has been proposed [173, 184–186]. Moreover, for systems far from equilibrium, the FDT which characterizes the balance between the environment fluctuations and dissipation is no longer rigorous. Instead, various forms of approximate FDR have been proposed [187–193], from which a local temperature can be extracted [139, 187–189, 193, 194]. For instance, Cugliandolo [194] and Puglisi *et al.* [139] have determined the local temperatures of non-equilibrium classical systems by scrutinizing the deviation of non-equilibrium FDR from equilibrium FDT. In the rest of this section, we shall instead focus on nanosystems in which quantum effects are prominent.

Third, a variety of physical properties sensitively depends on the local temperature [79]. This has facilitated the design of practical schemes for measuring a local temperature of non-equilibrium systems. Moreover, in practice it is ideal that a thermometer (such as a non-invasive thermal probe) should cause a minimal perturbation to the system under study when the measurement is conducted. Such a minimal perturbation condition (MPC) can be examined by

monitoring the evolution of a certain thermosensitive property of the system [140]. As a consequence, operational protocols based on the MPC have been proposed, with which the local temperature can be determined quantitatively by presuming the local equilibrium approximation [182, 183].

In Sec. 2.2 we will review the above three categories of theoretical definitions of local temperature. The physical essence and operational protocol of these definitions will be exemplified by specific examples, along with some remarks on their advantages and limitations. The experimental feasibility of these theoretical definitions will also be addressed.

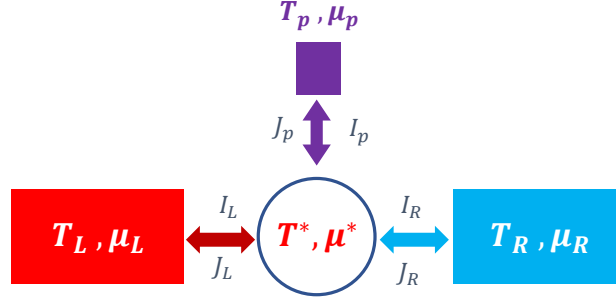


Figure 6: Schematic of a nanojunction. The central system (blue circle) is coupled to three leads – left lead, right lead, and probe, which are labeled by $\alpha = L, R, p$, respectively. Each lead can have a distinct background temperature (T_α) and electrochemical potential (μ_α). I_α is the electric current flowing into the α -lead, and J_α is the resulting heat current. The central system is considered to have a local temperature T^* and local electrochemical potential μ^* .

In the the rest of this section, we introduce some basic quantities which will be frequently used hereafter. To start, let us consider a nanojunction sketched in Fig. 6 as an example. The junction consists of a central system (such as a nanoelectronic device) coupled to a number of leads (labeled by α). Each lead has its own background temperature T_α and electrochemical potential μ_α . If T_α or μ_α of a certain lead is different from the counterpart of any other lead, the whole junction is out of equilibrium. In many of the existing theoretical approaches, the determination of a local temperature T^* requires the information of particle current and heat flux between the local system and the thermal probe. In the nanojunction depicted in Fig. 6, the electric current flowing into the α -lead and the resulting heat flux are denoted by I_α and J_α , respectively.

Consider $\{T_\alpha, \mu_\alpha\}$ to be all time-independent, so that the bias voltage and thermal gradient across any pair of leads are constant, and the whole junction has reached a stationary state. Under these conditions, the electric current flowing into α -lead ($\alpha = L, R, p$) can be expressed by the following Landauer formula [195]

$$I_\alpha = i \int d\epsilon \operatorname{tr} \{ \mathbf{\Gamma}_\alpha(\epsilon) \{ \mathbf{G}^<(\epsilon) + f_\alpha(\epsilon) [\mathbf{G}^r(\epsilon) - \mathbf{G}^a(\epsilon)] \} \}, \quad (16)$$

and the associated heat current is expressed by [196]

$$J_\alpha = i \int d\epsilon (\epsilon - \mu_\alpha) \operatorname{tr} \{ \mathbf{\Gamma}_\alpha(\epsilon) \{ \mathbf{G}^<(\epsilon) + f_\alpha(\epsilon) [\mathbf{G}^r(\epsilon) - \mathbf{G}^a(\epsilon)] \} \}. \quad (17)$$

Here, \mathbf{G}^r , \mathbf{G}^a and $\mathbf{G}^<$ are the retarded, advanced and lesser Green's functions, respectively, in the Keldysh, or non-equilibrium Green's function (NEGF), formalism, and the boldface indicates that these quantities are matrices in the Hilbert space of the central system. In particular, \mathbf{G}^r and \mathbf{G}^a describe the propagation of electronic excitations within the central system, while $\mathbf{G}^<$ describes the non-equilibrium electron distribution. $f_\alpha(\epsilon) = 1/[1 + e^{(\epsilon - \mu_\alpha)/T_\alpha}]$ is the Fermi distribution function of the α -lead, and $\mathbf{\Gamma}_\alpha$ is the hybridization (or linewidth) matrix characterizing the coupling strength between the central system and the α -lead. Note that Eq. (16) and Eq. (17) are formally exact even when the central system involves explicit electron-electron interactions [195].

For non-interacting or effectively non-interacting (mean-field) central systems, Eq. (16) and Eq. (17) can be sim-

plified as [195, 196]

$$I_\alpha = \sum_{\gamma \neq \alpha} \int d\epsilon \mathcal{T}_{\alpha\gamma}(\epsilon) [f_\alpha(\epsilon) - f_\gamma(\epsilon)], \quad (18)$$

$$J_\alpha = \sum_{\gamma \neq \alpha} \int d\epsilon (\epsilon - \mu_\alpha) \mathcal{T}_{\alpha\gamma}(\epsilon) [f_\alpha(\epsilon) - f_\gamma(\epsilon)], \quad (19)$$

where $\mathcal{T}_{\alpha\gamma} = \text{tr}\{\mathbf{\Gamma}_\alpha \mathbf{G}^r \mathbf{\Gamma}_\gamma \mathbf{G}^a\}$ is the electron transmission function from α -lead to γ -lead. Equation (18) is the well-known Landauer formula for a multi-terminal nano-conductor [27, 86, 197]. The above equations are of fundamental importance to quantum electron and thermal transport in nanoscopic/mesoscopic systems. It is important to point out, however, that the above equations do not include the influence of phonons. To account for the contribution of electron-phonon interactions, Eqs. (16)–(19) need to be modified, e.g., by including the self-energies due to phonon baths.

We now pay particular attention to the linear response regime because it is closely related to experiments. If I_α and J_α are driven by a small bias voltage, $\Delta\mu = \mu_L - \mu_R$, or a small temperature gradient, $\Delta T = T_L - T_R$, across the left and right leads, their expressions can be simplified as [198]

$$I_\alpha = -\mathcal{L}_{11} \frac{\Delta\mu}{T} - \mathcal{L}_{12} \frac{\Delta T}{T^2}, \quad (20)$$

$$J_\alpha = -\mathcal{L}_{21} \frac{\Delta\mu}{T} - \mathcal{L}_{22} \frac{\Delta T}{T^2}. \quad (21)$$

Here, T is the background temperature, and \mathcal{L}_{ij} ($i, j = 1, 2$) are the linear response coefficients [198, 199], which are closely related to the transport properties measured in experiments. The electric current induced purely by a small bias voltage reflects the electric conductance $G = -\frac{1}{T} \mathcal{L}_{11}$ [144, 198, 199], while the thermopower $S = \lim_{\Delta T \rightarrow 0} \frac{\delta V}{\delta T}|_{I_\alpha=0} = -\frac{1}{T} \frac{\mathcal{L}_{12}}{\mathcal{L}_{11}}$ measures the induced thermoelectric voltage in response to a temperature difference across the two leads [144, 198, 200]. In the situation in which $I_\alpha = 0$, the thermal flux can be simplified as $J_\alpha = -\kappa \Delta T$, with $\kappa = \frac{1}{T^2} (\mathcal{L}_{22} - \mathcal{L}_{22}^2 / \mathcal{L}_{11})$ being the thermal conductance. Moreover, the Onsager reciprocal relation $\mathcal{L}_{12} = \mathcal{L}_{21}$ has also been proved [198]. Particularly, the relation between the electronic contribution of κ and G of a metal (denoted κ_e and G_e , respectively) is revealed by the Wiedemann-Franz law, which states that the ratio of κ_e to G_e is proportional to the temperature of the system, $\kappa_e / G_e = LT$, with the proportionality constant L , known as the Lorenz number [201].

In addition to the NEGF method, there are some other approaches that can be used to describe quantum electron and thermal transport through nanojunctions. These include the QME approach and the HEOM approach [109, 202–206]. To simulate realistic nanojunctions from first principles, such as single molecular junctions [207–210] and graphene nano-devices [211–214], the above theoretical approaches must be combined with electronic structure methods. For instance, single-particle scattering theory has been combined with density functional theory (DFT) [215, 216] to simulate quantum electron transport through atomic or molecular electronic devices [210, 217–220]. In this approach, the Landauer formula of Eq. (18) for non-interacting systems is employed, since the Kohn–Sham reference system is effectively non-interacting. However, driven by a bias voltage or thermal gradient, the nanosystem is not in its ground state, and thus the use of ground-state DFT methods is only an approximation [221–223].

The time-dependent extension of DFT, time-dependent density functional theory (TDDFT), is capable of addressing excited-state properties of electronic systems [224], and, in principle, provides an exact theory for the total current flowing across the device [225]. TDDFT methods for open systems have also been developed. For instance, Burke *et al.* have constructed a Markovian QME including dissipation to phonons for the time-dependent Kohn–Sham system [226], while Di Ventra and D’Agosta have developed a stochastic time-dependent current-density functional theory method for open systems via the real-time propagation of a stochastic Schrödinger equation [227, 228]. Zheng *et al.* have proved the existence of a rigorous TDDFT for open systems with variable number of electrons [229], and developed a practical TDDFT scheme for open systems (TDDFT–OS) [230–232]. The TDDFT–OS method has been applied to perform atomistic simulations of real-time electron transport through nanojunctions [233].

With the latest DFT/TDDFT methods or their approximate variants, such as the density-functional tight-binding (DFTB) method [234], it is now possible to model and simulate a nanojunction consisting of tens of thousands of atoms at the quantum-mechanical level [235]. For instance, Yam *et al.* have employed a DFTB+NEGF method to

study the current-voltage characteristic of a junctionless silicon-nanowire field-effect transistor with more than 15000 atoms in the core region [236].

2.2. Definitions of non-equilibrium local temperatures

2.2.1. Definitions based on zero-current condition

As we have already briefly mentioned, in an early study, Engquist and Anderson proposed a local equilibrium condition [121] which has been employed extensively in the literature [237–240]. In their work, an ideal potentiometer/thermometer (a voltage/temperature probe) in the form of a one-dimensional chain of non-interacting electrons is weakly coupled to the non-equilibrium system of interest. Then the temperature T_p and electrochemical potential μ_p of the probe are adjusted until there is no net electric current I_p and heat current J_p flowing between the probe and the system. Such a condition is referred to as the zero-current condition (ZCC). Under the ZCC, the local temperature T^* and local electrochemical potential μ^* of the system are determined to be identical to those of the probe, respectively. Therefore, the ZCC can be expressed by the following form

$$\begin{cases} I_p|_{T_p=T^*, \mu_p=\mu^*} = 0, \\ J_p|_{T_p=T^*, \mu_p=\mu^*} = 0. \end{cases} \quad (22)$$

In some cases, for example, when the local probe exclusively couples to the vibrational DOF, the zero electric current condition is not relevant, since the phonon number is not conserved [237–239].

Caso *et al.* have applied the ZCC to study local temperatures of quantum systems driven out of equilibrium by external periodic fields [141, 142, 174]. Figure 7(a) displays the sketch of a quantum driven system. The central system is a nanowire modeled by a one-dimensional lattice, with its two ends connected to the left and right reservoirs. External fields which are periodic in time are applied to two separated sites of the nanowire. The periodic fields driving the electron and heat transport through the nanowire consist of both dc and ac components. The dc component creates a constant bias voltage which presents an energy barrier for electron transport [241, 242], while the two local ac fields have the identical amplitude and frequency but differ by a constant phase. In principle, the ac fields should lead to a local temperature which changes with time. To remove the time dependence, the authors investigated the local temperature in the low-frequency regime, where the periodic time of ac fields is much longer than the dwell time of electrons in the nanojunction so that the external field can be treated as an adiabatic perturbation. Therefore, the microscopic states of the system do not change significantly during the pumping process, and the ZCC results in a well-defined time-independent T_l^* for a given site l . More specifically, T_l^* is measured by monitoring the electric and thermal currents flowing into the third reservoir (the probe), which is weakly coupled to the l th site of the nanowire.

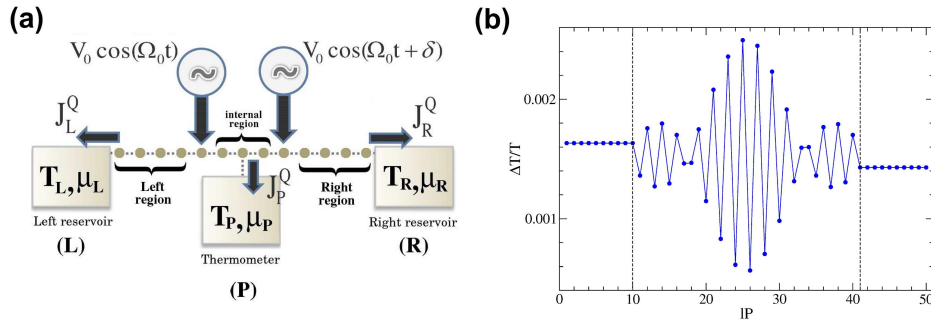


Figure 7: (a) Schematic of a quantum driven system. The central device is a nanowire connected to two reservoirs. The third reservoir P represents a local thermometer, which consists of a macroscopic system weakly coupled to a given point of the central device. (b) Local temperature along a lattice with $N = 50$ sites under two ac fields with a phase shift $\delta = \pi/2$ at the positions indicated by vertical dotted lines. Reprinted with permission from [142]. Copyright 2011 American Physical Society.

Figure 7(b) shows the spatial distribution of local temperature along the nanowire determined by Eq. (22). The value of T_l^* is plotted for each site for the situation of $T_L = T_R = T$, $\mu_L = \mu_R = \mu$ and a low driving frequency. From the profile of T_l^* one can easily recognize three regions in the nanowire. Clearly, the local temperature is almost constant in the left/right region. Note that the left end of the nanowire is slightly hotter than the right end because

the presence of the phase shift δ breaks the original symmetry of the nanowire [142]. In the internal region between two energy barriers, the local temperature oscillates periodically in space. The Friedel-like oscillation has also been observed in other nanostructures [145]. In the nanowire the two energy barriers act as local impurities in the charge transport, and the oscillation is a consequence of quantum interference generated by scattering processes between conduction electrons and local impurities [141, 142, 174]. The oscillations of local temperature have been observed in the left and right regions under a somewhat higher driving frequency [141].

The definition of local temperature based on the ZCC has the following advantages: (1) Recent theoretical research shows that the ZCC-defined T^* for a quantum system in steady state, arbitrarily far from equilibrium, with arbitrary interaction within the system, is unique when the solution of Eq. (22) exists [243]. (2) The ZCC reflects the zeroth law of thermodynamics because the nanosystem and the thermometer reach a local equilibrium state with no electron and energy exchange. As a result, the ZCC usually acts as a reference for other theoretical definitions.

Such a macroscopic definition of local temperature, however, does not reflect the microscopic change of the system state in a non-equilibrium situation and its experimental realization is not straightforward. For instance, the ZCC may appear to provide an operational definition with the aid of a non-invasive probe that can monitor the heat current through the probe-nanosystem coupling. This is, however, not the case. This is because it is difficult for present calorimeters to measure the heat current through a nanosized sample without the *a priori* knowledge of the local temperature of the sample, which defies the purpose. This issue will be discussed in detail in Sec. 3.

2.2.2. Definitions based on balance of local heat generation and dissipation

Chen *et al.* have suggested an alternative local equilibrium condition for nanoscale junctions [181]. The idea is that local thermal equilibrium is established when the local heating process within the nanojunction balances the local cooling due to heat dissipation into the environment. Assuming there is no inelastic electron-electron scattering, local ionic heating occurs in a nanoscale conductor when electrons release energy to the ions via inelastic scattering with phonons. Figure 8(a) shows the four main electron-phonon scattering processes which contribute to local heating of the junction. These scattering processes occur in the central region of the junction as well as within a few atomic layers of the bulk electrodes; see Fig. 8(b). Absorption and emission of energy through these scattering processes lead to the local heating and cooling effects, respectively;

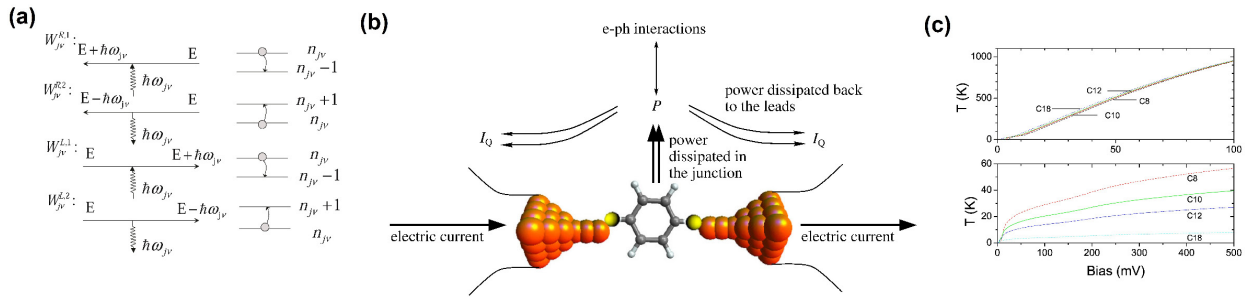


Figure 8: (a) Feynman diagrams of the four main electron-phonon scattering processes contributing to local heating of the junction. From top to bottom: (1) Cooling process due to absorption of a phonon from a left-moving electron; (2) heating process due to the emission of a phonon from a left-moving electron; (3) and (4) are the equivalent mechanisms corresponding to the right-moving electrons. Reprinted with permission from [181]. Copyright 2003 American Chemical Society. (b) A schematic representation of the mechanism of local ionic heating in nanoscale junctions. The thermal power generation P_{e-p} induced by the electric current is balanced by the heat dissipated into the electrodes $I_Q = J^{\text{out}} - J^{\text{in}}$. The balance between the thermal power in the junction and the heat current flowing out of the junction determines the local ionic temperature of the junction. Reprinted with permission from [144]. Copyright 2011 American Physical Society. (c) Local temperature calculated from DFT methods as a function of bias for various lengths of alkanethiols (color lines). Reprinted with permission from [244]. Copyright 2005 American Chemical Society.

Two scenarios have been considered in the literature [181]. In the first scenario, the central system is presumed to be thermally isolated from the environment and hence there is no heat current flow into the bulk electrodes. Consequently, local thermal equilibrium is reached when the local heating exactly cancels the local cooling by summing up the four electron-phonon scattering processes over all phonon modes in the central system. Such a balance of local

heating and cooling is expressed by [181, 244]

$$P_{\text{e-p}}(T^*) = \sum_{j,\nu} \left\{ W_{j\nu}^{R,2}(T^*) + W_{j\nu}^{L,2}(T^*) - W_{j\nu}^{R,1}(T^*) - W_{j\nu}^{L,1}(T^*) \right\} = 0. \quad (23)$$

Here, $P_{\text{e-p}}(T^*)$ is the thermal power generated within the central system due to electron-phonon interactions, $W_{j\nu}^{\alpha,k}$ is the contribution of ν th coordinate component ($\nu = x, y, z$) of the j th phonon mode to the junction thermal power, $\alpha = L, R$ represents the electrode from which the electron enters the junction, and $k = 1, 2$ indicates the phonon loses/gains energy. $W_{j\nu}^{\alpha,k}$ is a function of the local temperature T^* of the central system. This is because the value of $W_{j\nu}^{\alpha,k}$ depends on the occupation number of each phonon mode, $\langle n_{j\nu} \rangle = 1/(e^{E_{j\nu}/T^*} - 1)$ [245, 246]. The local temperature is thus determined by tuning the value of T^* until Eq. (23) holds.

In the second scenario, the energy stored locally in the junction is allowed to dissipate away into the bulk electrodes via elastic phonon scattering. Figure 8(b) shows the consequent thermal current J^{out} (denoted by I_Q in the figure) flowing into both the left and right electrodes with a background temperature T_0 . The heat is dissipated away into the bulk electrode at a rate of $J^{\text{out}} = \kappa_{\text{th}}(T^*)^4$, with κ_{th} being the bulk thermal conductance that can be estimated from a microscopic model [247]. The fourth power comes from the assumption of the bulk form of lattice heat conduction. If the electrodes are at a finite temperature ($T_0 > 0$), there is also a heat current flowing into the central system, *i.e.*, $J^{\text{in}} = \kappa_{\text{th}}T_0^4$. In this scenario, local thermal equilibrium is established when the thermal power generation $P_{\text{e-p}}$ balances the net heat flux [144]:

$$P_{\text{e-p}}(T^*) = J^{\text{out}} - J^{\text{in}} = \kappa_{\text{th}} \left[(T^*)^4 - T_0^4 \right]. \quad (24)$$

The local temperature T^* is determined by tuning T^* until Eq. (24) is satisfied.

Using Eq. (24), Chen *et al.* have studied the local temperature of alkanethiol chains of different lengths sandwiched between two electrodes [244]. The calculated T^* as a function of bias voltage are shown in Fig. 8(c). The results indicate that local temperature is considerably lowered by heat transfer into the electrodes even for relatively large biases. It was also found that the molecular length has an important effect on T^* when considering heat dissipation into the electrodes. Longer alkanethiols are more stable against current flow, which is consistent with experimental results on similar systems [248].

In real systems, the thermal power generation $P_{\text{e-p}}$ is a fraction of the total power of the entire circuit (nanojunction plus power source) [144]. The latter is given by $P = V_{\text{bias}}^2/R$, where V_{bias} is the bias voltage and R the junction resistance (assuming no resistance of the external circuit). A minimal bias V_c is necessary to excite the lowest-energy phonon mode of the nanostructure. $P_{\text{e-p}}$ can thus be estimated as

$$P_{\text{e-p}} = \Theta(V_{\text{bias}} - V_c) \alpha P = \Theta(V_{\text{bias}} - V_c) \left(\frac{\alpha}{R} \right) V_{\text{bias}}^2, \quad (25)$$

where $\Theta(x)$ is the Heaviside step function. The factor α describes the fraction of P dissipated into the ionic DOF of the junction due to electron-phonon interaction, and its value needs to be determined from a microscopic theory [249]. Combining Eq. (24) and Eq. (25) leads to [181]

$$(T^*)^4 = T_0^4 + \gamma_{\text{e-p}}^4 V_{\text{bias}}^2, \quad (26)$$

where $\gamma_{\text{e-p}} = \Theta(V_{\text{bias}} - V_c)(\alpha/R\kappa_{\text{th}})^{1/4}$ characterizes the contribution of the electron-phonon interaction to local ionic heating.

In the presence of electron-electron interactions, some part of the thermal power generated in the junction ends up heating the electrons [250], and that part of the power is no longer available to induce local ionic heating. This changes the balance of local heat generation and dissipation to the following form:

$$P_{\text{e-p}} - P_{\text{e-e}} = J^{\text{out}} - J^{\text{in}}. \quad (27)$$

In analogy to Eq. (26), the variation of local ionic temperature T^* with the bias voltage becomes [250, 251]

$$(T^*)^4 = T_0^4 + \gamma_{\text{e-p}}^4 V_{\text{bias}}^2 - \gamma_{\text{e-e}}^4 V_{\text{bias}}^4, \quad (28)$$

where γ_{e-e} describes the contribution of electron-electron interaction to local ionic heating. As the heated electrons carry energy away from the junction and eventually dissipate it to the bulk electrodes, the electron heating effect lowers the local temperature of the ions in the junction. Therefore, Eq. (28) also predicts a local ionic cooling with increasing bias, which has been observed in alkanedithiol stretching experiments using the MCBJ setup [175].

The method described above has the advantage of being able to treat realistic systems. However, it is not easily conducive to practical measurements. This is because tuning the temperature of a nanojunction implies that one has determined the local temperature prior to the temperature measurement. In addition, it is difficult to distinguish the thermal power $W_{jv}^{\alpha,k}$ for each scattering mechanism and to figure out how $W_{jv}^{\alpha,k}$ depends on T^* in practice.

2.2.3. Definitions based on thermodynamic relations

In classical thermodynamics, temperature measures the average kinetic energy of the particles in a system, $E_K = \frac{3}{2}k_B T$. Such a relation has been employed widely in molecular dynamics simulations [252–254]. In the framework of DFT, Ayers *et al.* have defined a local kinetic energy, $E_K[\Phi_{KS}[\rho]; \mathbf{r}]$, used to determine the local temperature $T^*(\mathbf{r})$ of the electron gas [255],

$$E_K[\Phi_{KS}[\rho]; \mathbf{r}] = \frac{3}{2}k_B T^*(\mathbf{r}). \quad (29)$$

Here, the determinantal Kohn-Sham wavefunction $\Phi_{KS}[\rho]$ describes a reference system with the electron density function $\rho(\mathbf{r})$. The validity of such a kinetic definition relies on the equipartition theorem, which is strictly proven only in the thermodynamic limit for systems whose energy is quadratic in the particle momenta [144].

To generalize the thermodynamic definition of Eq. (15) to a non-equilibrium nanosystem, various thermodynamic quantities, particularly the energy E_s and entropy S of the nanosystem, need to be properly defined within the framework of quantum mechanics. For a general dynamical variable \hat{O} , its expectation value has the form $O(t) = \langle \hat{O} \rangle = \text{tr}_s[\rho_s(t)\hat{O}]$. The energy $E_s(t)$ of the system at time t becomes

$$E_s(t) = \text{tr}_s[\rho_s(t)H_s]. \quad (30)$$

Although the definition of non-equilibrium entropy is still under debate [152–154], the von Neumann entropy has been widely used in the literature [149–151]. The von Neumann entropy of the system is defined as

$$S_{VN}(t) = -k_B \text{tr}_s[\rho_s(t) \ln \rho_s(t)], \quad (31)$$

where k_B is the Boltzmann’s constant. Clearly, both E_s and S_{VN} are functionals of ρ_s . Since Eqs. (30) and (31) extend the concept of energy and entropy to a time-dependent situation, a direct generalization of Eq. (15) is expressed by [149–151, 256–258]

$$T^*(t) = \left(\frac{\delta E_s(t)}{\delta S_{VN}(t)} \right)_{V,N}, \quad (32)$$

at a fixed “volume” V and “number of particles” N . However, it is not always clear how to define the volume V in generic quantum system, and the particle number N of many-body systems is not always a conserved quantity [151].

Di Ventra and Dubi have proposed an alternative definition based on thermodynamic relations [259]. They have defined a dynamical quantity, “information compressibility” $K_I(t)$, to characterize the ability of an open system to change its entropy in response to a variation of its energy as

$$K_I(t) = \frac{1}{k_B} \frac{\partial S_{VN}}{\partial t'} \left(\frac{\partial E_s}{\partial t'} \right)^{-1} \Big|_{t=t'}, \quad (33)$$

at the time t . Here, the energy E_s is given by Eq. (30) and the information entropy is the von Neumann one, S_{VN} . A theoretical analysis has shown that [259] for a two-level system coupled to external baths with different temperatures, the information compressibility K_I agrees exactly with the reciprocal of the local temperature $\beta^* \equiv 1/T^*$ measured at any given time by a weakly-coupled “temperature floating probe” [140], whose temperature is adjusted so that the system dynamics is minimally perturbed. The details of the latter approach to define a local temperature will be reviewed in Sec. 2.2.5.

Ali *et al.* have studied nonequilibrium thermodynamics of a single-particle quantum system in contact with a heat

bath [260]. Basic thermodynamic quantities, such as energy, entropy, and local temperature have been evaluated by Eqs. (30), (31), and (32), respectively. Referring to the definition of the Helmholtz free energy, the non-equilibrium free energy $F(t)$ has been defined as

$$F(t) = E_s(t) - T^*(t)S_{VN}(t). \quad (34)$$

Based on the non-equilibrium free energy $F(t)$, the non-equilibrium quantum thermodynamic work is defined, which is the time-dependent dissipative work done by the system, as the decrease of the non-equilibrium free energy of the system: $\delta W(t) = -dF(t)$. As a consequence of the first law of thermodynamics, the time-dependent heat $\delta Q(t)$ transferred into the system can be expressed by

$$\delta Q(t) = dE_s(t) + \delta W(t) = dE_s(t) - dF(t), \quad (35)$$

where $dE_s(t)$ is the change in the system energy during the non-equilibrium process.

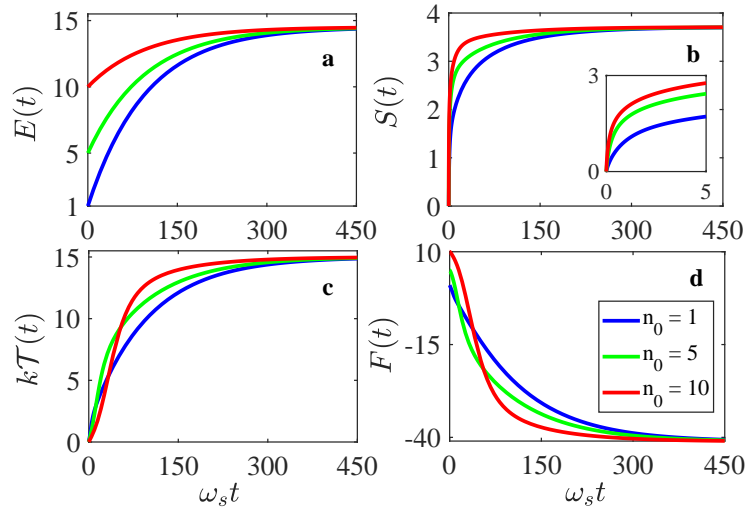


Figure 9: The non-equilibrium dynamics of the quantum system in terms of various thermodynamic quantities in the weak system-reservoir coupling regime with different initial states. Different colors represent initial states with system energy $E_0 = n_0 \omega_s$, $n_0 = 1, 5, 10$. (a) Internal energy; (b) Entropy; (c) Local temperature; (d) Free energy. Reproduced by permission of the authors of [260].

The above thermodynamic properties and the local temperature $T^*(t)$ have been applied to a single-mode photonic cavity in contact with a heat bath [260]. The frequency of the photon field in the cavity is denoted as ω_s . Initially, the system is assumed to be in the pure state with zero entropy at zero temperature, and the bath is at thermal equilibrium with a relative high temperature $k_B T_0 = 15 \omega_s$. Figure 9 shows the evolution of the above thermodynamic quantities in the weak-coupling regime for different initial states of the system with different energies. The entropy increases during the non-equilibrium processes. The increase of internal energy and the decrease of free energy amount to heat transfer into the system, resulting in the rise of the local temperature. Figure 9(c) clearly shows that the local temperature of the system becomes the same as the temperature of the reservoir. Therefore, the local temperature defined by Eq. (32) is physically meaningful because it coincides with the thermal equilibrium temperature when the system approaches the thermal equilibrium state with a reservoir in the weak-coupling regime. In the long-time limit, the free energy approaches a minimum value with maximum entropy in the equilibrium state.

The above analysis suggests that classical thermodynamic behaviors may emerge from quantum dynamics of a single-particle system in the weak system-reservoir coupling regime, without introducing any hypothesis on an equilibrium state. The main advantage of this approach is that a time-dependent local temperature is applicable to the real-time dynamics of nanosystems before the system approaches the steady state or thermal equilibrium. However, the thermodynamic relation-based definitions still face some challenges. For instance, from the theoretical point of view, the internal energy is a linear function of the reduced density matrix, while the entropy is a non-linear one [259]. Equation (32) may thus yield multiple values of local temperature at a specific time. In general, from the experimental

perspective, the practical implementation of, e.g., Eq. (32) requires the simultaneous measurement of the change in energy and entropy of the system. Although some efforts have been made to measure entropy in a nanosystem which consists of a few particles [261, 262, 262, 263], experimental measurement of energy change is a challenging problem, especially in a many-body system [264]. Therefore, it is not easy to realize the definition in practice, at least with the existing experimental techniques.

2.2.4. Definitions based on statistical relations

Since local temperature is closely related to a local Bose–Einstein distribution for bosonic systems (such as phonons) or a Fermi–Dirac distribution for fermionic systems (such as electrons), one can employ definitions based on local distribution functions [173, 265–267]. For an electronic system described by the Fermi–Dirac distribution, Pekola *et al.* have proposed a definition of T^* for spinless electrons in the normal-metal region of normal-metal-insulator-superconductor tunnel nanojunctions [173]. By using the Sommerfeld expansion, the local temperature is related to the thermal energy density of the electrons. In consideration of electron spin, Giazotto *et al.* [265] and Heikkilä *et al.* [266] have extended this definition to the spin-polarized tunneling junctions and the spin valve setups, respectively. In these works, a spin-dependent local temperature is defined as follows:

$$T_s^* = \frac{\sqrt{6}}{k_B \pi} \sqrt{\int_{-\infty}^{\infty} \{f_{\text{neq},s}(\epsilon) - [1 - \theta(\epsilon - \mu_s)]\} \epsilon d\epsilon}. \quad (36)$$

Here, μ_s is the electrochemical potential for the electrons in the normal-metal region, with $s = \uparrow (\downarrow)$ labeling the spin-up (spin-down) electrons, and $\theta(\epsilon - \mu_s)$ is the Heaviside step function. The spin-dependent non-equilibrium distribution function is expressed in terms of $f_{\text{neq},s} = n_{L,s} f_L + n_{R,s} f_R$, with $f_{\{L,R\}}$ the equilibrium Fermi–Dirac distribution and $n_{\{L,R\},s}$ the model-dependent weight coefficient of left/right leads [268, 269]. The term $1 - \theta(\epsilon - \mu_a)$ in Eq. (36) is equivalent to the equilibrium Fermi–Dirac distribution in the zero-temperature limit [265].

For a phonon system described by the Bose–Einstein distribution, Galperin *et al.* have proposed a definition of local temperature which directly compares the non-equilibrium local distribution function, f_{neq} , with an equilibrium one, $f_{\text{eq}}(E_a, T_a)$, with a given temperature T_a [267]. T^* is determined by varying T_a to give the best match. In short, the definition is expressed as

$$f_{\text{neq}}(\epsilon) \simeq f_{\text{eq}}(\epsilon, T^*). \quad (37)$$

The idea is to approximate f_{neq} by f_{eq} with a tunable local temperature T^* .

Galperin *et al.* have estimated the local phonon temperature as a function of voltage [267, 270] in a single-level model system coupled to one vibrational DOF. The system contacts with two leads which have the same temperature as that of the system (100 K) in the zero-bias limit. These authors have then compared the value of the local temperature defined by Eq. (37) with that defined by the ZCC. These two temperatures are termed $T^{*,BE}$ and $T^{*,ZCC}$, respectively, and are plotted in Figure 10.

The two definitions give similar values of local temperature at a large bias voltage, but $T^{*,BE}$ is substantially higher than $T^{*,ZCC}$ as the bias approaches zero. The ZCC gives a good estimation, while the equilibrium distribution-based definition produces an erroneous result. The reason for the deviation is that the equilibrium distribution function in Eq. (37) ignores the possible interaction between the phonon mode and the electrons in the molecule. The ZCC considers this contribution by coupling the whole molecule to an external probe, then adjusting the heat flux to zero. The agreement at a high voltage bias is partially an artifact of the single resonance level and/or the single vibrational mode model, whereby the results depend on properties of the phonon distribution at a relatively narrow frequency range and not on the full non-equilibrium distribution [270].

The above distribution-function-based definition of Eqs. (36) and (37) have the advantage that the local temperature is uniquely determined once the non-equilibrium distribution function is given. However, in principle, the validity of the two definitions requires that there is no significant difference between the non-equilibrium distribution function and an equilibrium one, namely, the nanosystem stays in a near-equilibrium state [271]. In addition, before the local temperature can be determined by using such definitions, one needs to know the non-equilibrium distribution function, while the values of T^* determined from different distribution functions may not agree with each other. Particularly, it is challenging for the definition of Eq. (36) to be applied to systems at a high temperature. This is because the Sommerfeld expansion is only valid for systems at sufficiently low temperatures.

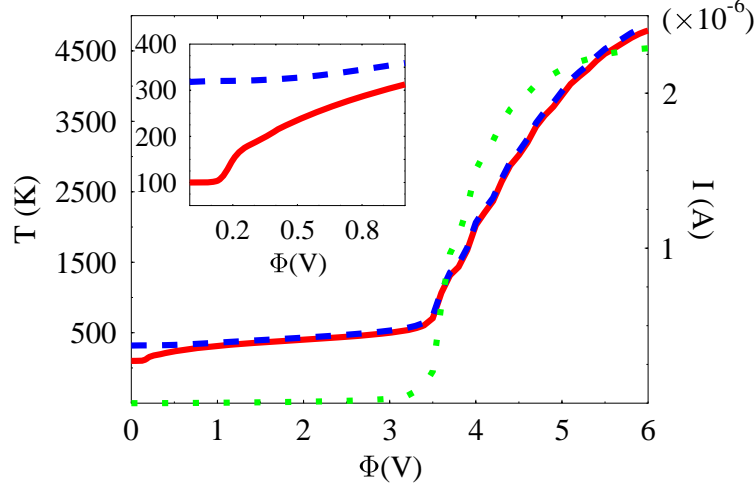


Figure 10: The local temperature $T^{*,BE}$ defined by the equilibrium distribution assumption, Eq. (37), (dashed line, blue) and $T^{*,ZCC}$ defined by the ZCC (solid line, red) plotted against the applied bias Φ , for a single-level model junction coupled to one vibrational DOF. The lead temperature is 100K. The inset shows the low bias region. The dotted line (green) shows the junction current (right vertical axis). $T^{*,ZCC}$ and $T^{*,BE}$ are the T_{th} and T_{BE} in the figure. Reprinted with permission from [270]. Copyright 2007 American Physical Society.

For the definitions of Eqs. (36) and (37), the key quantity, the non-equilibrium distribution function, is experimentally accessible at low temperature using the scanning tunneling spectroscopy [269, 272–274]. When a biased tunneling probe (such as the tip of an STM) approaches towards the surface of a sample, the electrons tunneling through the energy barrier between the sample and the probe produces a tunneling current. Since the tunneling current depends on the local electron distribution in the probe and at the coupled site of the sample, the local distribution function can be obtained by measuring the tunneling current [275] or the differential conductance [269] of the tunneling junction. This scanning tunneling technique has been applied to measure f_{neq} of electrons or quasi-particles which obey the Fermi–Dirac distribution in carbon nanotube junctions [276] and mesoscopic metallic wire junctions [277]. However, the technique is limited to nanoscale conductors because the tunneling barrier for an insulator is generally so high that electron tunneling is forbidden. Non-Fermi energy distributions could not be measured either [278].

Temperature not only determines the distribution function of a nanosystem, but also provides a measure of the magnitude of thermal fluctuations/excitations. The FDT connects the response of a system from a prepared non-equilibrium state to its statistical fluctuations at equilibrium [279]. However, when the system is far from equilibrium, for instance, driven by an external field, the detailed-balance relation may break down and the FDT does not hold exactly [280–284]. Nevertheless, an FDR between the response of a system in a non-equilibrium state to an external perturbation and the correlation functions computed in the unperturbed system, can still be derived for a large number of systems [139], from which a local temperature can be extracted.

Arrachea and Cugliandolo have developed a local FDR involving single-particle Green’s functions for a mesoscopic metallic ring driven by a time-dependent magnetic field and coupled to an electron reservoir [285]. Performing the Fourier transform for the Green’s function $G_{ij}^K(t, t')$ with respect to $\tau \equiv (t - t')$, the FDT for electrons at equilibrium reads [194]

$$G_{ij}^K(t, \omega) = \tanh\left(\frac{\beta\omega}{2}\right)[G_{ij}^r(t, \omega) - G_{ij}^a(t, \omega)], \quad (38)$$

where $G_{ij}^{K,a,r}$ are the causal, advanced and retarded Green’s functions; i and j label the site of the nanosystem (G^K was named Keldysh Green’s function in [285]). To extend Eq. (38) to a nanosystem driven out of equilibrium, the background temperature T (or $\beta = 1/T$) in the r.h.s. of Eq. (38) has been replaced by another parameter T' . Comparing the left and right hand sides of the inverse Fourier transform of Eq. (38) averaged over time t , these authors have adjusted T' such that the two sides of Eq. (38) fit with each other. This leads to a modification of the FDR for a non-equilibrium nanosystem by defining the local temperature $T^* = T'$ for such a system.

Caso *et al.* have formulated a similar modified FDR for a nanosystem driven by electrical fields, already shown in

Figure 7 [141, 142]. The local temperature can be extracted from the following equation [141, 142]

$$iG_{ll}^K(0, \omega) - iG_{ll}^K(0, \mu) = \tanh \left[\beta_l^* \left(\frac{\omega - \mu}{2} \right) \right] \bar{\varphi}_l(\omega), \quad (39)$$

for the site l of the system. Here, $\bar{\varphi}_l^*(\omega) = -2\text{Im}G_{ll}^r(0, \omega)$ and $G_{ll}^{K,r}(0, \omega)$ are the causal and retarded Green's functions, respectively, for the site l at time $t = 0$. The zero-time condition arises from the assumption that in the weak-driving adiabatic regime the driving frequency Ω_0 is much smaller than the inverse of the dwell time of the electrons within the central system, and the external field is treated as a perturbation [141, 142]. However, the local temperatures defined by Eqs. (38) and (39) are not directly accessible experimentally, because the Green's function is difficult to be directly measured in practice [285].

To find an experimentally feasible definition, an FDR has been developed in the framework of current-current correlation functions [174]

$$iC_{\alpha\alpha}^K(0, \omega) = \coth \left[\beta_\alpha^* \left(\frac{\omega}{2} \right) \right] \bar{\varphi}_\alpha^*(\omega), \quad (40)$$

where $\bar{\varphi}_\alpha^* = -2\text{Im}C_{\alpha\alpha}^R(0, \omega)$ and $C_{\alpha\alpha}^{K,R}(0, \omega)$ are causal and retarded current-current correlation functions for currents through the reservoir α at time $t = 0$. Compared with the Green's function involved in the definitions of Eqs. (38) and (39), current-current correlation functions are related to noise which is measurable in practice [286]. Therefore, Eq. (40) provides, in principle, an experimentally-accessible definition [287].

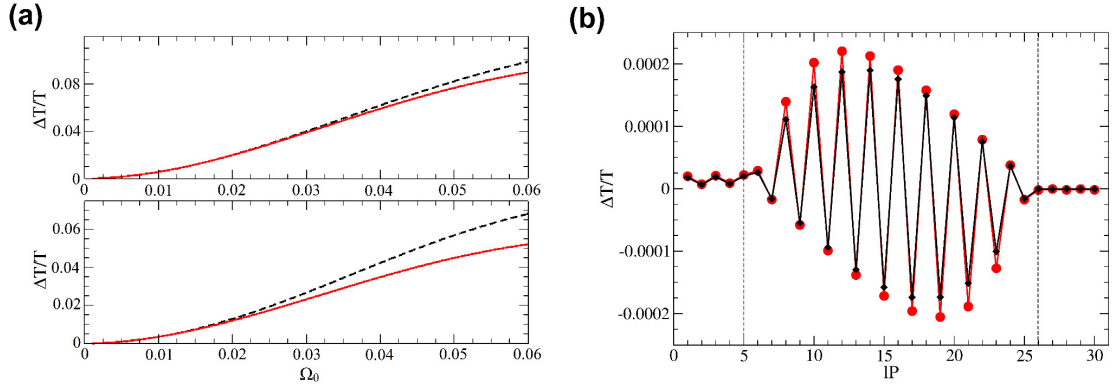


Figure 11: (a) Local temperature differences ΔT^{ZCC} (dashed black) and ΔT^{FDR} (solid red), relative to the temperature T of the reservoirs, $\Delta T/T$, for the site $l = 0$ connected to the left reservoir as a function of driving frequency Ω_0 , for the system depicted in Figure 7(a). The upper and lower panels correspond to $T = 0.016$ and $T = 0.005$, respectively. (b) Local temperature differences ΔT^{ZCC} (black diamonds) and ΔT^{FDR} (red circles) along a one-dimensional nanowire model system of $N = 30$ sites with two ac fields operating with a phase lag of $\delta = \pi/2$ at the positions indicated by dotted lines. Reprinted with permission from [174]. Copyright 2012 Springer Nature.

Caso *et al.* have compared the value of the ZCC-defined local temperature $T^{*,ZCC}$ and that of the local temperature $T^{*,FDR}$ defined by Eq. (40) in a one-dimensional model nanosystem [174]. The system is shown in Figure 7(a). Figure 11(a) shows ΔT^{FDR} and ΔT^{ZCC} calculated for the site $l = 0$ connected to the left reservoir, as a function of the driving frequency Ω_0 . Here, $\Delta T^{FDR} = T_l^{*,FDR} - T$ and $\Delta T^{ZCC} = T_l^{*,ZCC} - T$ are the differences between the temperature T of the reservoir and two local temperatures, respectively. The two local temperatures $T_l^{*,FDR}$ and $T_l^{*,ZCC}$ coincide with each other at a low frequency Ω_0 . As T increases, the region in which the two definitions agree quantitatively becomes broader; see the upper panel of Figure 11(a). Figure 11(b) exhibits a good agreement between the two local temperatures along the whole nanostructure, and an almost perfect agreement within the left and right regions. The Friedel-like oscillations appear in the central region. The local temperature oscillations here have the same microscopic origin as that of the temperature oscillations discussed in Sec. 2.2.1.

Similar to the equilibrium distribution definition, the FDR-based definition generalizes a statistical property established at equilibrium to the non-equilibrium situation by defining a local temperature. However, limited by the weak-driving adiabatic assumption, this definition is valid for near-equilibrium systems with slow dynamics. Nonetheless,

in view of the experimental developments of measuring current-current correlations and low-frequency noise (see, e.g., [286]), these definitions are experimentally conducive to the study of local temperatures in realistic nanosystems.

2.2.5. Definitions based on minimal perturbation condition

Dubi and Di Ventra have proposed an operational method to determine T^* by mimicking a probe-based thermometer technique [140]. The method is described as follows. As shown in Figure 6, one couples a thermal probe with temperature T_p to a local site of a nanosystem. Due to the interaction between the probe and the coupled site, the system dynamics is generally modified. Consequently, the QME of the system reduced density matrix ρ_s reads

$$\dot{\rho}_s = -i[H_s, \rho_s] + \mathcal{R}_{\text{env}}\rho_s + \mathcal{R}_{\text{probe}}(T_p)\rho_s, \quad (41)$$

where H_s is the system Hamiltonian, \mathcal{R}_{env} is a superoperator that represents the dissipative interactions between the system and its environment, and the temperature-dependent superoperator $\mathcal{R}_{\text{probe}}(T_p)$ corresponds to the influence of the thermal probe, with temperature T_p , on the microscopic states of the system. Then the temperature T_p is varied (or “floated” as discussed in their work) so that the perturbation on some local or global properties of the nanosystem is minimized (ideally to zero), and a local temperature is determined as $T^* = T_p$. This minimal perturbation condition (MPC), also named as the “temperature floating-probe method”, reads

$$\mathcal{R}_{\text{probe}}(T^*)\rho_s = 0. \quad (42)$$

Based on the MPC-based definition of local temperature, the temperature profile has been calculated for a one-dimensional model nanosystem [140]; see Figure 12(a). Figure 12(b) plots the local temperature at steady state for three different values of the lead-wire coupling strength g . At a weak coupling of $g = 0.01$, the temperature inside the wire is very low, but a “hot spot” develops in the cold lead. As g increases the hot spot vanishes and temperature oscillations emerge in the wire. At a strong coupling of $g = 0.8$, the temperature distribution along the system is uniform, and the wire equilibrates at a temperature that is roughly the average of T_L and T_R .

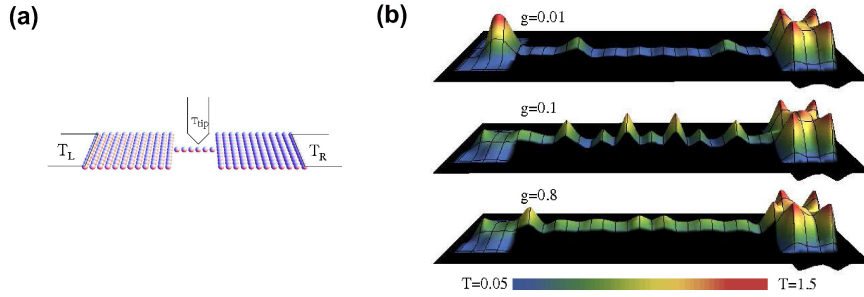


Figure 12: (a) Schematic representation of the calculation to determine the local temperature via the addition of a probe. A nanowire is coupled to the left and right leads with coupling strength g . The solid lines at the edges correspond to the contact area between the leads and the thermal baths at temperatures T_L and T_R , respectively. The T_{tip} represents the temperature of the probe. The left and right leads have the same chemical potential. (b) The local temperature along the nanostructure for three different values of the lead-wire coupling, $g = 0.01, 0.1, 0.8$. Three effects are observed: a hot spot in the cold lead at small coupling, temperature oscillations in the wire at intermediate coupling, and uniform temperature along the wire at large coupling. Reprinted with permission from [140]. Copyright 2009 American Chemical Society.

In its original formulation, the MPC approach of Eq. (42) only considered the energy exchange between probe and nanosystem, while particle transfer was excluded. This is a strong limitation, particularly for the studies of current-carrying nanoelectronic devices subjected to bias voltages. In order to overcome this limitation, Ye *et al.* have modified the original formulation of the MPC [182]. Another key quantity, the local electrochemical potential μ_p of the probe, was introduced; and the MPC was imposed on the expectation value of a specific system observable \hat{O} .

The modified MPC definition is described as follows. One varies T_p and μ_p , until the electric current I_p through the

probe vanishes and simultaneously the probe-induced perturbation $\delta O_p(T_p, \mu_p)$ on the observable \hat{O} gets minimized:

$$\begin{cases} I_p|_{T_p=T^*, \mu_p=\mu^*} = 0, \\ T^* = \arg \min_{T_p} \{\delta O_p(T_p, \mu^*)\}. \end{cases} \quad (43)$$

When Eq. (43) is satisfied, there is no particle exchange between the probe and the nanosystem, and the probe influence on the system is minimized (ideally to zero). This suggests that the system locally equilibrates with the probe to some degree. Therefore, this definition can be referred to as a “local-equilibrium condition” and be somewhat understood from the zeroth law of thermodynamics.

Particularly, when a nanosystem is connected to two leads, L and R , and under a voltage bias $V = \mu_R - \mu_L$, a convenient approximation for the local electrochemical potential μ_p is determined by a linear combination

$$\mu^* \simeq \zeta_L \mu_L + \zeta_R \mu_R. \quad (44)$$

Then the local temperature T^* is measured by varying T_p , with μ_p fixed at the value given by Eq. (44)

$$\delta O_p(T_p, \mu_p) = [\zeta_L O_p(T_L, \mu_L) + \zeta_R O_p(T_R, \mu_R)] - O_p(T_p, \mu_p). \quad (45)$$

Here, $O_p(T_p = T_\alpha, \mu_p = \mu_\alpha)$ denotes the local observable $\langle \hat{O} \rangle$ measured by setting the electrochemical potential and temperature of the probe to be identical with those of the leads $\alpha = L, R$. The subscript P represents the presence of the probe. The weight coefficients ζ_L and ζ_R in Eqs. (44) and (45) are determined by

$$\zeta_\alpha = 1 - \frac{I_p(T_\alpha, \mu_\alpha)}{I_p(T_L, \mu_L) + I_p(T_R, \mu_R)}. \quad (46)$$

Equations (44) and (46) are the result of the conservation of particle number in the system [182].

Ye *et al.* have utilized the MPC approach to a QD system described by a single impurity Anderson model [52], and have compared the value of the MPC-defined $T^{*,MPC}$ with the ZCC-defined $T^{*,ZCC}$ under the same situation [182]. To test the robustness of $T^{*,MPC}$ with respect to the choice of observables, two properties that are particularly sensitive to temperature variations have been chosen to impose the MPC: the local magnetic susceptibility $\chi^m = \frac{\partial \langle \hat{m}_z \rangle}{\partial H_z}|_{H_z \rightarrow 0}$ and the global spin-polarized current $I_\alpha^m = \langle \hat{I}_{\alpha\uparrow}^m \rangle - \langle \hat{I}_{\alpha\downarrow}^m \rangle$ through the lead α . Here, \hat{m}_z is the dot magnetization operator due to the dot spin polarization, H_z is the magnetic field, and $\hat{I}_{\alpha s}^m$ is the electric current operator for spin- s .

The results in Figure 13 show a remarkable agreement with the local temperature T^* determined by the minimal perturbation of either I_α^m or χ^m , thus confirming its robustness with respect to the choice of observables. Figure 13(a) and (b) illustrate that the MPC-defined $T^{*,MPC}$ also agrees closely and consistently with that obtained with $T^{*,ZCC}$ in a large range of background temperatures. This is because the electric and heat currents flowing into the probe are both close to zero when the minimal perturbation is satisfied. This result numerically confirms the notion that the MPC can be referred to as a local equilibrium condition to some degree.

Although the Kondo effect is evident from the inset of Figure 13(b), which shows that the QD exhibits more prominent Kondo features when T is low (as confirmed by the higher and sharper Kondo peak centered at $\omega = \mu$), the MPC definition applies equally well for a QD system from non-interacting to the Kondo-correlated regime. These results highlight the generality of the MPC.

In contrast to the ZCC-based definitions, the MPC method relies on the measurement of local (or semilocal) observables, instead of the heat current through the probe. Therefore, one of the advantages of the MPC method is that it offers an operational protocol for local temperature measurement that is feasible for experimental implementations.

2.3. Uniqueness/non-uniqueness of local temperature out of equilibrium

In principle, for systems at a global equilibrium state, the value of temperature should be uniquely determined by any thermometer or by any theoretical definition that is physically sound. Let us instead discuss the uniqueness of the values of local temperature for systems out of equilibrium. Ideally, the various definitions should produce the same (or at least similar) values of local temperature for a given system under a given non-equilibrium condition. For macroscopic systems out of equilibrium, it has been shown that different definitions give the same temperature as long

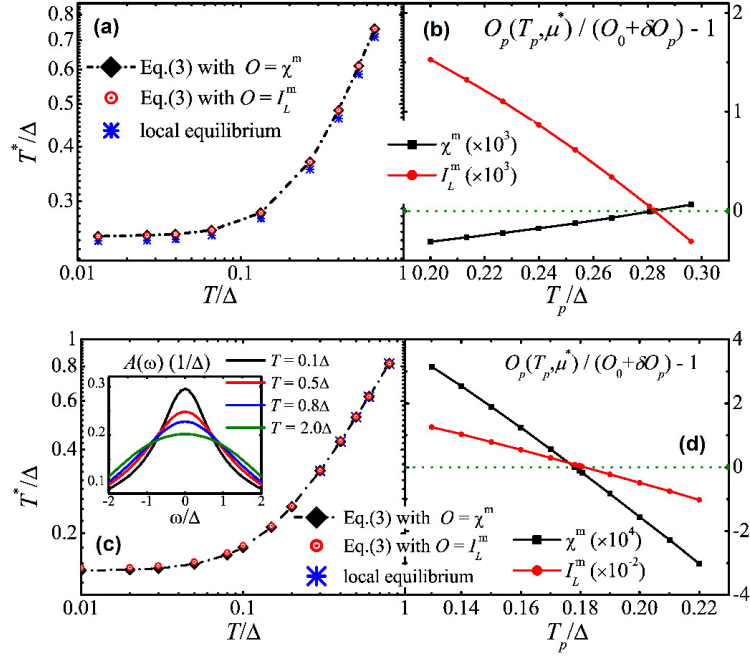


Figure 13: Local temperature T^* of a single-level QD determined by different protocols versus background T . (a) A noninteracting QD without electron-electron Coulomb interactions; (b) An interacting QD with electron-electron Coulomb interactions; The inset shows the Kondo spectral peak of the dot at various T . (c) and (d) are variations δO_p of system observables χ^m (local magnetic susceptibility) and I_α^m (global spin-polarized current) with μ^* determined for a noninteracting/interacting QD, respectively. Reprinted with permission from [182]. Copyright 2015 American Physical Society.

as the local equilibrium condition is satisfied [138]. However, the situation is more complicated for nanosystems out of equilibrium.

Summarizing the various definitions of local temperature that have been introduced in this section, we indeed find that they yield similar quantitative results in many cases. For instance, it has been shown analytically in [259] that for a two-level system, the $T^{*,MPC}$ determined by imposing the MPC condition on the reduced density matrix is exactly equivalent to T^* defined based on the thermodynamic-type relation of Eq. (33). By performing numerical calculations on QDs under low temperatures, Ye *et al.* [182] have shown that the $T^{*,MPC}$ extracted from the local magnetic susceptibility or spin-polarized current agrees closely with $T^{*,ZCC}$ in a wide range of temperatures, even in the presence of strong electron correlations; see Figure 13. As for $T^{*,BE}$ reviewed in Sec. 2.2.4, a numerical analysis has shown that $T^{*,ZCC}$ coincides with $T^{*,BE}$ in a single-level nanosystem subjected to a high bias voltage.

Caso *et al.* have compared the difference between the $T^{*,FDR}$ and $T^{*,ZCC}$. It has been shown analytically that the $T^{*,FDR}$ determined by the single-particle Green's functions is in good agreement with the $T^{*,ZCC}$ at a low background temperature and in the weak-driving regime [141, 142]. For the $T^{*,FDR}$ derived from the current-current correlation function, the correlation functions involve the equilibrium Fermi-Dirac function f_p , and thus depend on the temperature T_p and the electrochemical potential μ_p of the probe. To clarify the influence of such dependency on the value of local temperature defined by FDR, three different choices of T_p and μ_p have been considered [174]. In the first choice (Case I), μ_p is considered to be equal to the reservoir electrochemical potential μ , and T_p is equal to the local temperature $T_l^{*,ZCC}$. The second choice (Case II) also considers $\mu_p = \mu$, but $T_p = T_l^{*,FDR}$. In the third choice (Case III), $T_p = T_l^{*,FDR}$ is adopted, while $\mu_p = \mu_l^{*,ZCC}$ (the ZCC-defined local electrochemical potential for site l). Figure 14 shows that the local temperatures $T^{*,FDR}$ and $T^{*,ZCC}$ calculated for the above three cases agree well with each other in the slow-driving regime. When the driving frequency Ω_0 is further reduced, the differences among the values of local temperatures determined by different definitions become vanishingly small. Conspicuous deviations only emerge in the high-frequency region.

The above results confirm that in near-equilibrium nanosystems, such as the systems subjected to slow driving

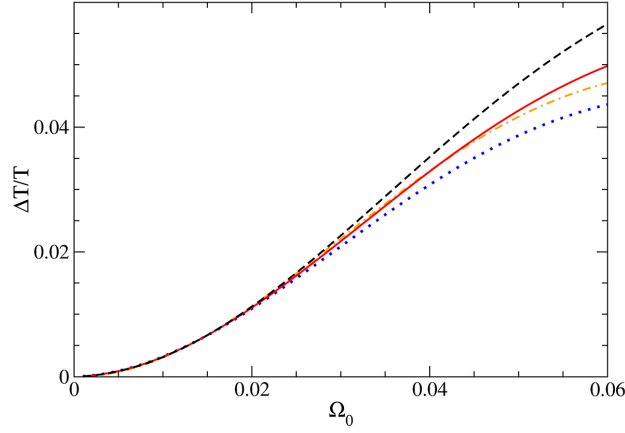


Figure 14: Local temperature differences $\Delta T^{*,ZCC}$ (dashed black) and $\Delta T^{*,FDR}$ for Case I (solid red), Case II (dotted blue) and Case III (dashed and dotted orange), relative to the temperature T of the reservoirs, for the site connected to the left reservoir as a function of driving frequency Ω_0 (see the main text for a detailed explanation of the three cases). Reprinted with permission from [174]. Copyright 2012 Springer Nature.

fields or low biases, the local temperatures determined by different definitions agree quantitatively with each other. This is consistent with the intuition that the local temperature should inherit all the physical implications of the conventional concept of temperature, if the local system can be properly described by a local equilibrium approximation. Moreover, it is remarkable that for certain systems subjected to rather large biases or involving strongly correlated states, such as the systems studied in Figure 10 and Figure 13, the different definitions of local temperature still yield similar values. This suggests that the physical considerations behind these definitions are somewhat universal and may remain valid even in the far-from-equilibrium or quantum regime.

Of course, in some circumstances the local temperatures resulted from different definitions may differ distinctly from one another. The reason is mainly twofold. First, in a general non-equilibrium situation, the various physical implications of the concept of temperature (as presented in Sec. 1.3) may become independent of each other. For instance, it is difficult to define a unique local temperature if nonlocal excitations emerge in the system [183]. Second, the practical implementation of a theoretical definition may involve non-universal approximation or parametrization procedure. For example, as shown in Figure 14, the value of $T^{*,FDR}$ relies heavily on the specific choice of the temperature or electrochemical potential of the probe in the fast-driving regime [174].

Ye *et al.* have compared the calculated $T^{*,MPC}$ and $T^{*,ZCC}$ of QDs [183]. Under a low background temperature, the local excitations on the QD are dominated by the scattering events and correlation effects among electrons, while the phonon modes are not promoted. Figure 15(a) shows the $T^{*,MPC}$ as a function of energy level ϵ_d for a non-interacting QD and Figure 15(c) shows $T^{*,ZCC}$ as a function of Coulomb interaction energy U for an interacting QD. In a non-interacting QD, the ZCC predicts an almost constant $T^{*,ZCC}$ over a large range of ϵ_d . In contrast, the MPC results in a conspicuous fluctuation of $T^{*,MPC}$ around $\epsilon_d = -0.7\Delta$, where the magnitude of $T^{*,MPC}$ differs significantly from $T^{*,ZCC}$. The vertical lines mark the three distinct regions. The three regions of $T^{*,MPC}$ have also been observed in an interacting QD, while the change in $T^{*,ZCC}$ is negligibly small with increasing U .

The existence of the three distinct regions can be explained by the changes in peak positions of the spectral function $A(\omega)$, as shown in Figure 15(b) and (d). With increasing ϵ_d or U , the spectral peak gradually approaches the thermal activation window. As a result, the dot-lead resonances become stronger, and long-range nonlocal excitations emerge in the system. For a dot in the region I of Figure 15 the dot level is off-resonant with the lead states. The electronic excitations are largely local on the dot, and $T^{*,ZCC}$ precisely captures the magnitude of these local excitations. In contrast, for a dot in the regions II and III, the spectral peak approaches towards, and finally enters into the thermal activation window. Electronic excitations can then occur inside the leads to create hot electrons (holes) above (below) the Fermi energy. Such excitations are hence nonlocal. In particular, Figure 15(a) and (c) illustrate that, for a dot in the region II where both local and nonlocal excitations take place, the $T^{*,MPC}$ effectively characterizes the magnitude of the nonlocal excitations, while $T^{*,ZCC}$ does not.

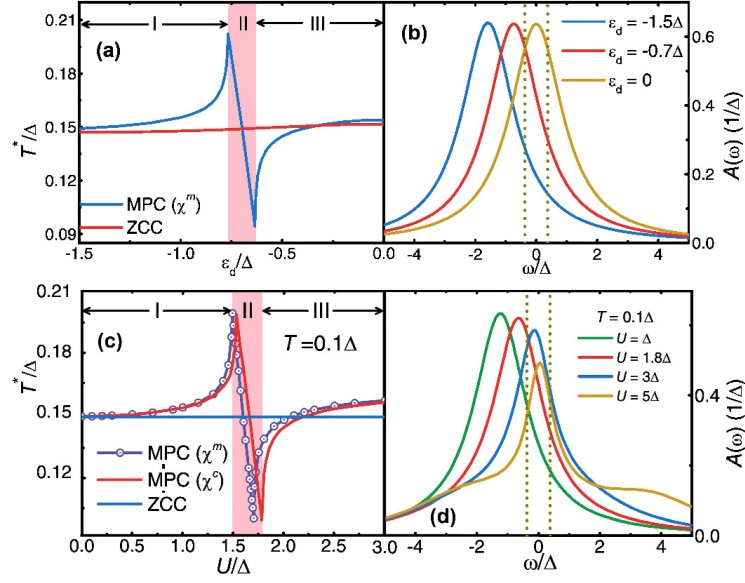


Figure 15: (a) Calculated T^* versus single-particle energy level, ϵ_d , for a noninteracting QD under a bias voltage V ; (b) Dot spectral function $A(\omega)$ for different ϵ_d ; (c) Calculated T^* versus interaction strength, U , for an interacting QD under a bias voltage V ; (d) Dot spectral function $A(\omega)$ of a non-equilibrium QD with varying U . The region between the two vertical dot lines in (c) is the excitation window in which the dot level is strongly resonant with the lead states. Reprinted with permission from [183]. Copyright 2016 American Physical Society.

3. Experimental measurement of non-equilibrium local temperatures

3.1. Experimental strategies to measure the local temperature

A variety of experimental strategies for measuring the local temperatures of non-equilibrium nanosystems have been proposed. Like the theoretical definitions of local temperature reviewed in Sec. 2, the existing experimental efforts on local temperature measurement can also be ascribed to three general categories.

First, from the thermodynamical point of view, the local temperature can be determined by monitoring local equilibration of energy and particles within a non-equilibrium nanosystem. According to the ZCC-based definition reviewed in Sec. 2.2.1, the fulfillment of the local equilibrium condition can be examined by probing the particle and heat currents flowing through a probe which is weakly coupled to the nanosystem; see Eq. (22). However, it is worth pointing out that, while the particle current (such as the electric current) through a nanostructure can be measured directly with a high-precision instrument (such as an ammeter) [288], the measurement of heat current at the nanoscale is much less straightforward and more challenging. Because of its importance for characterizing the thermal properties of nanomaterials, as well as its close connection to the measurement of local temperature, we shall briefly review the development of nanocalorimetry in Sec. 3.2, and discuss its relevance to the local temperature measurements. We will then review the experimental progress on local temperature measurements on current-carrying nanosystems with the use of MCBJ setups in Sec. 3.3.1.

Second, from the statistical perspective, the local temperature determines the distribution of particles among the microscopic states of a nanosystem. For instance, as discussed in Sec. 2.2.4, the local distribution of electrons in a nanowire has been obtained by measuring the tunneling current or differential conductance between the nanowire and a biased probe [269, 275]. Alternatively, the local distribution function can be extracted from the fluctuation-dissipation relations by exploring the statistical features of measured local physical observables (such as the shot noise spectra) [286, 289, 290]. Moreover, the deviation of local temperature from the background temperature reveals how the magnitude of local excitations/fluctuations in a non-equilibrium system differs from the thermal equilibrium situation. Experimentally, the local excitations/fluctuations can be probed by spectroscopic techniques which monitor the scattering processes between the nanosystem and incident particles (such as photons or electrons). In spectroscopy experiments, the local distribution of particles and the magnitude of local excitations can be characterized and quantified by the line shapes of the measured spectra. Particularly, with a spectroscopy measurement, it is possible to

extract both the local phonon temperature (T_{ph}^*) and local electron temperature (T_e^*) which are distinctly different in a non-equilibrium nanosystem [176]. In Sec. 3.3.2 we will review the spectroscopic techniques for local temperature measurement.

Third, the temperature of a local region of a nanostructure or material can be measured by nano-sized thermometers which are fabricated through the miniaturization of conventional thermometers. The nano-sized thermometers include thermal sensors or probes as their key components. Thus, they are capable of detecting thermally sensitive properties or behaviors within the studied local region, such as thermovoltage due to the Seebeck effect [291, 292], change of electric resistance [293, 294], thermal expansion due to local heating [79], etc. In practice, a nano-sized thermometer can be mounted on or integrated into the atomically sharp tip of a STM or AFM to form a scanning thermal microscopy (SThM). Nanoscopic thermal imaging techniques can then be realized based on the SThM apparatus [295, 296], which enables a non-invasive measurement of the temperature field of nanostructures under applied bias voltage or thermal gradient. In Sec. 3.3.3 we will review the SThM techniques.

The following subsections will cover the working principles and practical implementations of the experimental techniques mentioned above. The advantages and limitations of these techniques will be analyzed. At the end of this section, we will relate the existing experimental strategies for local temperature measurement to the theoretical definitions presented in Sec. 2.

Before going to the next subsection, we shall mention that the term “effective temperature” (T_{eff}) is often adopted in the literature (experimental works particularly). In this section, any experimentally measured T_{eff} is regarded as a “physical” temperature as long as it has certain characteristics of the thermodynamical temperature.

3.2. Measurement of heat current at the nanoscale

3.2.1. General principle of nanocalorimetric techniques

Calorimetry at the nanoscale has developed into a crucial and useful technique for quantifying the generation, dissipation and transport of heat in a nanosystem. Recent advancement in the experimental instruments and operational protocols has enabled the measurement of heat flow through nano-devices with a resolution of picowatts [297–302]. Presently, the calorimeters have been applied to monitor cellular activities [303, 304]; and to study radiative heat transfer [305–310], thermal conductivity of nanostructures [311–315], and phase transitions of nanomaterials [316].

To explain the working principle of a nanocalorimeter and elucidate its relation to the local temperature measurement, we consider the nano-contact between a non-equilibrium nanosystem (with a local temperature T^*) and a probe (with a background temperature T_p). As discussed in the paragraph after Eqs. (20) and (21), in the absence of electric current and considering only the linear response, the heat current flowing into the probe through the nano-contact (J_p) follows the Fourier’s law [144, 317] of

$$J_p = -\kappa \Delta T. \quad (47)$$

Here, κ is the thermal conductance of the nano-contact. From Eq. (47), the magnitude of the heat current J_p can be deduced from the preset or measured thermal gradient $\Delta T = T_p - T^*$ (or vice versa) provided that κ is known.

In the following, we will focus on two types of nanocalorimeters that are widely used in current experimental studies: the bimaterial cantilever-based calorimeters and the resistance-based calorimeters. The readers may refer to [316, 318, 319] for other types of nanocalorimeters.

3.2.2. Bimaterial cantilever-based calorimeters

In this subsection, the voltage bias across a sample is left out of consideration, and temperature gradient is the only force to drive the heat flow from the hot side of the sample to the cold side. The heat flow J leads to heating in the cold side, and in experiments it is generally quantified by the thermal power P , the amount of incident thermal energy per unit time, *i.e.*, $J = P$. The Fourier’s law of Eq. (47) is always considered valid.

The design and implementation of the bimaterial cantilever-based calorimeter was pioneered by Gimzewski and co-workers [297, 320]. They have demonstrated a calorimetric technique with a sensitivity to heat flux of 1 nW, and measured the heat generation of the catalytic conversion of hydrogen and oxygen to form water over a platinum surface [297, 320]. The same device has been used for measurements of photothermal power with a resolution of 100 pW [321, 322]. Figure 16(a) illustrates the working principle of the cantilever-based calorimeter. The incident heat current (or thermal power) results in a deflection of the cantilever due to the mismatch in thermal expansion of

the two beam materials. The cantilever deflection can be detected and measured by optical means, from which the temperature profile along the cantilever can be deduced.

Assuming that temperature is constant at any cross section of the cantilever, the relation between the cantilever deflection and temperature profile is described by [323]

$$\frac{d^2\delta}{dx^2} = 6(\alpha_1 - \alpha_2) \frac{t_1 + t_2}{t_2^2 K} \Delta T(x). \quad (48)$$

Here, $\delta(x)$ is the vertical deflection of the cantilever at position x along its length L , $\Delta T(x)$ is the change of local temperature at x with respect to the ambient temperature T_0 , t_i (α_i) is the thickness (thermal expansion coefficient) of the i th layer ($i = 1, 2$) of the beam, and K is a constant determined by the thicknesses and Young's moduli of the two beam materials.

If the thermal power P is fed to the loose end of the cantilever, such as by a laser beam, the temperature profile along the cantilever $\Delta T(x)$ can be evaluated via the Fourier's law as

$$\Delta T(x) = \frac{P}{w(\kappa_1 t_1 + \kappa_2 t_2)} x, \quad (49)$$

where κ_i is the thermal conductivity of the i th layer and w is the cantilever width. It is assumed that most of the heat absorbed by the cantilever is finally conducted into the bulk reservoir at temperature T_0 through the fixed end, and the heat dissipation through air is negligible. The cantilever deflection at the free end of the cantilever can be obtained by solving Eq.(48) as [322]

$$\delta(x = L) = 2(\alpha_1 - \alpha_2) \frac{t_1 + t_2}{t_2^2 K} \frac{L^3 P}{w(\kappa_1 t_1 + \kappa_2 t_2)}. \quad (50)$$

Based on Eq. (49) and Eq. (50), the temperature profile $\Delta T(x)$ and the incident heat current $J = P$ are determined simultaneously once $\delta(x = L)$ is measured.

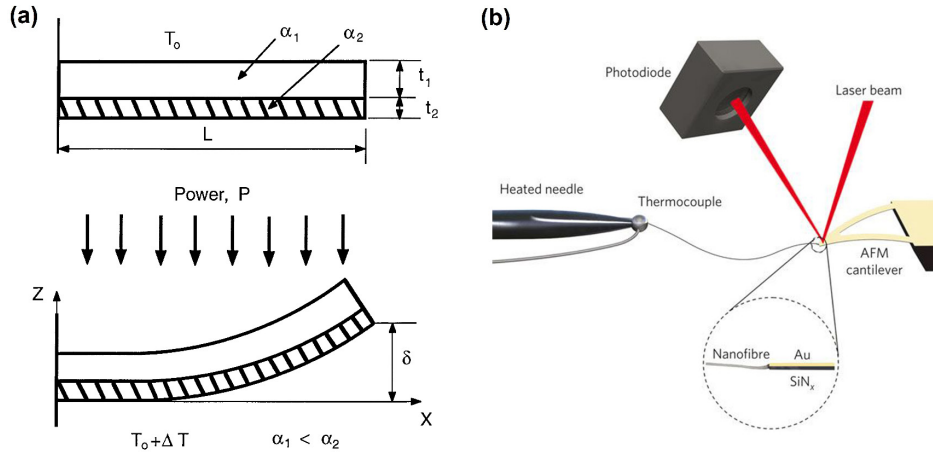


Figure 16: (a) Schematic illustration of a bimaterial cantilever beam heated uniformly by an incident thermal flux P . One end of the cantilever is connected to a bulk reservoir of ambient temperature T_0 , while the other end experiences a deflection due to the unbalanced thermal expansion of the two beam materials. The meanings of the symbols are explained in the main text. Reprinted with permission from [324]. Copyright 1997 Elsevier. (b) An AFM setup which includes a bimaterial cantilever-based calorimeter for the measurement of heat transport through one-dimensional nanosystems. In the depicted setup, a nanofibre connects the bimaterial cantilever to a thermocouple. The deflection of the cantilever is measured by focusing a laser beam onto the cantilever and receiving the reflected beam with a photodetector. Reprinted with permission from [325]. Copyright 2010 Springer Nature.

Figure 16(b) depicts an experimental setup in which the bimaterial cantilever-based calorimeter is integrated into an AFM. Such a setup has been employed to study thermal transport in one-dimensional nanosystems [325]. As shown in Fig. 16(b), a nanofibre connects the bimaterial cantilever to a micro thermocouple. The temperature of the

thermocouple can be adjusted to create a thermal gradient across the cantilever, and the deflection of the cantilever is measured by focusing a laser beam onto the cantilever and receiving the reflected beam with a photodetector. Note that the heat current reaching the cantilever (J_c) consists of two components: the heat conducted through the nanofibre (J_n) and the heat generated by the laser beam (J_l). Since J_l is controllable (by tuning the laser intensity) and J_c is measurable from the cantilever deflection via Eq. (50), the heat current through the nanofibre can be determined as $J_n = J_c - J_l$.

Using the setup of Fig. 16(b), Shen *et al.* have measured the thermal conductivity of polyethylene nanofibres [325]. They kept the laser power J_l constant and changed the temperature of the thermocouple from T_a to T_b (here a and b label two different temperatures). As a result, the heat conducted through the nanofibre varies from $J_{n,a}$ to $J_{n,b}$, and $J_{n,a} - J_{n,b} = J_{c,a} - J_{c,b}$. Thus, by measuring $J_{c,a}$ and $J_{c,b}$ with the bimaterial (Au/Si₃N₄) cantilever-based calorimeter and using the Fourier's law of Eq. (47), the thermal conductance of the nanofibre is determined by $\kappa = (J_{c,a} - J_{c,b})/(T_a - T_b)$. Shen *et al.*'s experimental findings indicate that nanofibres with diameters of 50 ~ 500 nm and lengths up to tens of millimeters may possess thermal conductivities larger than many pure bulk metals.

It is interesting to note that the ZCC-based definition of local temperature discussed in Sec. 2.2.1 is, in principle, realizable with the use of a bimaterial cantilever-based calorimeter. For instance, to measure the local temperature T^* of a nanosystem, the fixed end of the cantilever (the probe) can be connected to a metal lead with a tunable T_p and μ_p , while the loose end of the cantilever is placed close to the examined nanosystem to achieve local equilibration. Then, one tunes T_p and μ_p until the ZCC is satisfied, which means $I_p = 0$ (no electric current through the metal lead, measured by an ammeter) and $J_p = 0$ (no deflection on the bimaterial cantilever), and the local temperature is determined as $T^* = T_p$. Of course, there are surely many practical issues to address before such an experiment can be actually conducted.

3.2.3. Resistance thermometry-based calorimeters

Another widely used type of calorimetric device is the resistance thermometry-based calorimeter. Figure 17(a) illustrates the setup and working principle of a resistance thermometry-based calorimeter. Two nanopads of different temperatures (T_1 and T_2) are thermally connected by a bridging conductor with a thermal conductance κ . Except the bridging conductor, the nanopads are considered to be thermally isolated from the surrounding environment, with other means of heat exchange (such as heat radiation) presumed to be negligible. The temperature of each nanopad is measured by a resistance thermometer which includes a temperature-dependent resistive element (the serpentine white lines in Fig. 17). The heat current flow from one nanopad to another through the bridging conductor is thus determined by Eq. (47), provided the thermal conductance of the conductor κ is known.

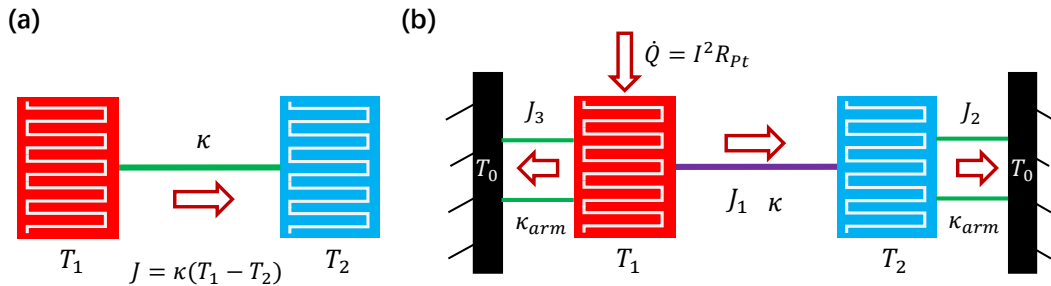


Figure 17: (a) Schematic illustration of the setup and working principle of a resistance thermometry-based calorimeter. The nanopads 1 (red) and 2 (blue) are connected by a conductor with a thermal conductance κ . The temperature of each nanopad is measured by a resistance thermometer (the serpentine white line), and the heat current through the conductor is determined as $J = \kappa(T_1 - T_2)$. (b) Schematic illustration of measurement of the thermal conductance κ of a one-dimensional nanobeam (purple). Each of the two nanopads is suspended to a bulk material (black) of temperature T_0 by an arm (green) with a thermal conductance κ_{arm} . A Pt resistance line (serpentine white line) with an electric resistance R_{pt} is integrated on each nanopad, which serves as both a resistance heater and a thermometer. The detailed procedure of measuring κ is explained in the main text.

The setup displayed in Fig. 17(a) can be utilized to study thermal transport in one-dimensional nanostructures. For instance, Fig. 17(b) illustrates how the unknown κ of a one-dimensional nanobeam (purple) can be determined by using a resistance thermometry-based calorimeter. To carry out the measurement, each of the two nanopads is suspended to a bulk material of ambient temperature T_0 by an arm of thermal conductance κ_{arm} . A serpentine Pt

resistance line is integrated on each pad and is used as both a resistance heater and a thermometer. Measurement of κ of the central nanobeam proceeds as follows [311, 313].

As illustrated in Fig. 17(b), an electric current I flows through the serpentine Pt resistance line integrated on the pad 1, which generates a Joule heat with the rate $\dot{Q} = I^2 R_{\text{Pt}}$, where R_{Pt} is the electric resistance of the Pt line. The Joule heat raises the temperature of the pad 1 to $T_1 \equiv T_0 + \Delta T_1$, with T_0 being the environmental temperature. Some of the Joule heat transfers across the central nanobeam (denoted as J_1), and raises the temperature of the pad 2 to $T_2 \equiv T_0 + \Delta T_2$ (measured by the Pt resistance line in the pad 2), while the rest of the generated heat dissipates into the environment through the suspended arms in contact with the pad 1 (J_3) and pad 2 (J_2). Again, other means of heat dissipation (such as by air or by radiation) are considered to be negligible. In the steady state, the heat dissipation into the environment through the suspended arms should balance the Joule heat generated by the incident electric current. This implies $\dot{Q} = J_1 + J_3$ and $J_1 = J_2$. Assuming the Fourier's law of Eq. (47) is valid for $J_i (i = 1, 2, 3)$, one has the following relations [311, 313]:

$$J_1 = \kappa(T_1 - T_2) = \kappa(\Delta T_1 - \Delta T_2), \quad (51)$$

$$J_2 = \kappa_{\text{arm}}(T_2 - T_0) = \kappa_{\text{arm}}\Delta T_2, \quad (52)$$

$$J_3 = \kappa_{\text{arm}}(T_1 - T_0) = \kappa_{\text{arm}}\Delta T_1. \quad (53)$$

The thermal conductance of the nanobeam can then be easily deduced as

$$\kappa = \frac{I^2 R_{\text{Pt}} \Delta T_2}{\Delta T_2^2 - \Delta T_1^2}. \quad (54)$$

Using the above technique, Shi and co-workers have measured the thermal conductances of nanowires and carbon nanotubes, and observed a dependence of κ on temperature [313, 326–328]. Lee *et al.* have measured the electronic contribution to the thermal conductance of a VO_2 nanowire and found the breakdown of the Wiedemann–Franz law [201] at high temperatures ranging from 240 to 340 K in the vicinity of its metal-insulator transition [311]. The violation of the Wiedemann–Franz law is attributed to the formation of a strongly correlated, incoherent non-Fermi liquid, in which charge and heat are independently transported.

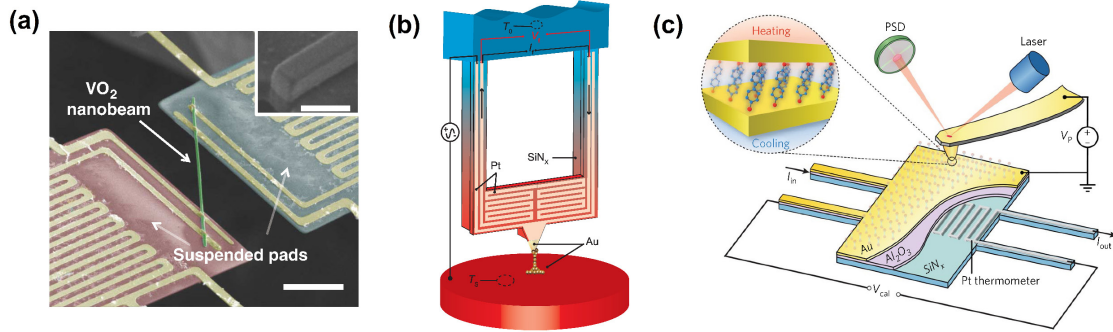


Figure 18: Several experimental setups using resistance thermometry-based calorimeter. (a) False-color SEM image of a nanojunction setup. A VO_2 nanobeam bridges two suspended pads, and heat transports from the heated pad (red) to the sensing pad (blue) through the nanobeam (green). The Pt resistance line integrated on each pad acts as both a micro-heater and a thermometer. The inset shows the SEM image of the rectangular cross section of the nanobeam. Reprinted with permission from [311]. Copyright 2017 AAAS. (b) A custom-fabricated calorimetric SThM probe for thermal conductance measurement of atomic contact junctions. The serpentine Pt thermometer is integrated on the probe of the SThM. Reprinted with permission from [329]. Copyright 2017 AAAS. An AFM-based calorimetric device for investigating the Peltier cooling effect in molecular junctions. A serpentine Pt thermometer is embedded into the SiN_x substrate. Reprinted with permission from [330]. Copyright 2018 Springer Nature.

Cui *et al.* have investigated the thermal transport in single atomic junctions [329, 331]. Figure 18(b) shows the experimental setup, in which a custom-fabricated high-resolution Pt resistance thermometer is integrated on the probe of an SThM. An atomic junction is formed when the SThM probe is in contact with a heated metallic substrate. Driven by the temperature difference between the substrate and the probe, the heat current across the atomic junction gives

rise to a change of the probe temperature, which can be quantified by the resistance change of the Pt thermometer. Consequently, the incident heat current can be determined from Eq. (47) with the known thermal conductance of the probe.

Cui *et al.* have also investigated local heating and Peltier cooling in molecular junctions by integrating a Pt thermometer-based calorimeter into a conducting-probe AFM; see Figure 18 [330]. Molecular junctions are created by placing the tip of an AFM probe in gentle contact with a self-assembled monolayer of molecules formed on the substrate. Current flow across the molecular junctions gives rise to heat generation or cooling due to Joule heating or Peltier cooling effect, which in turn results in a temperature change ΔT of the calorimeter on the substrate that can be quantified by the integrated Pt resistance thermometer. The total cooling or heating power P can be directly determined from $P = \kappa \Delta T$, where κ is the predetermined thermal conductance of the device [329, 330].

3.2.4. Advantages and limitations of nanocalorimetric techniques

The present nanocalorimetric techniques allow for measuring heat flow through nano-devices with a picowatt resolution. For the bimaterial cantilever-based calorimeter, Lai *et al.* have optimized the beam materials and the thickness ratio of two beam layers to achieve measurement of thermal power within 76 pW [324]. Varesi *et al.* have modulated the incident laser at sufficiently high frequency, which has enabled detection of thermal power within 40 pW [298]. Canetta and Narayanaswamy have used two laser beams with different wavelengths to heat up the cantilever and detect its deflection. They have also optimized the geometry of the cantilever. The resulting calorimeter is capable of measuring thermal power with a resolution of less than 1 pW [332]. Regarding the resistance thermometry-based calorimeter, Sadata *et al.* have used a high-resolution resistance thermometer with a sensitivity to temperature in the range of 20-100 μ K [299], and reported measurement of heat currents with a resolution of ~ 5 pW [300].

In practical applications, the main difficulty for reaching higher resolutions is the noise. For a cantilever-based calorimeter, noise may arise from external sources such as electronic components, mechanical vibrations of the cantilever beam [333], and intensity fluctuations in the laser source [321]. For a resistance thermometry-based calorimeter, the noise can be either intrinsic (such as Johnson–Nyquist noise and shot noise) or non-intrinsic (such as low frequency noise and electronic components noise) [299].

We now relate the nanocalorimetric techniques to local temperature measurements. As discussed in Sec. 3.2.2, in principle, with a bimaterial cantilever-based-calorimeter, the incident heat current and the local temperature profile of the cantilever are determined simultaneously by measuring the cantilever deflection; see Eqs. (48)–(50). However, with most of the existing experimental instruments and setups, the measurement of heat current usually requires the knowledge of temperature gradient (and thus the local temperature) as a prerequisite condition, *i.e.*, the heat current is determined by measuring the temperature, rather than the other way around.

There are also some practical limitations concerning the application of nanocalorimeters. One of them is spatial resolution. While a local temperature has been defined for a single molecular junction and atom-sized regions of nanostructures [142, 145, 334], experimental measurements of heat current were done for nanojunctions consisting of a large number of molecules [330] and one-dimensional nanowires with diameters of hundreds of nanometers [311–314, 326–328, 335]. Moreover, as discussed in Sec. 3.2.1, the present nanocalorimetric techniques presume that the Fourier’s law of Eq. (47) generally holds for nano-sized systems. However, it is well-known that the Fourier’s law does not properly describe ballistic phonon transport when the material dimension is similar to or even smaller than the phonon mean free path [88, 89, 336–339].

3.3. Measurement of local temperatures of non-equilibrium nanosystems

3.3.1. Mechanically-controlled break junction techniques

MCBJ has become a versatile and useful platform for the study of electron transport through single molecules, with which many important measurements/observations have been made [23, 61, 340–344]. Figure 19 gives schematic representations of two typical MCBJ setups. Specifically, Figure 19(a) depicts an AFM-based MCBJ setup, in which the cantilever (or probe) is gently brought into contact with a molecule adsorbed on the bottom substrate. Likewise, STM-based MCBJs have also been constructed, in which the probe also acts as an electrode. Figure 19(b) demonstrates an MCBJ setup with a metallic point contact, in which the mechanical force at the contact is controlled by adjusting a push rod integrated under the substrate. More details about the design and working mechanisms of MCBJ setups can be found in Refs. [345–348].

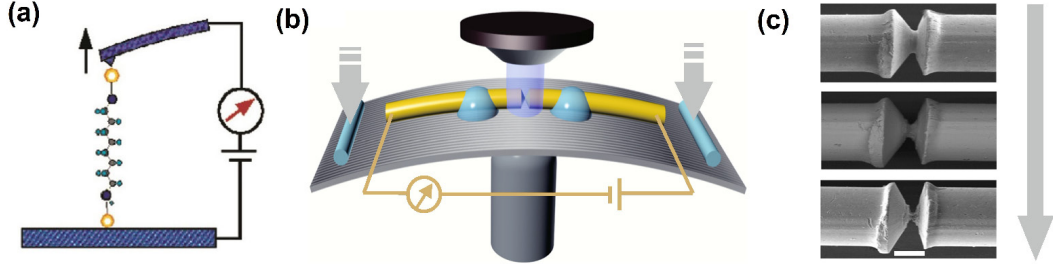


Figure 19: (a) A schematic of an AFM-based MCBJ setup. The cantilever (probe) is gently brought into contact with a molecule adsorbed on the bottom substrate. Continuously pulling the tip of the probe away from the substrate finally breaks the molecular junction. The breaking force is recorded. Reprinted with permission from [28]. Copyright 2006 American Chemical Society. (b) A schematic of MCBJ for metallic point contacts. A metallic nanowire (yellow) is fixed to two electrodes (blue) at a flexible substrate. One makes a notch near the middle of the nanowire to reduce the cross section of the line. A push rod is integrated under the substrate. A vertical movement of the rod bends the substrate. As the beam is bent, the metal wire starts to elongate, which results in the reduction of the cross section at the notch and finally results in a complete fracture of the metallic nanowire. (c) SEM images of the notched Au nanowire during the stretching process. The scale bar marks the length of $50\mu\text{m}$. (b) and (c) reprinted with permission from [349]. Copyright 2019 Springer Nature.

Based on an MCBJ setup, one method for measuring a local temperature is to study the force at which an molecular junction breaks with the increasing current-induced local heating. The idea behind the method is that the breakdown process is thermally activated. Consequently, the higher the local temperature is in the molecule-electrode contact, the smaller the average breakdown force it requires [28, 175]. A large number of breaking experiments were carried out repeatedly to obtain breakdown force histograms for subsequent statistical analyses; see Fig. 20(a). The broad distribution of the breakdown force reflects different molecule-electrode contact configurations, and the peak position gives the most probable force F^* required to break a molecular junction. Local temperatures T_{ph}^* can be extracted from the most probable breakdown force F^* as [29]

$$F^* = \frac{E_b}{x_\beta} + \frac{k_B T_{ph}^*}{x_\beta} \ln \left(\frac{r_F t_{\text{off}} x_\beta}{k_B T_{ph}^*} \right). \quad (55)$$

Here, E_b is the dissociation energy of the junction, x_β is the average thermal bond length along the pulling direction until breaking, r_F is the force loading rate, and t_{off} is the lifetime of the bond before it breaks down. Considering current-induced forces which may reduce the dissociation energy barrier and thus yield a smaller breakdown force, t_{off} can be expressed by $t_{\text{off}} = t_D \exp[-(E_b - \alpha V_{\text{bias}})/k_B T_{ph}^*]$ with t_D the diffusion relaxation time [30]. The empirical coefficient α describes the influence of current-induced forces.

The temperature T^* in Eq. (55) was originally described as an effective temperature of the molecular junction in Ref. [28]. Nevertheless, as it will be discussed below, the agreement between the experimental results and theoretical estimates of Eq. (26) indicates that the obtained T^* can provide a quantitative measure of the thermal excitation of local phonon modes. We thus assign T^* to the local temperature of local phonon modes (T_{ph}^*) in the following text.

Huang *et al.* have investigated current-induced local heating in single molecular junctions [28]. They used an STM-based MCBJ to measure the variation of local temperature versus bias voltage V_{bias} for an octanedithiol molecule connected in the junction. The results show that local heating raises the local temperature $T_{ph}^* \sim 30$ K above the ambient temperature T_0 at a bias voltage of ~ 1 V. Higher bias makes the single molecule junction unstable [350, 351]. The experimental data shown in the inset of Fig. 20(b) roughly agree with theoretical predictions from Eq. (26) at high bias. This agreement suggests that the electron-phonon scattering dominates the local heating in the octanedithiol junction, while the effect of electron-electron scattering in the junction is relatively weak [28]. A possible reason for the deviation in the low-bias region is that a low bias voltage cannot provide sufficient energy to excite the local phonon modes in the molecule.

Huang *et al.* have also measured local phonon temperatures of alkanedithiols of different lengths covalently bonded to two gold electrodes [175]. Their experimental results shown in Fig. 21(b) indicate that T_{ph}^* first increases with voltage bias, and then decreases after reaching a peak value. The measured data are in general agreement with the theoretical prediction of Eq. (28) (solid lines) regardless of the length of the molecule. This suggests that

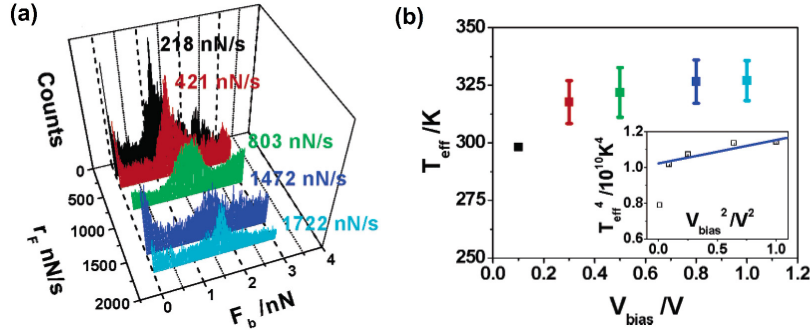


Figure 20: (a) Breakdown force histograms are constructed from ~ 500 measurements for individual force curves at each loading rate. (b) Local temperature of an octanedithiol molecule, extracted from F^* as a function of bias voltage. The inset shows that the local temperature has a fourth-power dependence on the square of the bias. The blue line in the inset is the best fit of the data using Eq. (26). Reprinted with permission from [28]. Copyright 2006 American Chemical Society.

both electron-phonon and electron-electron scattering occur in the alkanedithiols junctions. In the same experiment, Fig. 21(b) also suggests that the lengths of alkanedithiols have a non-negligible impact on local temperature. Under a given bias voltage the local temperature increases with decreasing molecular length. Based on DFT calculations, Chen *et al.* have attributed such a behavior to the insulating character of alkanedithiols [244]. In other words, the increasing electronic resistance of longer alkanedithiols weakens the Joule heating effect in nanojunctions.

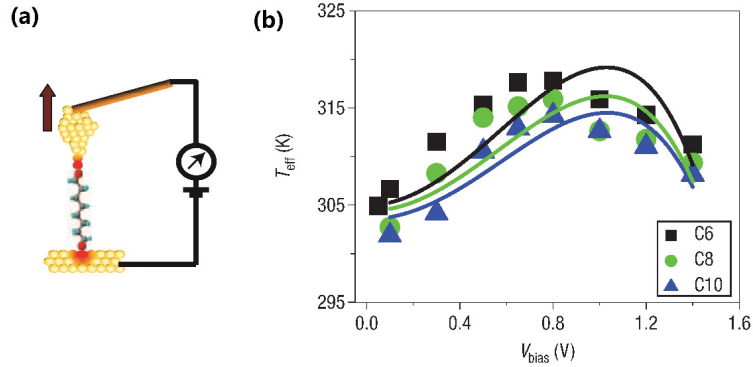


Figure 21: (a) A schematic of STM-based MCBJ setup. Molecules may bridge between the STM probe and the substrate via covalent bonds and form a molecule junction. Pulling the probe away from the substrate results in a breakdown of individual molecules from contacting the electrodes. (b) Local ionic temperature of a molecular junction, for three different types of molecule n -alkanedithiol, with $n = 6$ (squares), $n = 8$ (circles), and $n = 10$ (triangles). The solid lines are best fit to the theoretical estimation of Eq. (28). Reprinted with permission from [175]. Copyright 2007 Springer Nature.

For atom-sized contacts, an alternative method to evaluate local temperatures is to measure the change of electric conductance when the junction heats up. The principle is described as follows. The atomic configuration of the atom-sized contact corresponds to a local potential minimum. When the contact is stretched by an external force, the configuration will become unstable and then transform to a different configuration corresponding to a new local potential minimum [352]. Since the electric conductance of atom-sized metal contacts depends sensitively on the atomic configuration of the junction, a rearrangement in the contact geometry will lead to a sudden jump in electric conductance. For example, when there are two stable atomic configurations, a two-level conductance fluctuation emerges [353, 354]. The atomic rearrangement is achieved by atom jump between two distinct positions. The atom jump is a thermally activated process. Thus, the rate of the conductance fluctuation depends on local temperature as follows

$$\nu = \nu_0 \exp\left(-\frac{E_B - \alpha V_{\text{bias}}}{k_B T_{ph}^*}\right), \quad (56)$$

where ν_0 is the transition rate between two stable atomic configurations, E_B is an energy gap between two configurations, and α characterizes the influence of current-induced force [355].

Using the MCBJ setup, Tsutsui *et al.* have studied local heating in atom-sized Au contacts [356]. Figure 22(a) demonstrates an entire trace of two-level fluctuations of electric conductance under a given bias voltage. The frequency ν is derived by counting the number of these conductance switching cycles in the entire trace. A large number of repeated measurements were performed to generate a sufficient amount of data for the subsequent statistical analysis. This gives rise to the most probable rate of the conductance fluctuation, with which the local temperature is determined from Eq. (56). In Figure (5) of Ref. [356], the local temperature of the Au contact is plotted as a function of bias. The measured data exhibit a $\sqrt{V_{\text{bias}}}$ dependence of T^* , which agrees well with the theoretical prediction of Eq. (26), though the measured data are distributed within a limited range of bias voltage. This also suggests that electron-phonon interactions contribute significantly to the current-induced local heating at the atom-sized Au contact, while the contribution of electron-electron interaction may be small at a high bias.

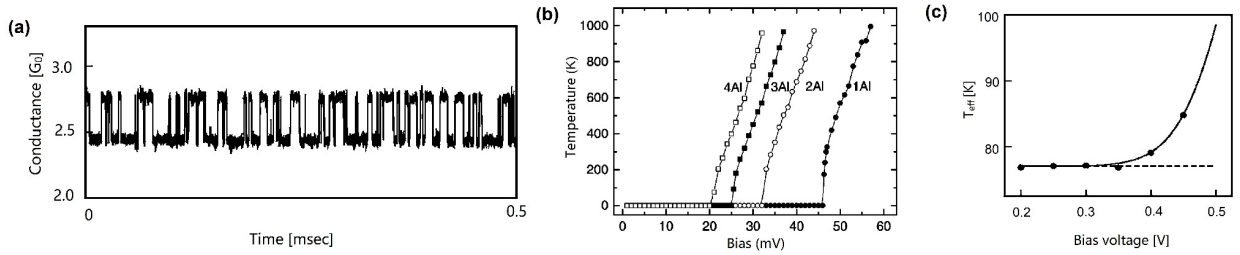


Figure 22: (a) A typical two-level fluctuation trace of electric conductance obtained at 0.35 V for atom-sized metal contacts. (b) Local temperature calculated from Eq. (23) as a function of bias for Al nanowires of different lengths. The calculation assumes there is no heat dissipation into the bulk electrodes. (a) and (c) reprinted with permission from [357]. Copyright 2007 American Institute of Physics. (c) Local ionic temperature of an atomic-size Zn contact with the ambient temperature $T_0 = 77$ K. The solid curve is a fit to the relation $T_{\text{ph}}^* = aV_{\text{bias}}^3$. The dash line is the initial slope of the curve. (b) reprinted with permission from [358]. Copyright 2005 American Physical Society.

Yang *et al.* have investigated local heating in Al nanowires in a junction using DFT calculations. They calculated the local temperature of the nanowire with Eq. (23) by assuming that there is no heat dissipation into the bulk electrodes [358]. They have found that, a bias larger than the lowest vibrational frequency of the junction is necessary to generate heat. Once above that threshold, a severe overheating occurs in the nanowire, which results in a drastic elevation of local temperature with a slightly increased bias by only a few mV; see Fig. 22(b). Tsutsui *et al.* have studied local heating in atom-sized Zn contacts at the ambient temperature of $T_0 = 77$ K [357]. Figure 22(c) exhibits a similar dependence of local temperature on bias. The local temperature remains unchanged when the bias is below 0.35 V, while it rises rapidly as the bias increases further. The experimental data fit well to the relation $T_{\text{ph}}^* = aV_{\text{bias}}^3$ with a being a fitting parameter. The sharp increase of local temperature has been attributed to contact overheating [357], which implies the heat generated is not efficiently dissipated into the electrodes and severely accumulates at the atom-sized Zn contact.

The MCBJ techniques have the following advantages: They allow for the measurement of local temperature in single-molecule and atom-sized junctions under bias voltages. Besides measuring local electric properties, MCBJ can also be combined with other techniques in practice, such as noise spectroscopy and surface enhanced Raman spectroscopy [346], to characterize voltage noise and Raman scattering.

Since the present MCBJ setups can measure local properties of nanojunctions, this platform is promising for the practical implementation of MPC-based definitions such as that described by Eq. (43). A possible scheme is described as follows. By using a specialized detector, one can monitor the variation of a certain local property of the nanosystem as the probe approaches the system. When the probe is weakly coupled to the system, one can tune the temperature and the applied bias on the probe until the electric current through the probe vanishes and the local property is minimally perturbed by the probe. Thus, the local temperature and local electrochemical potential are determined to be equal to the probe counterparts. Such a scheme would require a high-precision measurement of the local property.

Nevertheless, there are still some limitations to the MCBJ techniques. For instance, it is difficult to precisely control the microscopic details of the break process, such as the atomic configuration of the contacts. To minimize

the uncertainty, a large number of repeated measurements are required to obtain sufficient data for statistical analysis.

3.3.2. Spectroscopic techniques

An alternative method makes use of spectroscopic techniques, including optical interferometry [359, 360], Raman spectroscopy [361] and luminescence [362–366]. The technical details of the above spectroscopic techniques can be found in relevant reviews [367–370]. For spectroscopic techniques, the height, width, and peak position of measured spectral lines reflect local excitations in nanosystems and the distribution of relevant microstates of the particles. The principle behind spectroscopic techniques is that the change of local temperature has an impact on the distribution of particles and local excitations in nanosystems, which changes the shape and peak position of spectral lines.

Raman spectroscopy has been applied to the study of electrically-heated suspended carbon nanotubes [371, 372], and to measure local temperature of high energy optical phonons of G_+ and G_- bands. Generally the G band is related to the different C-C vibrational modes in a carbon nanotube [373]. In carbon nanotubes, the G band is split into many spectra lines around 1580 cm^{-1} [374]. Here, the G_+ and G_- bands are characteristic of the transverse and longitudinal optical phonon modes at the Γ point, respectively. Figure 23(a) shows the Raman shifts of the G_+ and G_- bands, along the length of the nanotube with $5 \mu\text{m}$ length, for $V_{sd} = 0 \text{ V}$ and 1.2 V . The G bands downshift significantly in response to the voltage bias. To image the temperature profiles along the nanotubes, Deshpande *et al.* have measured the G band shifts with a varying temperature; see the inset of Figure 23(b) [372]. The local temperature at each point is obtained by dividing the voltage-induced downshift of G bands in Figure 23(a) by the slope of the contour line in the Figure 23(b)'s inset. Figure 23(b) and (c) show the profiles of phonon temperature along $2 \mu\text{m}$ and $5 \mu\text{m}$ carbon nanotubes under the bias $V_{sd} = 1.2 \text{ V}$, respectively. The voltage-induced local heating is prominent in the middle of the nanotubes. Particularly, the local temperature of the G_- mode significantly varies along the $2 \mu\text{m}$ nanotube, while the local temperature of the G_+ mode is around the ambient temperature. This is because the electrons are preferentially coupled with the G_- mode phonons [371, 375], and induce critical local ionic heating.

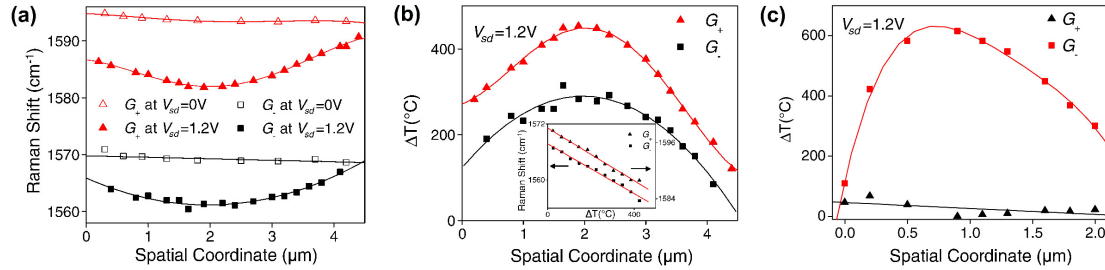


Figure 23: (a) Spatial profile of Raman shifts of G_+ and G_- bands for a $5 \mu\text{m}$ carbon nanotube at $V_{sd} = 0 \text{ V}$ and 1.2 V . (b) Temperature profiles of G_+ and G_- bands for $5 \mu\text{m}$ carbon nanotube at $V_{sd} = 1.2 \text{ V}$. (c) Temperature profiles of G_+ and G_- bands for $2 \mu\text{m}$ carbon nanotube at $V_{sd} = 1.2 \text{ V}$. $\Delta T = T^* - T_0$ with T_0 being the room temperature. Reprinted with permission from [372]. Copyright 2009 American Physical Society.

Iof *et al.* have directly monitored the local phonon temperature in a current-heating molecular junction, using a surface-enhanced Raman spectroscopy technique that can simultaneously measure both the Stokes, I_S , and anti-Stokes, I_{AS} , components of the Raman scattering [376]. The idea is that the ratio between the Stokes and anti-Stokes intensities is directly related to their non-equilibrium populations, from which a local phonon temperature T_{ph}^* can be extracted by the following equation [377]

$$\frac{I_{AS}}{I_S} = A_v \left[\frac{\omega_L + \omega_v}{\omega_L - \omega_v} \right]^4 \exp \left[\frac{-\hbar\omega_v}{k_B T_{ph}^*} \right], \quad (57)$$

where $I_{AS(S)}$ is the intensity of the anti-Stokes (Stokes) Raman mode, $\omega_{L(v)}$ is the frequency of the laser (Raman mode) and $\hbar\omega_v$ is the Raman shift. A_v is a bias-dependent correction factor related to the ratio of the anti-Stokes and Stokes cross sections.

In Figure 24 the local temperature is plotted as a function of voltage bias for different phonon modes of a biphenyldithiol nanojunction. Although the temperature is slightly different between different modes (due to the different electron-phonon coupling strengths and symmetries), the overall voltage dependence shows roughly similar

features. An apparent decrease in local temperature has also been observed at high bias, which roughly agrees with results in Figure 21(b). This agreement suggests that both electron-electron and electron-phonon interaction contribute to local heating in the junction.

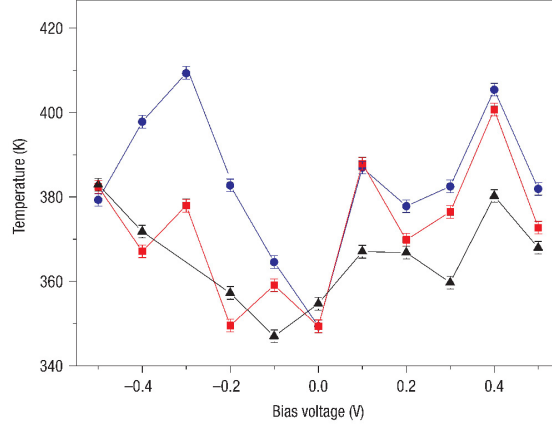


Figure 24: Plot of T_{ph}^* as a function of bias voltage V for the $1,585\text{ cm}^{-1}$ (black triangles), $1,280\text{ cm}^{-1}$ (blue circles) and $1,083\text{ cm}^{-1}$ (red squares) modes in biphenyldithiol nanojunction. While the temperature is slightly different, the overall voltage dependence shows roughly similar features. Reprinted with permission from [376]. Copyright 2008 Springer Nature.

Ward *et al.* have shown that the anti-Stokes component of surface-enhanced Raman scattering could be used to determine the local electron temperature [176]. The idea is that the intensity of the anti-Stokes scattering $I_{AS}(\epsilon)$ at a specific shift ϵ is proportional to the joint DOS $J(\epsilon) = \int g(E + \epsilon)f(E + \epsilon, T_e^*)g(E)[1 - f(E, T_e^*)]dE$ for electrons at energy $E + \epsilon$ and holes at energy E , with $g(E)$ being the density of electrons and holes [378]. The integral over the conduction band is related to the local electron temperature [176],

$$I_{AS}(\epsilon) \propto \int f(E + \epsilon, T_e^*)[1 - f(E, T_e^*)]dE \simeq \frac{\epsilon}{\exp[\epsilon/(k_B T_e^*)] - 1}, \quad (58)$$

when the band densities of states vary slightly over the anti-Stokes shift range of interest. Here $f(E, T)$ is the Fermi-Dirac function.

Figure 25(a) and (b) depict the local phonon temperature as a function of V in an OPV₃ molecule junction (OPV₃, three-ring oligophenylene vinylene terminating in amine functional groups). However, local ionic cooling at a high bias does not appear. An approximately linear increase of local phonon temperature T_{ph}^* for measured Raman modes is observed with increasing $|V|$, while T_{ph}^* does not act as $T_{ph}^* \propto \sqrt{V}$ predicted by Eq. (26) at low biases, as would be expected for heat dissipation to environment (bulk substrates and electrodes) via elastic scattering between phonons of the nanojunction and phonons of the bulk system. This suggests that local vibrational relaxation to environment takes place by other means, such as coupling to phonons with reduced DOF [176].

Figure 25(c) and (d) plot the local temperature of electrons as a function of V_{bias} for the bare nanojunction without any molecule and OPV₃ molecule junction, respectively. The nanogap between the two electrodes allows a relatively large tunneling current through the bare junction, while the presence of the OPV₃ molecule limits the electric current through the junction. A linearly increasing T_e^* with respect to V is consistent with the prediction for local electron heating in nanoscale conductors when no electron-phonon interaction is present [250].

Mecklenburg *et al.* have developed a non-invasive thermometric technique, plasmon energy expansion thermometry, which can measure local electron temperatures of bulk systems with nanometer-scale spatial resolution [379, 380]. Incorporating electron energy loss spectroscopy (EELS) with scanning tunneling electron microscopy (STEM), the thermometry can measure local temperatures from the minimally required energy E to excite a bulk plasmon, which represents the oscillations of electron density around ion cores within the bulk material containing an electron gas. The principle behind is that the temperature-induced change of free electron density ρ_e of bulk plasmon affects the plasmon energy E . When the temperature of a bulk material rises by ΔT above room temperature T_0 , the material

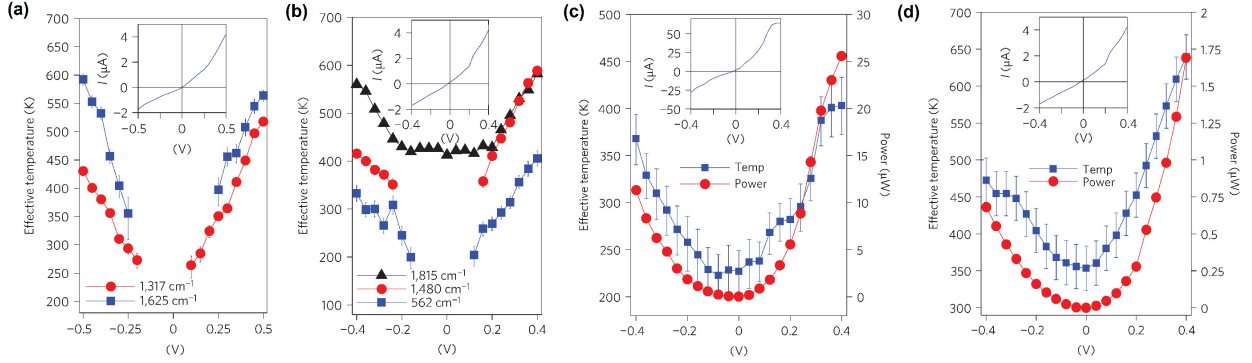


Figure 25: Local phonon (a,b) and electron (c,d) temperature as a function of V . Inset: $I - V$ curve for each device. For OPV₃ molecule junction, (a) shows local temperatures for two vibrational modes: 1,317 cm^{-1} (red) and 1,625 cm^{-1} (blue), and (b) exhibits another three modes: 1,815 cm^{-1} (black), 1,480 cm^{-1} (red) and 562 cm^{-1} (blue). The vibrational modes in (a) are pumped by charge flow through the molecule and the vibrational pumping for modes in (b) results from both current and optical excitation. The curve is limited below $|V| \leq 0.2\text{V}$ by the detector noise floor for anti-Stokes signal, except for the mode with 1,815 cm^{-1} . (c) and (d) show local electron temperature (blue; left axis) and dissipated electrical power (red; right axis) for the bare nanojunction without any molecule and OPV₃ molecule junction, respectively. The nanogap between the two electrodes allows a relatively large tunneling current through the bare junction. Reprinted with permission from [176]. Copyright 2011 Springer Nature.

expands. The thermal expansion of a bulk material changes its density, as well as the density of free electrons inside the material $\rho_e(T) \approx \rho_e(T_0)[1 - \alpha_1\Delta T - \alpha_2(\Delta T)^2]$. Here, α_i ($i = 1, 2$) are the first-order and second-order coefficients of thermal expansion. Since the energy E of free electrons depends on ρ_e , given by $E = \sqrt{4\pi\rho_e e^2/m}$, the temperature rise ΔT is related to the change in plasmon energy $\Delta E(T) = E(T) - E(T_0)$ by the following equation

$$\Delta T = \frac{\alpha_1}{2\alpha_2} \left(\sqrt{1 - \frac{8\alpha_2\Delta E(T^*)}{3\alpha_1^2 E(T_0)}} - 1 \right). \quad (59)$$

By focusing the STEM electron beam into a nanometer-sized probe, placing it over the sample, and analyzing the shift of the plasmon peak in EELS according to Eq. (59), one obtains an image for the temperature map of the sample; see Figure 1 in [379].

In this way, Mecklenburg *et al.* have imaged the local temperature distribution of a serpentine Al nano-device subjected to a bias voltage [379]. Figure 26(b) reveals the spatial resolution of the temperature field of the nano-device is, technically, less than 2 nm. However, as stated by Mecklenburg *et al.*, temperature differences do not exist on the length scales smaller than the mean free path of a particle. Since the electron transport is ballistic over distances less than the electron mean free path, l_e , the setup cannot measure a temperature gradient for separations smaller than l_e . Thus l_e provides the minimal spatial resolution of local electron temperature, estimated as $l_e \leq 4 - 15$ nm in their experiment. The precision of the temperature measurement is limited to several Kelvins (standard error of ~ 3 to ~ 5 K).

Another application of STEM-EELS to the temperature measurement has been reported by Lagos *et al.* [381, 382]. When an electron probe of the STEM setup is coupled to a nanostructure, the incident high energy electron from the probe will be scattered elastically and inelastically, producing a large variety of vibrational/phonon excitations. For an inelastic process involving the transfer of the energy ΔE and momentum Δq between the electrons and phonons in materials, the detailed balance relation associates the scattering probability of a loss energy event with that of a gain energy process

$$\frac{P(\Delta E, \Delta q)}{P(-\Delta E, -\Delta q)} = e^{-\beta_{ph}^* \Delta E}, \quad (60)$$

thus providing a straightforward access to temperature information on objects through scattering measurements. Here, $\beta_{ph}^* \equiv 1/T_{ph}^*$ and P is the probability of energy loss or gain in scattering. Although the detailed balance relation is only

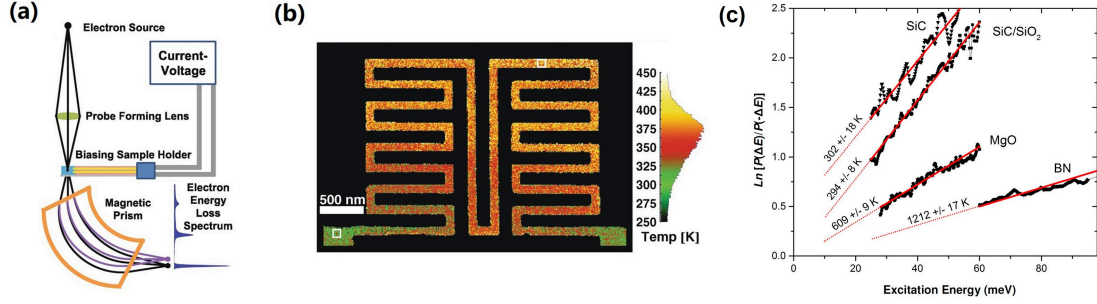


Figure 26: (a) Schematic of the plasmon energy expansion thermometer. It consists of a STEM, a biasing sample holder, a power source for Joule-heating the sample, and an EELS spectrometer; (b) A false-color temperature map of a serpentine aluminum wire heated by the electrical current. The histogram indicates the color scale and bins each pixel according to its temperature. (a) and (b) reprinted with permission from [379]. Copyright 2015 AAAS. (c) The result of the bulk and surface phonon scattering in different nanostructures: a single SiC nanoparticle and a SiO₂/SiC interface sample at room temperature and for a single MgO nanosphere and a BN flake at high temperatures. The plots follow the linear behavior as predicted by the detailed balance relation. The measured temperature values for each nanosystem are shown over the dotted lines. Reprinted with permission from [381]. Copyright 2018 American Chemical Society.

valid for equilibrium systems, Lagos *et al.* have held a view that this technique is still applicable for nonequilibrium nanosystems, which violate the FDT [381]. The energy gain and loss by phonons in inelastic scattering have been measured for different nanostructures [381, 383]. The logarithm of the ratio of the loss and gain scattering is fitted as a function of the excitation energy. Figure 26(c) shows that all of the curves exhibit the typical linear behavior, with slope scaling like T^{-1} , as described by Eq. (60). Using an energy gain and loss spectroscopy, one can measure the local temperature of a nanosystem with precision down to about 1 K. The spatial resolution depends on the type of scattering signal used to determine the local temperature: short wavelength bulk phonons technically provide a highly localized scattering signal down to the atom-level ($\sim 2\text{\AA}$).

Some efforts have been made to incorporate an AFM setup with spectroscopic techniques. For instance, Aigouy *et al.* have developed a scanning thermal imaging method based on a temperature-sensitive phenomenon: fluorescence [384]. Fluorescent nanoparticles have been glued on the apex of an AFM probe, as a temperature sensor. When nanoparticles are in thermal equilibrium with the measured sample, the population of energy levels in fluorescent nanoparticles is ruled by the Boltzmann distribution [385, 386]. The relative intensity of the two fluorescent lines is linked by the following relation [385, 387, 388]

$$\frac{I_{\nu_1}}{I_{\nu_2}} = A \exp\left(-\frac{\Delta\hbar\omega}{k_B T^*}\right). \quad (61)$$

Here, I_ν is the intensity of each peak located at specific frequency ν , $\Delta\omega$ is the energy separation between these two groups of lines, and A is a parameter that depends on the fluorescent material. By scanning the surface of the sample and calculating the ratio of the intensity of the two fluorescence lines, one can obtain information on the temperature distribution over the sample.

The spectroscopic techniques described above have the following advantages: some of the spectroscopic techniques enable temperature measurements with atom-level spatial resolution; since spectroscopic techniques are mainly based on statistical properties of nanosystems, they have the potential to realize the theoretical definitions in Sec. 2.2.4. In addition, spectroscopic techniques are non-invasive in the sense that the measurement has a minor effect on the measured system's temperature [379]. This is different from the MCBJ techniques which require breaking the nanojunction by applying mechanical forces. On the other hand, the spatial resolution of some spectroscopic techniques, such as Raman spectroscopy and infrared thermography may be restricted by the diffraction limit (around half wavelength) [367]. Moreover, the techniques with a high spatial resolution, such as plasmon energy expansion thermometry, are only valid for metals and semiconductors which have sufficiently sharp plasmon resonances [379].

Finally, it should be pointed out that, since some spectroscopic techniques probe locally the energy space rather than the real space, the measured non-equilibrium temperature is spatially nonlocal. Notable examples are the mode-specific local phonon temperature T_{ph}^* exhibited in Figures 24 and 25, and the mode-specific temperature of magnons

(quasi-particles representing the collective excitations of electronic spins) defined by an energy repartition principle in spin systems at a non-equilibrium steady-state [135]. Such non-equilibrium temperatures should be distinguished from the local temperatures that are truly local in real space.

3.3.3. Scanning thermal microscope

The SThM, designed for measuring the temperature distribution of a large nanostructure, is widely used to investigate thermal transport of nanoscale/mesoscopic structures [389–391]. Figure 27 shows the setup of an AFM-based SThM. The principle of an SThM is that the local temperature is obtained from the value of a temperature-dependent property, measured by the thermal sensors integrated onto the AFM probe. In practice, the probe closely approaches a sample and scanning its surface to obtain information of its topography and temperature simultaneously but independently. Various thermal sensors have been developed based on different thermally-sensitive properties or phenomena, such as thermoelectricity [392, 393], change in electrical resistance [394, 395], thermal expansion [396], or fluorescence [397]. Here, we first review two types of widely-used thermal probes.

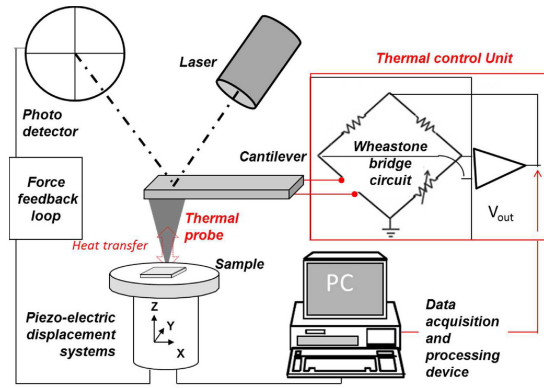


Figure 27: The set-up of an AFM-based SThM system. Here, the output signal is the voltage delivered by a “thermal control unit” and a balanced Wheatstone bridge can be used to maintain the probe mean temperature at constant value. Reprinted with permission from [398]. Copyright 2015 John Wiley and Sons.

The first type of probe is based on a resistance thermometer. The temperature dependence of the resistance R_p can be expressed as [398]

$$R_p(T) = R_p(T_0)[1 - \alpha(T - T_0)], \quad (62)$$

where T_0 is a reference temperature and α is the temperature coefficient of its electrical resistivity. The probe determines the local temperature by measuring the variation of the electrical resistance R_p of the probe in response to a temperature change. Although the resistance thermometer has been used in the nanocalorimeters we previously reviewed, the experimental utilization of a resistance thermometer in SThM is different that in calorimetry. Here, a resistance thermometer is integrated on the SThM probe, and can measure the temperature of a local region of the sample. In nanocalorimeters, a resistance thermometer is embedded into the pad, and can only measure the temperature for one end of the nanostructures.

To improve the spatial resolution of a resistance thermometer-based SThM a carbon nanotube has been proposed as a thermal probe because of its small tip radius and high thermal conductivity [399, 400]. Tovee *et al.* have developed a carbon nanotube-based SThM probe, as shown in Figure 28(a). Compared with the conventional Pt tip with the ~ 100 nm spatial resolution [367], this probe could achieve a spatial resolution of ~ 30 nm [401].

The second type of probe is the thermocouple-based SThM probe. Based on the Seebeck effect between two different types of metals, a thermocouple uses the thermoelectric voltage V_{TE} to carry out the temperature measurement [402]

$$S_{Sb} = \frac{V_{TE}}{T_1 - T_2}, \quad (63)$$

where S_{sb} is the Seebeck coefficient of the thermocouple, T_1 and T_2 are temperatures of the two different metals. Given the excellent thermal contact between the thermocouple and the sample, T_1 can be assumed to be the same as the local temperature T^* of the measured region of the sample. Given excellent thermal contact between the thermocouple and the tip, T_2 is equivalent to the probe temperature T_p . Since the thermoelectric voltage V_{TE} across the thermocouple is directly proportional to T^* of the sample, one can quantitatively determine T^* by measuring V_{TE} with a known S_{sb} .

A point-contact thermocouple has been developed by Sadat *et al.* [403]. The thermocouple forms when a Pt-coated AFM probe at the ambient temperature is brought into physical contact with the surface made by another type of metal. This method can map the temperature field of metallic surfaces with a ~ 0.01 K temperature resolution and < 100 nm spatial resolution [403].

Kim *et al.* have reported an ultra-high-vacuum (UHV)-based SThM technique [404]. A nanoscale Au-Cr thermocouple coats the SiO_2 tip of the probe, as shown in Figure 28(b). Since an UHV environment eliminates heat transport between the tip and the sample through air, the UHV-SThM is capable of quantitatively mapping temperature fields with the ~ 15 mK temperature resolution and ~ 10 nm spatial resolution on metal and dielectric surfaces. Figure 29(a)

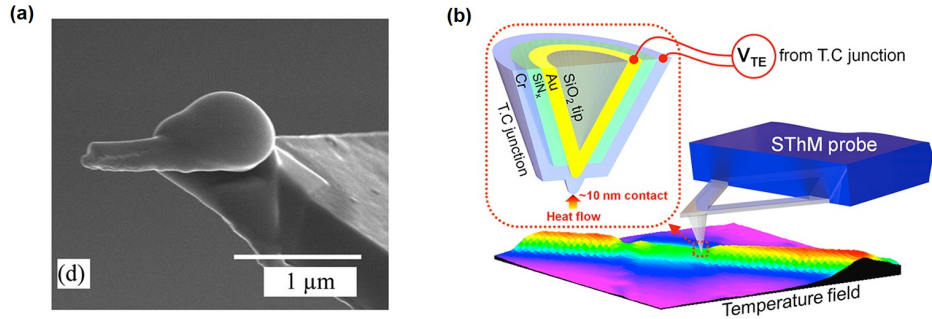


Figure 28: (a) SEM images of the SThM probe assembling carbon nanotube. High thermal conductivity and small tip radius of the carbon nanotube improve the thermal resolution of SThM. Reprinted with permission from [401]. Copyright 2014 Royal Society of Chemistry. (b) Schematic illustrating the UHV-SThM technique. The device resides in a UHV chamber. The nano-thermocouple junction fabricated by Au and Cr layers is assembled outside the end of the tip. The thermoelectric voltage V_{TE} generated from the Au-Cr junction is directly proportional to local temperature of the sample at the contact region. Reprinted with permission from [404]. Copyright 2012 American Chemical Society.

and (c) show the topographical image of 200 nm (narrow) and 1 μm (wide) Pt lines, respectively. The local temperature decays rapidly in the direction perpendicular to the Pt lines; see yellow lines in Figure 29(b) and (d). When the narrow Pt line (through which an electrical current flows) is connected to the wide Pt line (through which no electrical current passes), the temperature rise of the 200 nm line is significantly lower in the region where it intersects the 1 μm line; see Figure 29(e) and (f). This is because heat current dissipates from the 200 nm Pt line by the 1 μm Pt line in the cross section.

Varesi and Majumdar have developed a scanning Joule expansion microscopy (SJEM), an AFM-based setup that can image both surface topography and Joule heating-induced thermal expansion of a sample [32, 405]. The thermal expansion ΔL_z of the sample thickness is related to the rise of local temperature $T^* - T_0$ via the following equation [32, 405]

$$\Delta L_z = \alpha L_z (T^* - T_0), \quad (64)$$

where T_0 is the background temperature, α is the linear thermal expansion coefficient, and L_z is the local thickness of the sample, which is obtained from the surface topography. According to Eq. (64), the change in local temperature can be determined by detecting the thermal expansion ΔL_z of the sample. It is reported that the spatial resolution of SJEM has reached ~ 20 nm [406].

SJEM has also been applied to investigate temperature fields of various nanosystems, such as nanowires [406], two-dimensional metallic films [407], and graphene-metal contacts [22]. Using SJEM, Xie *et al.* have investigated the temperature profile of three single-wall carbon nanotubes subjected to a bias voltage [408]. Figure 30(a) shows the topographical image of three single-wall carbon nanotubes. Compared with nanotube A and C, nanotube B has

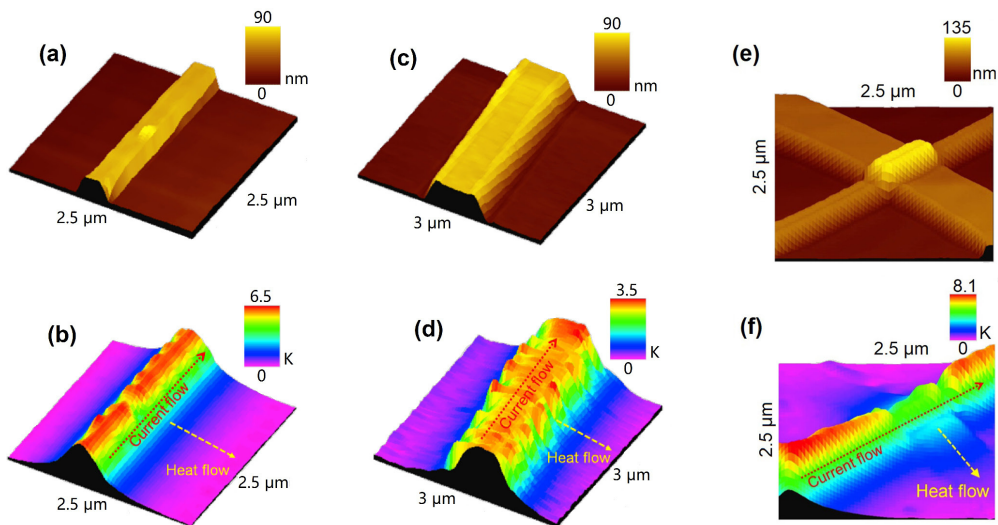


Figure 29: Simultaneously-measured topographical and temperature images on (a), (b) 200 nm and (c), (d) 1 μm wide Pt lines, respectively. The directions of current and heat flow are represented on temperature images. The measured temperatures decay rapidly away from the Pt lines. Simultaneous-measured topographical and temperature (e), (f) images, respectively, on a 2.5 μm - 2.5 μm region where the 200 nm wide Pt line lies on top of a 1 μm wide Pt line. The 1 μm wide Pt line acts as a fin for the 200 nm Pt line in the cross sections. Reprinted with permission from [404]. Copyright 2012 American Chemical Society.

high combined electrical resistance in the electrode-nanotube contacts. There is a prominent “kink” in the middle of nanotube C. The “kink” arises from the growth process of the carbon nanotube and can be considered as a topographic defect. AC voltage bias is applied to three nanotubes and provides Joule heating. Figure 30(b) illustrates the SJEM image of the nanotubes under AC voltage with a frequency $f = 30$ kHz. Nanotube A exhibits nearly uniform thermal expansion along its length. Nearly no topographical signal is obtained from nanotube B due to its high resistance. Nanotube C shows a sharp peak corresponding to the site of the “kink” defect, indicating substantial local heating. Under a high frequency voltage with $f = 155$ kHz, the overall image of Figure 30(c) is similar to that of Figure 30(b). This defect-induced local heating can be used to examine whether a topographic defect exists in carbon nanotubes [408].

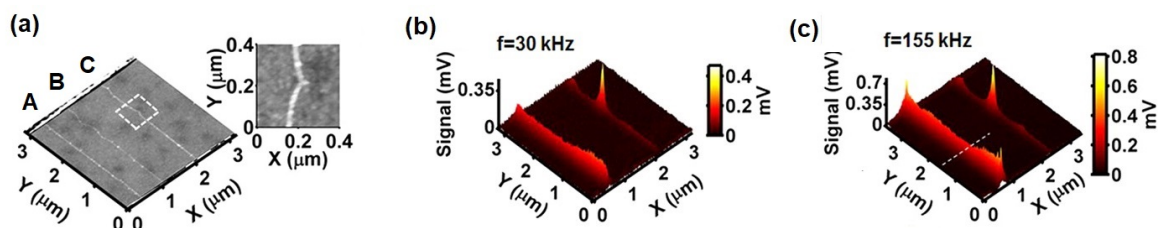


Figure 30: (a) Topographical AFM image of three single-wall carbon nanotubes. The inset provides a magnified view of a “kink” in one of the single-wall carbon nanotubes. (b) SJEM image of the same nanotubes at low frequency. A strong peak appears at the position of the kink, illustrating significant heat generation at this location. (c) SJEM image of the carbon nanotubes at high frequency. f is the frequency of the AC voltage bias. The overall shape of (c) is similar to that of (b). Reprinted with permission from [408]. Copyright 2012 American Chemical Society.

Combining AFM with spectroscopic techniques, Aigouy *et al.* have proposed a SThM setup based on fluorescence [386, 397, 409]. Rare-earth ion-based fluorescent particles are attached to the apex of the AFM probe. Scanning a Ni nanoscale (Joule) heater, they have imaged the topography and the temperature profile of the whole nanostructure; see Figure 8(a) and (b) in [397]. The temperature cross section exhibits a homogenous temperature distribution along the axis direction of the Ni heater; see Figure 8(c) in [397]. The spatial resolution is in the range of the fluorescent particle size (smaller than 500 nm), and the temperature sensitivity is smaller than 5 K [409].

A large advantage of the SThM is simultaneously imaging surface topography and temperature field. Under an UHV environment, a custom-fabricated thermocouple can reach a high spatial resolution with an accuracy of ~ 10 nm [404]. However, a limitation is that the SThM generally demands physical contact with nanosystems. The thermal probe inevitably perturbs the local properties of nanosystems to some extent, and therefore disturbs the value of the local temperature [379]. More strengths and limitations of SThM have been analyzed by Brites *et al.* [367], Gomès *et al.* [398] and Kim *et al.* [369].

3.3.4. Relation between experiments and theories

In Sec. 3.3 we have reviewed the present thermometric techniques designed for a variety of non-equilibrium nanosystems, ranging from one-dimensional molecular junctions and nanowires to two-dimensional nanosheets and layered nanostructures. Besides these works, there are still many other experimental efforts on thermometers at the nanoscale which are not covered in the above discussion, such as [367–369, 398]. In the following, we establish the connections between the existing experimental efforts presented in this Section and the theoretical definitions of local temperature reviewed in Sec. 2.

First, it is important to recognize that some theoretically proposed schemes for local temperature measurement have been realized in real experiments. For instance, the extraction of a local temperature from the local distribution function of particles has been realized by spectroscopic techniques. As reviewed in Sec. 3.3.2, both the local phonon temperature and local electron temperature of a molecular junction have been obtained by analyzing the surface enhanced Raman spectroscopy [176]. Moreover, experimental observations have confirmed some theoretical predictions. For instance, as reviewed in Sec. 3.3.1 the local temperatures measured by MCBJ-based techniques agree well with the theoretical prediction of Eq. (28) which quantifies the contribution of electron-phonon and electron-electron couplings to current-induced local ionic heating. Furthermore, the advancement of experimental instruments and techniques has encouraged novel theoretical proposals. For instance, the latest SThM has achieved high-precision measurement of local physical properties which are highly sensitive to the local temperature. This would make some newly proposed protocols, such as the MPC-based definitions reviewed in Sec. 2.2.5, practically feasible and potentially promising.

Second, there is a still noticeable gap between the experiments and the theories. On the experimental side, many experimental measurement approaches are based on the miniaturization of conventional macroscopic thermometers [367]. For instance, as reviewed in Sec. 3.3.3, the application of SThM has presumed that the local thermal properties or phenomena of nano-sized materials, such as thermoelectricity, thermal expansion, and temperature-dependent electrical resistance, preserve their conventional relations or forms as in bulk materials. The validity of such a presumption requires the nano-sized material should include a sufficiently large number of DOF. As discussed in Sec. 1.2.2, the minimal length scale for the existence of a local Boltzmann distribution is estimated to be ~ 100 nm for real materials [79]. Such a length scale coincides with the typical spatial resolution of the temperature field measured by a resistance thermometer-based SThM [367]. In contrast, on the theoretical side, the proposed local temperature definitions are, in principle, suitable for general nanosystems of all sizes. However, numerical simulations of real nano-devices or materials for practical purposes are often limited by the computational capabilities of modern computers. Consequently, most of the reported theoretical studies were carried out for nano-sized devices or materials with a relatively small number of DOF, such as nanojunctions consisting of a single molecule and QDs with a few energy levels.

Third, a number of theoretical definitions have not been put to experimental test. This is because some key quantities involved in these definitions cannot be measured directly with the existing instruments/apparati. For instance, despite the possible scheme presented at the end of Sec. 3.2.2, the ZCC-based definitions have not been realized, because of the difficulty in measuring the heat current without the prerequisite knowledge of the temperature gradient. As for the thermodynamic relations-based definitions, the measurement of thermodynamic entropy for nanosystems which is at the heart of many definitions, has remained a formidable challenge for experiments [63]. In addition, some dynamic response properties required for the statistical relations-based definitions, such as the NEGFs, are also hard to access directly in experiments.

The above discussion suggests that there is plenty of room for improvement for both experimental and theoretical studies regarding the determination of local temperatures for non-equilibrium nanosystems. Particularly, it is important for the experimental techniques to go beyond the conventional strategies for classical systems and be able to account for the quantum effects at the nanoscale. On the other hand, it is also crucial for theoretical proposals to pay more attention to their practical feasibility, so that they can be realized by the existing experimental setups. For instance, the MPC-based definitions discussed in Sec. 2.2.5 were designed with unambiguous operational protocols,

and their implementation does not require the potentially difficult procedure of measuring the heat current or thermodynamic properties. Thus, these operational definitions are expected to be promising candidates for future practical applications.

4. Implications and applications of non-equilibrium local temperatures

4.1. Physical Implications

4.1.1. Generalization of the thermodynamic laws

For a nanosystem in a non-equilibrium steady state, Stafford *et al.* have shown that the ZCC-defined local temperature is consistent with the thermodynamic laws, if a broadband probe is weakly coupled to the system.

The Zeroth Law – The zeroth law has been discussed in two scenarios. The first one is as follows [143, 410]: If the local temperatures and the local electrochemical potentials of two non-interacting fermionic systems, as measured by a probe, are equal, the two systems will be in thermal and electrical equilibrium with each other when connected by a transmission line coupled locally to the same two positions.

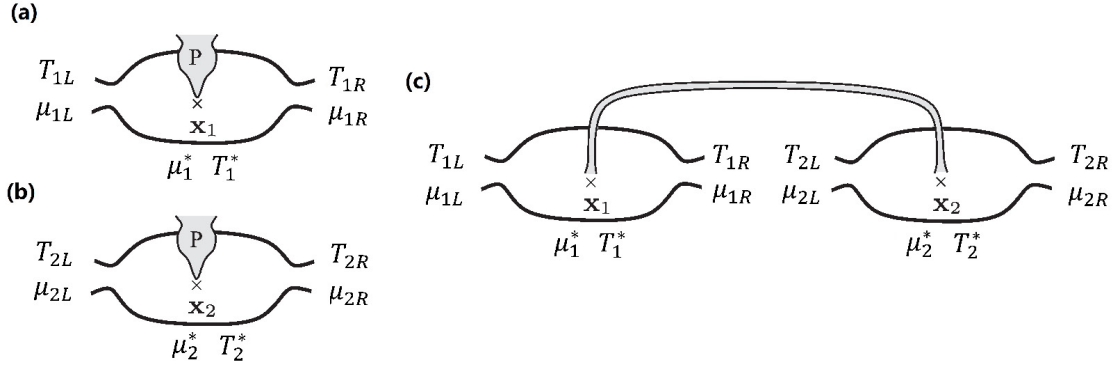


Figure 31: (a) and (b): Two independent systems sequentially probed by the same probe at local positions x_1 and x_2 . (c) A transmission line is locally coupled to the positions at x_1 of system 1 and x_2 of system 2. Here, T_1^* (T_2^*) and μ_1^* (μ_2^*) are the probe-measured local temperature and local electrochemical potential of system 1 (2). Reprinted with permission from [143]. Copyright 2014 American Physical Society.

Figure 31(a) and (b) show two independent two-terminal nanojunctions. The electron reservoirs in contact with the systems are in an equilibrium state in the absence of the thermal and electrical biases across the junction. The values of the equilibrium temperature and electrochemical potential are assumed to be T_0 and μ_0 for each reservoir [199]. Once the thermal and electrical biases are imposed on the junctions, there is a pair of positions x_1 of system 1, and x_2 of system 2, in which a probe measures the identical μ^* and T^* . A transmission line then connects the position x_1 of system 1 to the position x_2 of system 2, with the same coupling strength as that of the probe; see Figure 31(c). When the bias voltage is sufficiently small, the net electric currents I and thermal current J between the two systems can be evaluated as [143]:

$$\begin{bmatrix} I \\ J \end{bmatrix} = \begin{bmatrix} \mathcal{M}(E) & a \partial_E \mathcal{M}(E) \\ a \partial_E \mathcal{M}(E) & \mathcal{M}(E) \end{bmatrix}_{E=\mu_0} \begin{bmatrix} \mu_2^* - \mu_1^* \\ (T_2^* - T_1^*)/T_0 \end{bmatrix}, \quad (65)$$

in the linear response regime. Here the coefficient $a = (\pi k_B T_0)^2/3$, and $\mathcal{M}(E)$ is the transmission coefficient between the two connected systems. Equation (65) implies that the net currents through the line cancel when the local temperature and the local electrochemical potential of the connected positions are identical. In this case, the two systems will be in equilibrium with each other, when connected by a transmission line coupled locally to the connected positions. This equilibrium condition has been extended to a non-interacting electron system beyond the linear response regime [410]: If the T^* and μ^* of the two systems under small bias are equal, there will be no energy/particle flow between the systems when connected by a transmission line coupled locally to the connected positions.

Another scenario has also been discussed: Under what conditions two different thermometers yield the same value of local temperature for the same non-equilibrium system [410]? A sufficient condition has been proposed for

the zeroth law as follows. Consider an electron system consisting of many orbitals, denoted by i, j, \dots , weakly coupled to a probe with a broadband width. If the probe is only coupled to a single orbital n of the system, the probe-system tunneling matrix $\Gamma^p(\omega)$ has only one non-zero element $\Gamma_{ij}^p(\omega) = \bar{\Gamma}^p(\mu_0)\delta_{i,n}\delta_{n,j}$. In the case of such system-probe coupling, the values of local temperature and local electrochemical potential depend only on the non-equilibrium state of the system to which the probe is coupled. These values are thus independent of the properties of the probe. The weak system-probe coupling ensures that a temperature measurement does not strongly perturb the microstates of the system.

The First Law – Consider a fermionic non-interacting system subjected to bias. A broadband probe is coupled to a single orbital of the system and obtains the local temperature T_1^* and local electrochemical potential μ^* . A small change is imposed on the bias. This change finally leads the system to a new non-equilibrium steady state which is assumed to be characterized by the same value of the local electrochemical potential μ^* , but by a different local temperature T_2^* . In absence of the work done by the environment on the system, the heat flowing into the system can be evaluated by the first law [410]: $\Delta Q \equiv \Delta\langle E - \mu^*N \rangle$, where $\langle N \rangle$ and $\langle E \rangle$ are the mean occupation number and the energy of the orbital coupled to the probe, respectively. It has been found that if the local specific heat C_s of the system is properly defined, the heat ΔQ will satisfy [410]

$$\Delta Q = C_s(T_1^* - T_2^*). \quad (66)$$

The local specific heat C_s depends on both the local occupation number and the local DOS of the system sampled by the probe. Equation (66) shows that the first law associates the absolute local temperature difference $T_1^* - T_2^*$ with the heat ΔQ into the system [410].

The Second Law – For an interacting fermionic system in a steady state arbitrarily far from equilibrium, it has been shown that the local temperature is consistent with the Clausius's statement of the second law [410], that heat spontaneously flows from a hot body to a cold body.

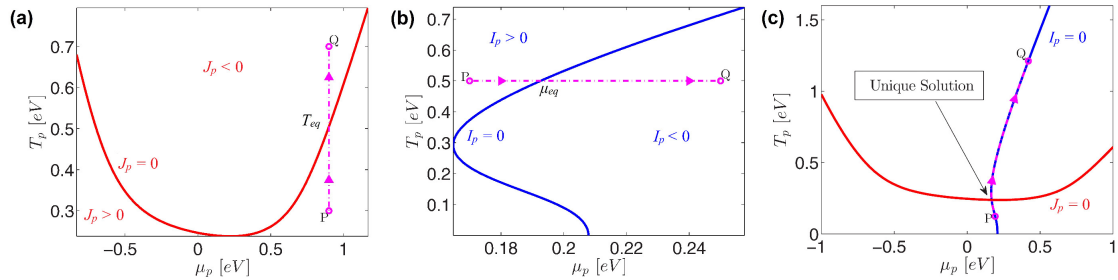


Figure 32: (a) Schematic diagram of the measurement of local temperature in a two-level system when $J_p = 0$. T_p largely depends on μ_p . The line from P to Q is at a constant electrochemical potential of the probe, and cuts the contour $J_p = 0$ at the point T_{eq} . In the point P , $J_p > 0$ means that the heat current flows into the probe, and in the point Q , $J_p < 0$ means that the heat current flows out of the probe. (b) Schematic diagram of the measurement of local electrochemical potential in a two-level system when $I_p = 0$. μ_p largely depends on T_p . The line from P to Q is at a constant temperature of the probe, and cuts the contour $I_p = 0$ at the point μ_{eq} . In the point P , $I_p > 0$ means that the charge current flows into the probe, and in the point Q , $I_p < 0$ means that the charge current flows out of the probe. (c) Schematic diagram of the simultaneous measurement of T^* and μ^* defined by ZCC. The contour PQ along $I_p = 0$ cuts the contour J_p once exactly, which implies the unique result of Eq. (22) when it exists. Reprinted with permission from [243]. Copyright 2016 American Physical Society.

Consider, for instance, a temperature probe weakly coupled to a two-level system sandwiched by two electron reservoirs under bias voltage [243]. The local temperature T^* of the system is determined as $T^* = T_p$ when the heat current between the system and the probe vanishes, namely $J_p(\mu_p, T_p) = 0$, so that a thermal equilibrium state is considered to be established between the system and the temperature probe. By keeping $J_p(\mu_p, T_p) = 0$ in the temperature measurement, the probe temperature T_p can be expressed as a function of the electrochemical potential μ_p of the probe; see Figure 32(a). When the probe is biased away from the thermal equilibrium state of the system, the probe temperature T_p will become hotter or colder than T_{eq} , the value of the contour $J_p = 0$ at a specific μ_p ; see the line PQ in Figure 32(a). Consequently, a temperature gradient is established across the system-probe contact, and the heat current driven by this temperature gradient will flow through the contact. If T_p is hotter than T_{eq} , such as the point Q in Figure 32(a), the heat current will flow from the probe into the system, namely $J_p < 0$, and vice

versa. Analogously, when a voltage probe is weakly coupled to the two-level system [243], the local electrochemical potential of the system is obtained as $\mu^* = \mu_p$ in the case of $I_p(\mu_p, T_p) = 0$. Figure 32(b) shows the dependence of the probe electrochemical potential μ_p on the probe temperature T_p . The charge current will spontaneously flow from the side with a high electrochemical potential to the side with a low one. From the above analysis, the direction in which heat/charge current flows through the system-probe contact has been pointed out: heat spontaneously flows from a hot body to a cold body, and charge spontaneously flows from a body with a high electrochemical potential to a body with a low one. Therefore, the local temperature/chemical potential defined by the ZCC is consistent with the Clausius's statement of the second law.

Since T_p largely depends on μ_p for the temperature measurement, the unique measurement of local temperature T^* requires the knowledge of μ_p . Similarly, a known T_p is necessary for the unique measurement of local electrochemical potential μ^* . In a word, to obtain a unique result of T^* and μ^* , it is necessary to measure both temperature and voltage simultaneously. Jacquet has analytically shown that the values of T^* and μ^* are uniquely determined by simultaneous voltage and temperature measurements for a non-interacting electron system in the linear response regime [411]. Stafford *et al.* have analytically and numerically shown that the simultaneous measurement of temperature and electrochemical potential uniquely yields T^* and μ^* in an interacting electron system arbitrarily away from equilibrium [243]. Figure 32(c) shows the numerical simulation for simultaneous measurements of T^* and μ^* defined by the ZCC in a two-level system. Only one point can be found along $I_p = 0$ that also satisfies $J_p = 0$, which implies a unique result of the ZCC.

The Third Law - By carefully defining a local non-equilibrium entropy of a fermionic system in a non-equilibrium steady state, the local temperature has been found to be consistent with the Nernst's statement of the third law [412–414], that it is impossible for any process, no matter how idealized, to reduce the entropy of a system to its absolute-zero value in a finite number of operations [415]. The local non-equilibrium entropy $S(\mathbf{x})$ is defined as follows [414]

$$S(\mathbf{x}) = \sum_{\alpha} \int d\omega g_{\alpha}(\omega; \mathbf{x}) s(f_{\alpha}) + \sum_l |\psi(\mathbf{x})|^2 s(f_l). \quad (67)$$

Here, $g_{\alpha}(\omega; \mathbf{x}) = \text{tr}\{A_{\alpha}(\omega; \mathbf{x})\}$ is the local DOS at the position \mathbf{x} of the system due to scattering states incident on the system from reservoir α . The spectral function $A_{\alpha}(\omega) = \frac{1}{2\pi} \mathbf{G}(\omega) \mathbf{\Gamma}(\omega) \mathbf{G}^{\dagger}(\omega)$ takes into account the system-reservoir tunneling matrix $\mathbf{\Gamma}$ and the NEGF \mathbf{G} ; $s(f_{\alpha})$ is defined as $s(f_{\alpha}) = -k_B \{f_{\alpha}(\omega) \ln f_{\alpha}(\omega) + [1 - f_{\alpha}(\omega)] \ln [1 - f_{\alpha}(\omega)]\}$, where f_{α} is the Fermi-Dirac function of the reservoir α ; f_l is the occupation number of the l -th localized state of the system, and $\psi_l(\mathbf{x})$ is the wave-function of the l -th localized state. It has been analytically shown in [412–414] that the local entropy $S(\mathbf{x})$ asymptotically converges to zero as $T^* \rightarrow 0$, consistent with the third law of thermodynamics.

4.1.2. A scale of local thermal fluctuations and excitations

As already reviewed in Sec. 2.2.4, the FDR-based definition of local temperature provides a measure of local fluctuations in a non-equilibrium nanosystem. Here, we will go beyond the FDR, focus on the attempts to establish a generic non-equilibrium FDT in an open quantum system out of equilibrium, and analyze the applicability of the existing FDT to define a local temperature.

Prost *et al.* have proposed a generic FDT applicable for any system with Markovian dynamics in a non-equilibrium steady state [416]. The small variations of observables are applied around the steady state of a classical system which is defined by a set of observables denoted by \mathbf{c} , such as positions, velocities and other parameters. The state of the system is controlled by a set of parameters λ . For fixed values of the control parameters λ , a steady state is assumed which is characterized by its probability distribution function $\rho_{\text{ss}}(\mathbf{c}; \lambda)$. When small variations of the control parameters $\delta\lambda(t) \equiv \lambda(t) - \lambda^{\text{ss}}$ are imposed on a steady state value λ^{ss} , the non-equilibrium FDT reads [416]:

$$\left\langle \frac{\partial \phi(\mathbf{c}(t); \lambda^{\text{ss}})}{\partial \lambda_{\alpha}} \right\rangle = \int_{t_i}^t dt' \chi_{\alpha\gamma}(t - t') \delta\lambda_{\gamma}(t'), \quad (68)$$

where $\chi_{\alpha\gamma}(t - t')$ is the response function in the steady state of the system, and the potential $\phi(\mathbf{c}; \lambda)$ is defined by $\phi(\mathbf{c}; \lambda) = -\log[\rho_{\text{ss}}(\mathbf{c}; \lambda)]$. The FDT of Eq. (68) has been generalized to any Markovian quantum system [417]. Although the temperature is not explicitly involved in Eq. (68), the changes of temperature still have an effect on the parameters λ [416], and the response function may depend on temperature.

Zhang *et al.* have presented a general theory of non-Markovian dynamics for an open quantum system consisting of non-interacting particles [136, 418]. A non-equilibrium FDT has been proposed [136, 419]

$$v(\tau, t) = \int_{t_0}^{\tau} d\tau_1 \int_{t_0}^{\tau} d\tau_2 u(\tau, \tau_1) \tilde{g}(\tau_1, \tau_2) u^{\dagger}(t, \tau_2), \quad (69)$$

where the NEGF u describes the dissipation dynamics of the system, and the NEGF v characterizes the non-equilibrium fluctuations inside the open system. The non-Markovian interactions between the system and the environment are taken into account by the self-energy correction \tilde{g} .

In the steady state limit $t \rightarrow \infty$, the function v can be expressed as $v(t, t)|_{t \rightarrow \infty} \equiv \int d\omega \chi(\omega)$ [418, 420, 421]. The non-equilibrium FDT then reads [420, 421]

$$\chi(\omega) = [D_l(\omega) + D_d(\omega)]f(\omega, T^*), \quad (70)$$

in a steady state. Here, the first term $D_l(\omega)$ on the r.h.s. of Eq. (70) arises from the particles in localized bound states of the system, and the dissipation spectrum $D_d(\omega)$ is the contribution from the particles moving into the environment. $f(\omega, T^*)$ is the Bose or Fermi distribution function of particles, depending on the system being made of bosons or fermions. If there is no particle in the localized states, $D_l(\omega)$ will become zero, then [418, 421]

$$\chi(\omega) = D_d(\omega)f(\omega, T^*). \quad (71)$$

Equation (71) resembles the formulation of the equilibrium FDT at temperature T^* in the particle number representation [418, 421]. T^* in Eq. (71) then provides a scale of local fluctuations of a nanosystem in a non-equilibrium steady state.

4.1.3. Local properties of nanosystems

Ye *et al.* have studied the effect of bias-induced electronic excitations on a local observable $\langle \hat{O} \rangle$ [183]. For a non-interacting QD, it has been analytically shown in [183] that the MPC-defined local temperature not only characterizes the magnitude of the electronic excitations, but also establishes a correspondence relation for $\langle \hat{O} \rangle$ between a non-equilibrium QD and a reference equilibrium QD

$$O_0(T_L, \mu_L; T_R, \mu_R) = O_0(T^*, \mu^*; T^*, \mu^*), \quad (72)$$

in the broadband limit, provided that the zero perturbation condition

$$\frac{\delta O_p(T_p, \mu_p)}{\Delta_p} \Big|_{T_p=T^*, \mu_p=\mu^*, \Delta_p \rightarrow 0} = 0, \quad (73)$$

can be satisfied. Here, Δ_p is the dot-probe coupling strength, and $O_o(T_L, \mu_L; T_R, \mu_R)$ is the expectation value of $\langle \hat{O} \rangle$ in the absence of the probe, with the lead $\alpha = L, R$ subjected to T_α and μ_α . As shown in Figure 33(a), the physical significance of T^* is clarified as follows: the electronic excitations induced by a bias voltage or temperature gradient can be equivalently characterized as thermal excitations induced by a uniform equilibrium temperature. This relation provides a microscopic interpretation of the MPC-based definition of local temperature.

When the bandwidth of the leads is finite, the correspondence relation still holds under a small bias voltage $V = (\mu_R - \mu_L)$:

$$O_0(T_L, \mu_L; T_R, \mu_R) = O_0(T^*, \mu^*; T^*, \mu^*) + O(V^2), \quad (74)$$

provided the zero perturbation condition of Eq. (43) is satisfied. Here, a voltage-dependent higher order term $O(V^2)$ emerges due to the finite bandwidth.

Figure 33(b) shows the numerical verification for the correspondence relation between a non-equilibrium QD and a reference QD, by comparing the relative deviation for local magnetic susceptibility χ^m of the two systems. For T^* determined by the MPC, the deviation appears to be vanishingly small in regions I and III; while in region II the deviation remains appreciable. The explanation of such large deviation is that the dot is in a near-resonance situation, local and non-local excitations could both take place, and the zero perturbation condition of Eq. (73) is not achievable.

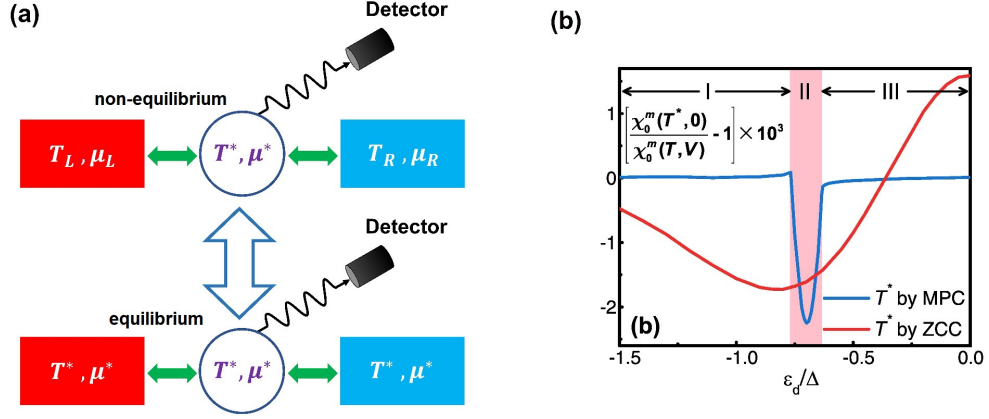


Figure 33: (a) Schematic illustration of the relation defined by Eq. (72). The local observable $\langle O_o \rangle$ of a non-equilibrium QD (upper panel) can be made equivalent to that of a reference equilibrium QD (lower panel), provided the two dots have the same local temperature T^* . (b) The relative deviation between $\chi^m(T, V) \equiv \frac{\partial \langle \hat{n}_z(T, V) \rangle}{\partial H_z} |_{H_z \rightarrow 0}$ and $\chi^m(T^*, 0)$ versus ϵ_d for a non-interacting QD under a bias voltage V . The temperature gradient across two leads is set to zero, $T_R = T_L = T$. Reprinted with permission from [183]. Copyright 2016 American Physical Society.

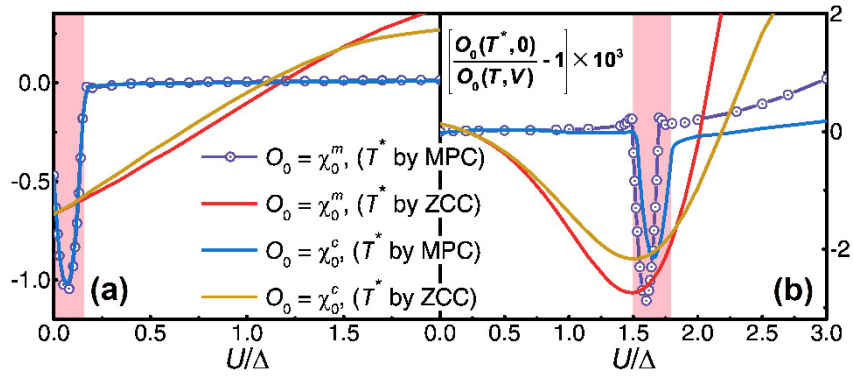


Figure 34: The relative deviations between $O_0(T, V)$ and $O_0(T^*, 0)$ for two observables O_0 versus the Coulomb interaction energy U for an interacting QD under a bias voltage V at the background temperature (a) $T = \Delta$ and (b) $T = 0.1\Delta$. The MPC is imposed on the local magnetic susceptibility $\chi^c \equiv -\frac{\partial \langle \hat{n}_d \rangle}{\partial \epsilon_d}$ and local charge susceptibility χ^m . The temperature gradient across two leads is set to zero, $T_R = T_L = T$. Reprinted with permission from [183]. Copyright 2016 American Physical Society.

The correspondence relation for an interacting QD has been verified by employing a numerical approach [109]. The relative deviations between $O_0(T, V)$ and $O_0(T^*, 0)$ are shown in Figure 34 for two choices of the local observable $\langle \hat{O} \rangle$ —the local magnetic susceptibility χ^m and the local charge susceptibility χ^c . The MPC-defined T^* leads to rather minor deviations so long as the zero perturbation condition can be achieved, except for the interaction strength in the shaded region of Figure 34. In that case, as for non-interacting electrons, the dot is in a near-resonance situation, and the local and non-local excitations could both take place, where the correspondence relation for local observables does not hold.

In Figure 34(b), the deviation between $\chi^m(T, V)$ and $\chi^m(T^*, 0)$ appears to be a small but finite value around the Coulomb energy $U = 3.0\Delta$. This is because the Kondo resonant states inside the QD start to emerge as U increases. Under a bias voltage, the Kondo resonant states facilitate the electron co-tunneling processes, which can be understood as the concurrence of local spin-flip and non-local electron-transfer excitations. Therefore, as in the case of the shaded region, the correspondence relation for local observables does not hold since local and non-local excitations both take place.

4.2. Practical applications

4.2.1. Quantum oscillations of local temperature in nanostructures

When a classical bulk system is in contact with two heat baths with different temperatures, heat will transfer from a hot bath, through the system, to a cold bath. The thermal transport finally establishes a temperature distribution across the system. When a bulk system is in the linear response regime, the Fourier’s law provides a good description for the thermal transport and the temperature distribution. However, if the size of the system is reduced to the nanoscale, which is comparable to or even smaller than the wavelength or mean free path of its constituent particles, the energy transport process will be significantly different from that in a bulk system due to the emergence of quantum coherence effects. The quantum effects will then give rise to quantum oscillations of the local temperature in the entire nanostructure as predicted in [140]. It has been found that the temperature oscillations in nanowires [140–142] strongly violate the Fourier’s law which predicts a linear temperature profile along a one-dimensional nanosystem [337, 422–424].

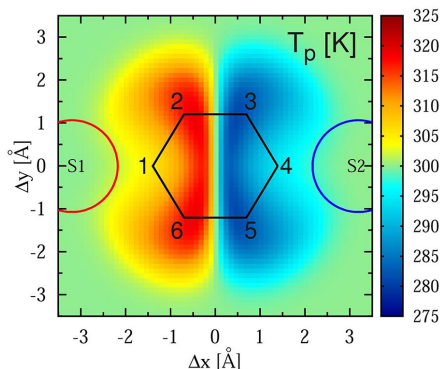


Figure 35: The calculated local temperature distribution of the BDT junction. Quantum oscillations of local temperature are visible in the vicinity of the molecule, which can be explained in terms of the charge transfer between the electrodes and the benzene ring. The ambient temperature is taken as $T_0 = 300$ K. Reprinted with permission from [425]. Copyright 2013 American Chemical Society.

Bergfield *et al.* have investigated the local temperature distribution in a benzenedithiol junction subjected to a thermal bias [425]. Figure 35 illustrates spatial oscillations of the local temperature around the molecule. The oscillations have been explained by the charge transfer from the electrodes with different temperatures into the benzene ring. The electrons from the electrodes with a specific temperature carry finite thermal energy, which can lead to local heating/cooling in nanostructures. Assuming that the left electrode is hotter than the ambient temperature and the right one is colder, the charge transfer mechanism between the electrodes and the molecule [425] indicates that electrons from the hot side (S1) can move to atoms 2, 4, and 6, while electrons from the cold side (S2) can move to atoms 1, 3, and 5. Therefore, the atoms 3 and 5 appear colder than the ambient temperature and the atoms 2 and 4 appear hotter, as displayed in Figure 35. Taking into account that the atoms 1 and 4 are in proximity to the hot and cold

electrodes, respectively, the temperature of the electrodes washes out the temperature oscillations around the atoms 1 and 4. Therefore, local temperature oscillations could be understood as a result of the quantum interference of heat flow from the electrodes with different temperatures [425].

Other numerical calculations have predicted the emergence of quantum oscillations of local temperature in various nanostructures [243, 334, 412, 425]. However, the ranges of these temperature oscillations in nanosystems are usually less than 1 nm, which is beyond the spatial resolution of the present thermometry [404]. To find a condition under which the range of the temperature oscillations can be brought within the spatial resolution of present techniques in thermal microscopy, theoretical efforts have been made to simulate the local temperature distribution in a realistic system, such as a graphene flake under a thermal bias [145]. It has been found that the wavelength of the temperature oscillations in a graphene flake is related to that of the Friedel oscillations, an equilibrium property that results from long-range interferences in the local DOS. The wavelength of the Friedel oscillations λ in a graphene flake can be controlled by the Fermi energy μ of the flake, namely $\lambda \propto (\mu - \mu_{\text{Dirac}})^{-1}$. As the Fermi energy μ approaches the Dirac point μ_{Dirac} of the graphene, the wavelength of the temperature oscillations grows dramatically [145]. Figure 36(a)

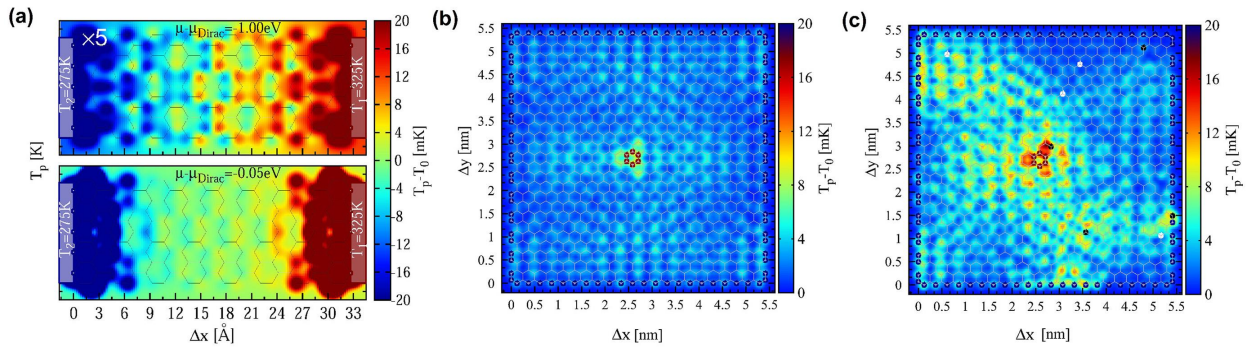


Figure 36: (a) The calculated spatial temperature profile for a graphene flake. The values in the upper panel are multiplied by a factor of five. By adjusting $\mu - \mu_{\text{Dirac}}$ the temperature oscillation wavelength can be tuned. The ambient temperature is taken as $T_0 = 300 \text{ K}$. (a) from [426]. The simulated temperature distribution of a graphene flake without (b) and with (c) impurities (white and black circles). A hot needle-like terminal (red circles) is located in the center of the flake, and the edge of the flake held at ambient temperature $T_0 = 300 \text{ K}$ by cold electrodes (blue circles). The existence of impurities significantly affects the temperature field. Reprinted with permission from [145]. Copyright 2015 American Physical Society.

shows that when $\mu - \mu_{\text{Dirac}} = -1.00 \text{ eV}$ in the upper panel Figure 36(a) the quantity λ is evaluated as 3.8 \AA [426], and there are relatively large oscillations in the middle of the graphene. When $\mu - \mu_{\text{Dirac}} = -0.05 \text{ eV}$ in the lower panel Figure 36(a) the wavelength λ increases to $\sim 10 \text{ \AA}$ [145]. The temperature oscillations almost vanish in the middle of the graphene flake due to its finite size. In practice, the Fermi energy of a graphene flake can be continuously tuned by applying a gate voltage on the flakes [427, 428]. Thus, the local temperature oscillations may be observed in a realistic system by applying a proper gate voltage. In addition, the numerical simulation of local temperature has been carried out on a graphene flake doped with impurities and vacancies [145]. Figure 36(b) and (c) suggest that these defects have a strong influence on the temperature distribution. Long-range temperature oscillations appear across the doped graphene. This result suggests that doping a graphene flake with defects may be an experimentally feasible method to observe local temperature oscillations in a realistic system.

4.2.2. Recovering Fourier's law at the nanoscale

The above studies suggest that quantum effects can produce spatial oscillations of the local temperature in nanostructures, thus violating the Fourier's law. This motivates the search for the conditions under which the quantum temperature oscillations vanish, and the Fourier's law is restored.

Efforts to understand how the Fourier's law in a one-dimensional model system may be recovered have been made previously by Dubi and Di Ventra [88, 89]. They considered a nanowire subjected to a thermal bias, and randomly tuned every on-site energy of the wires (for example, ϵ_i at the i th point of the wires) in a limited range $[-W, W]$, with W being the disorder strength [88]. The MPC-defined local electron temperature is then calculated as a function of

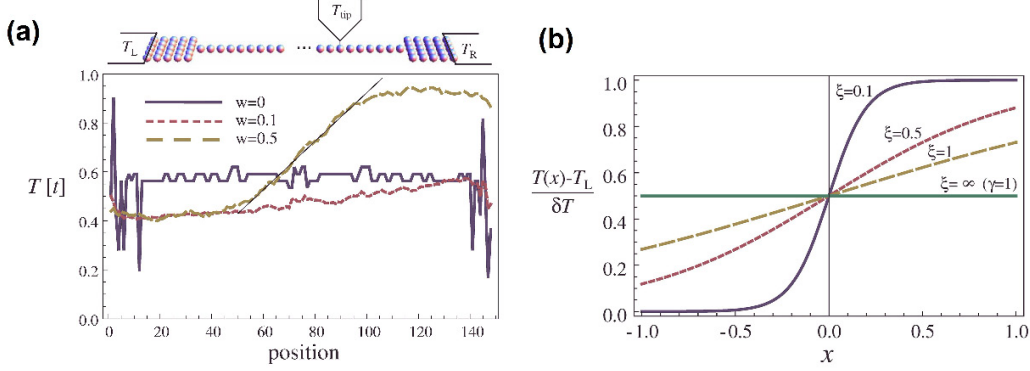


Figure 37: (a) Upper panel: Schematic representation of the calculation to determine the local temperature via the addition of a probe. A nanowire is coupled to the left and right leads (the solid lines at the edges). Lower panel: Local temperature as a function of the position x along the wire. The local temperature is calculated for three different values of disorder strength W . For the wire with $W = 0$ the temperature hardly changes along the wire, while a uniform temperature gradient builds up as the disorder strength W increases (showed by a thin solid line). Reprinted with permission from [88]. Copyright 2009 American Physical Society. (b) The normalized local temperature $[T(x) - T_L] / \delta T$ as a function of the position variable x along the wire. The local temperature is calculated for three different values of dephasing length L_ϕ . Here, ξ in the figure is the L_ϕ in the main text. In this figure, the position variable is defined as $x \equiv \frac{l}{L} - 1$, with the position l , and the length of the nanowire L . The value $x = -1$ is equivalent to $l = 0$ and $x = 1$ corresponds to $l = L$. $\delta T \equiv T_R - T_L$ is the temperature gradient across the nanowire. The temperature T in the two figures is the local electron temperature defined by Eq. (42). Reprinted with permission from [89]. Copyright 2009 American Physical Society.

the positions along the wire under different W . The results in Figure 37(a) illustrate that strong disorder strength gives rise to the Fourier's law at the nanoscale.

This crossover from the ballistic (the Fourier's law is invalid) to diffusive (the Fourier's law is valid) regime could be interpreted in terms of electronic dephasing. To discuss the condition for the dephasing, the characteristic length L_ϕ is introduced, which describes the length over which the electronic wave-function retains its phase [89]. If the length L_ϕ is greater than the length of the nanowire L , namely $L_\phi \geq L$, the dephasing has no effect and thermal transport is ballistic, while for $L_\phi \leq L$ the thermal transport is in the diffusive regime due to the dephasing effect. Figure 37(b) shows the local temperature distribution under different characteristic lengths. With increasing L_ϕ the temperature gradient across the system vanishes, and a uniform temperature profile emerges as $L_\phi \rightarrow \infty$. This change of the temperature profile corresponds to the crossover of thermal transport from the ballistic to the diffusive regime. The disorder in a nanowire breaks the quantum phases of the electronic wave-functions [429–431] and reduces the length L_ϕ . When the disorder becomes sufficiently strong, $L_\phi \leq L$, and electronic dephasing occurs in the nanowire. The Fourier's law is thus retrieved in such a strongly-dephased system [89].

Since the dephasing mechanism has successfully explained how the Fourier's law can be recovered in some model systems, several theoretical efforts were made to explain the emergence of the Fourier's law in realistic systems by disorder or dephasing [432]. However, retrieving the Fourier's law in realistic systems, such as molecular junctions, would require a very strong disorder or dephasing to make L_ϕ shorter than the scale of the junction. This, in turn, would likely destroy the covalent bonds of the molecule [432, 433], effectively breaking the molecule.

To address this issue, Inui *et al.* have studied the Fourier's law in graphene flakes subjected to a thermal bias [433]. Figure 38 shows the calculated local temperature distribution for two different graphene-electrode contact geometries [433]. In the type I contact only the left and right edges of the flake couple to the electrodes, while for type II contact two electrodes cover three edges of the flake, leading to a stronger coupling. Compared with the temperature distribution for the type I contact, the temperature distribution for the type II contact is closer to the classical results predicted by the Fourier's law. This can be seen clearly from Figure 39(a) which compares the temperature profiles along the line $y = 0$ for each contact type.

The different nature of thermal transport for the contact types I and II can be understood from the DOS of the system, $g(E)$, shown in Figure 38. For the type I contact, $g(E)$ exhibits a sequence of sharp peaks, corresponding to the energy eigenfunctions of the graphene flake. A sharply peaked DOS implies that the system is in the resonant-tunneling regime, where thermal transport is controlled by the wave-function of a single resonant state. In contrast, the type II contact has a smooth DOS which indicates that many quantum states contribute to thermal transport, so that

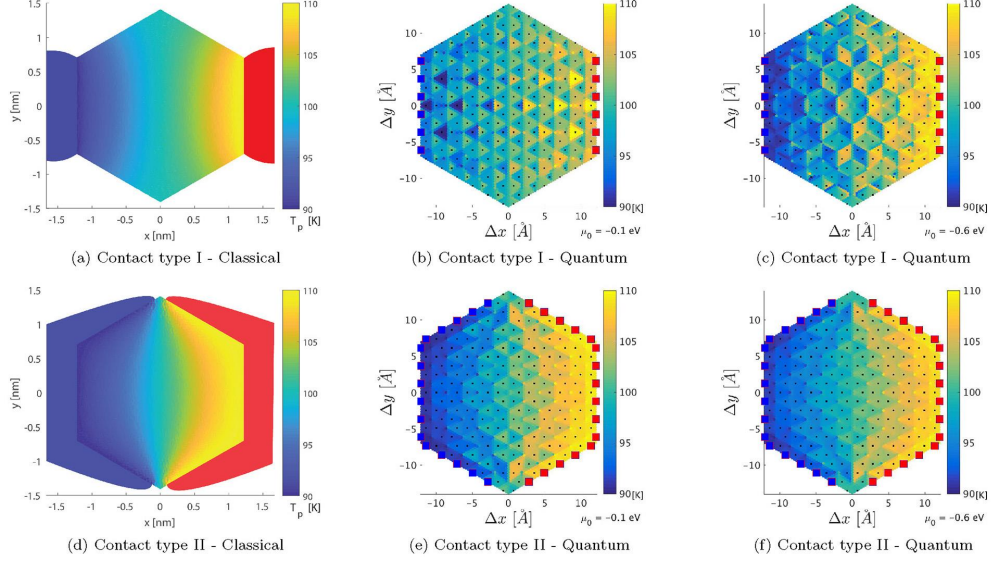


Figure 38: The classical (a, d) and local (b, c, e, f) temperature distribution of a graphene flake under thermal bias for two contact geometries. In type I contact (top panels), only the left and right edges of the flake couple to the electrodes. In type II contact, two electrodes cover three edges of the flake, leading to a stronger coupling. The classical temperature distribution is evaluated by the Fourier's law, and the local temperature is given by Eq. (22). The local temperature calculations are at Fermi energies $\mu_0 - \mu_{Dirac} = -0.1$ eV (b, e) and $\mu_0 - \mu_{Dirac} = -0.6$ eV (c, f). The hot electrode (red) and cold electrode (blue) is held at 110 K, and the cold electrode (blue) is held at 90 K. The squares indicate the carbon atoms covalently bonded to the hot (red) and cold (blue) electrodes. The local temperature distributions for type I contact exhibit strong oscillations that depend on μ_0 , while for type II contact, the distributions resemble the classical distribution. Reprinted with permission from [433]. Copyright 2018 American Chemical Society.

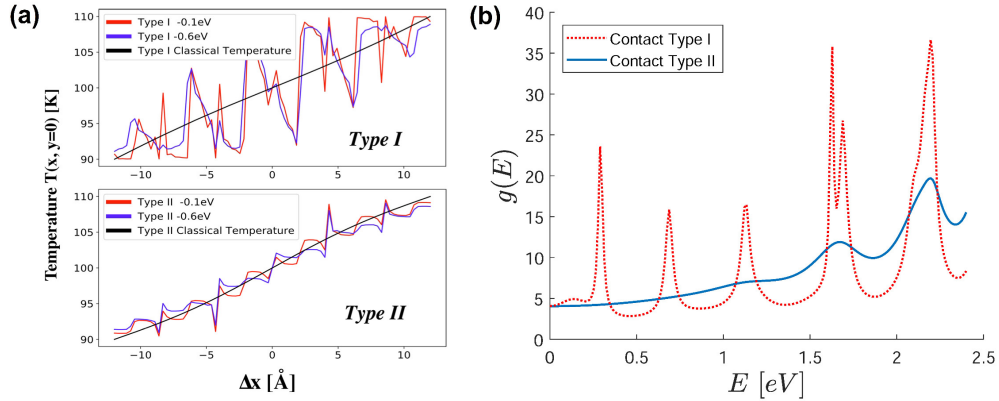


Figure 39: (a) Temperature profiles along the centerline of the system ($y = 0$) for each contact type and the Fermi energy shown in Figure 38. In the type II contact, the temperature profile is much closer to that predicted by the Fourier's law. (b) Calculated DOS, $g(E)$, of a graphene flake junction for two different contact geometries. The DOS for the type I contact exhibits a sequence of sharp peaks, while the type II contact exhibits a smooth, nearly featureless DOS. Reprinted with permission from [433]. Copyright 2018 American Chemical Society.

temperature oscillations tend to average out. From the above analysis, these authors have put forward the following hypothesis for recovering Fourier’s law in a realistic system [433]: if sufficient quantum states participate in thermal transport across the system, the Fourier’s law will emerge; when transport occurs in or near the resonant-tunneling regime, there is no classical behavior for the temperature distribution.

4.2.3. Laser-induced ultrafast adsorption dynamics of molecules on metal surfaces

The dynamics of molecules from one adsorption site to another is the most elementary process of bond-breaking and -making on a surface, and is a key step in processes such as catalysis [434]. The time when reactants are rearranged into products is merely of the order of a few hundred femto-seconds. Therefore, understanding ultrafast adsorption dynamics of these molecules on metal surfaces is of fundamental importance in the field of catalysis. Numerous experiments have studied the ultrafast elementary motions of adsorbates on metal surfaces by means of high time-resolution techniques [435–440]. In these experiments, the molecular motion is generally triggered by femto-second laser pulses, which rapidly excite surface electrons to a high energy level. To characterize the magnitude of the thermal excitation for electrons or vibrational modes, the concept of the electron or phonon temperature has been used in adsorption dynamics. The temporal and spatial evolution of these two temperatures can be evaluated quantitatively by the two-temperature model [70, 441, 442], which describes the thermal response of a metal surface to a ultrashort laser pulse. The changes of two temperatures reflect the energy exchange between the laser-excited surface electrons and the vibrational modes of the adsorbates and surface lattice.

Based on the two-temperature model, Lončarić *et al.* have theoretically investigated the laser-induced desorption of O₂ from Ag(110) [443], using the Langevin equation to describe the dynamics of each atom of the molecule [444, 445]. Figure 40(a) shows the model of the molecule position in the four adsorption sites, and Figure 40(b) shows the time dependence of the electron and phonon temperatures obtained by the two-temperature model, in comparison with the time evolution of the desorption rate for each adsorption site. Laser pluses imposed at the initial time rapidly excite electrons in the metal surface to several thousands Kelvin due to a relatively low electron heat capacity of metals. The electron-phonon interaction then transfers the energy from electrons to phonons which finally reach a thermal equilibrium state with each other. Compared with the evolution of the two temperatures, the behavior of the desorption rate of different positions illustrates that the desorption mechanism for O₂ depends on the adsorption configuration. The desorption rates for the hollow positions (H001 and H110) seem to follow the time evolution of the electron temperature, but with some time delay. These results suggest desorption from the hollow sites is mainly an electron mediated effect, where the energy transfer from the electrons excited by the laser pulse to the adsorbed molecule plays a dominant role [443]. In contrast, the desorption rates from the bridge sites (SB and LB) do not seem to be very much affected by the high increase of electron temperature at the beginning. In these sites, the highest values of the desorption rates occur at longer times, once the electron and phonon temperatures are equilibrated. This suggests that the heating of electrons is not that important for desorption from the bridge sites, and that the laser mediated phonon excitation is the relevant mechanism in these sites [443].

Novko *et al.* have also used the two-temperature model to understand the laser-induced ultrafast dynamics of CO adsorbates on Cu(100) [446]. A DFT calculation has been employed to investigate the frequency and linewidth changes of the CO internal stretch mode on the metal surface. It has been found that two distinct processes give rise to these changes: electron-hole pair excitations result in the frequency shifts, while electron-mediated vibrational mode coupling gives rise to linewidth changes. Since the electron temperature affects the electron-hole pair excitations and the electron-mediated vibrational mode coupling depends on both electron and phonon temperatures [447], the electron and phonon temperatures play an important role in laser-induced ultrafast dynamics.

4.2.4. Local temperature of Kondo systems

Lobaskin and Kehrein have used a time-dependent local temperature to characterize the formation of the Kondo singlet [448]. These authors have focused on a Kondo model system under a small periodic perturbation with frequency ω . The local temperature $T^*(t_w)$ is defined by the FDR expressed as follows [448, 449]:

$$\lim_{\omega \rightarrow 0} \frac{\text{Im}R(\omega, t_w)}{\omega} = \frac{1}{2T^*(t_w)} C_{[A,A]}^{(\text{cum})}(\omega = 0), \quad (75)$$

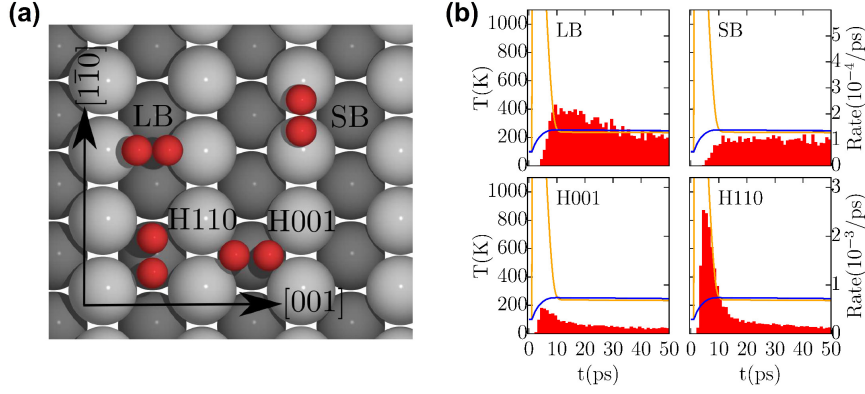


Figure 40: (a) Sketch of the position of the O_2 molecules (red ball) in the four adsorption sites: long bridge (denoted LB), short bridge (denoted SB), hollow along the $[1\bar{1}0]$ direction (denoted H110), and hollow along the $[001]$ direction (denoted H001). (b) The electron (orange line) and phonon (blue line) temperatures calculated from the two-temperature model as a function of time from the four adsorption sites. The electronic temperature peaks at values larger than 6000 K. The desorption rates are also shown by the histograms. Reprinted with permission from [443]. Copyright 2016 American Physical Society.

in the zero frequency limit. Here, the imaginary part of the response function $R(\omega, t_w)$

$$R(\omega, t_w) = 2i \int d\tau \theta(\tau) C_{[A,A]}(t_w + \tau, t_w) e^{i\omega\tau} = i \int d\tau \theta(\tau) \langle [\hat{A}(t_w + \tau), \hat{A}(t_w)] \rangle e^{i\omega\tau}, \quad (76)$$

describes the energy dissipated from the system after time t_w . $C_{[A,A]}^{(\text{cum})}(\omega)$ is the Fourier transform of the second-order cumulant of the two-time correlation function $C_{[A,A]}(t, t') = 1/2 \langle \{\hat{A}(t), \hat{A}(t')\} \rangle$, and reads

$$C_{[A,A]}^{(\text{cum})}(t, t') = C_{[A,A]}(t, t') - \langle \hat{A}(t) \rangle \langle \hat{A}(t') \rangle, \quad (77)$$

with an operator \hat{A} .

Equation (77) has been applied to a Kondo model system at zero temperature. The local temperature is defined from the above FDR imposed on the spin-spin correlation function $C_{S_z, S_z}^{(\text{cum})}$ with S_z being the impurity spin. The system is prepared in an initial state with a frozen impurity spin, then allowed to relax after $t_w = 0$. Figure 41 shows a relaxation of the non-equilibrium initial state towards an equilibrium state. The local temperature first rises up quickly as a function of time until it reaches a maximum of $T^* \simeq 0.45T_K$ at $t_w = 0.03t_K$. After that, T^* decreases and nearly reaches zero. Here, T_K is the Kondo temperature and t_K is the time scale, defined as $t_K = 1/T_K$. This aging effect is interpreted in terms of the formation of the Kondo singlet. The Kondo singlet starts building up at $t_w = 0$. In the vicinity of the impurity, the conduction band electrons get locally heated up due to the release of the binding energy, when the Kondo singlet is being formed. After a sufficiently long time the Kondo singlet has been formed, the binding energy diffuses away, and the local temperature nearly becomes zero.

Kehrein *et al.* have calculated the local temperature defined by the FDR imposed on various operators [450, 451], and have presented a dependence of T^* on the choice of the operator \hat{A} . It has been found that a large deviation among these local temperatures, calculated from different operators, starts to emerge when the system-bath coupling becomes strong [451].

4.2.5. Local electrochemical potential of two-dimensional networks

Analogous to the role of local temperature in thermal transport at the nanoscale, the knowledge of local electrochemical potential is not only important as a source of information about electrical properties of a nanosystem, but also is of fundamental importance to understand and explore charge transport at the nanoscale [452–454]. In practice, a local electrochemical potential of electrons can be measured by a scanning tunneling potentiometry with the spatial resolution down to several nanometers [455–458]. Figure 42(a) exhibits the principle of a scanning tunneling potentiometry: when the potentiometry probe is above the site \mathbf{r} of the sample, the electrochemical potential of the probe

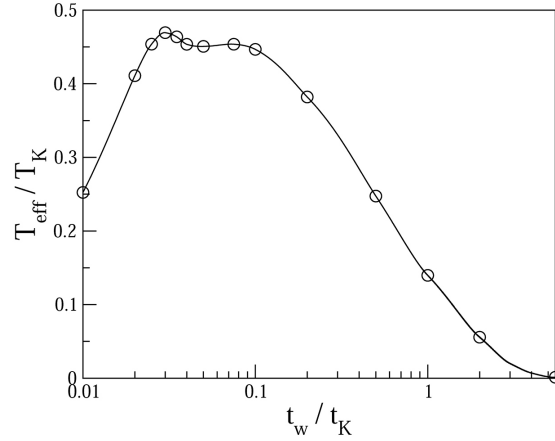


Figure 41: Local temperature T^* as a function of time t_w in a Kondo model. After a rapid increase to the maximum, T^* eventually approaches zero. The size of the circles indicates the magnitude of the numerical error of the calculated data. T_K is the Kondo temperature and t_K is the time scale, defined as $t_K = 1/T_K$. T_{eff} is T^* in this review. Reprinted with permission from [448]. Copyright 2006 Springer Nature.

$\mu_p(\mathbf{r})$ is adjusted such that there is a zero net electric current flowing between the probe and the network [452].

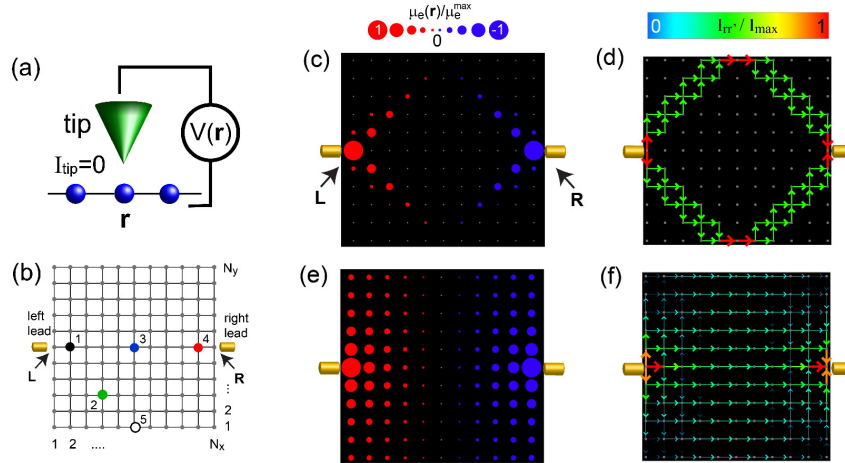


Figure 42: (a) Schematic representation of the principle of a scanning tunneling potentiometry: when the potentiometry probe is above a site \mathbf{r} of the network, its potential $\mu_p(\mathbf{r}) = eV(\mathbf{r})$ is adjusted so that there is a zero net current flowing between the probe and the network. Here $V(\mathbf{r})$ is the voltage of the probe. (b) Schematic of the two-dimensional network of electronic sites that are coupled to two narrow leads with different voltages. (c-d) plot the normalized μ^*/μ_{max} for electron-phonon interaction strength $g = 0.01t^2$ and $g = 500t^2$ with the energy scale t , and (e-f) plot the corresponding normalized current $I(\mathbf{r}, \mathbf{r}')/I_{\text{max}}$. Reprinted with permission from [12]. Copyright 2017 American Physical Society.

Referring to the principle of a scanning tunneling potentiometry, a theoretical approach based on the ZCC has been proposed to image the local electrochemical potential distribution of a two-dimensional network [12, 459–461]: one weakly couples a voltage probe to a two-dimensional network shown in Figure 42(b), and shifts the $\mu_p(\mathbf{r})$ at every site such that the current $I_p(\mathbf{r})$ between the probe and a site \mathbf{r} in the network vanishes. By keeping $I_p(\mathbf{r}) = 0$, the local electrochemical potential $\mu^*(\mathbf{r})$ is determined to be identical $\mu_p(\mathbf{r})$. Both the network and the probe are assumed in thermal equilibrium with the environment, and heat current between the probe and the network is not considered in [12].

Morr has studied the relation between the ZCC-defined local electrochemical potential and the electric current inside a two-dimensional network from the quantum to classical charge transport regime [12]. In the quantum regime, the electron-phonon interaction strength $g = 0$ describes a fully coherent system with an infinitely large elastic mean

free path of electrons. The increasing strength of the electron-phonon interaction strength g reduces the mean free path to a value much smaller than the scale of the network. A strong electron-phonon interaction leads to the electronic dephasing, and the charge transport in the network is in the classical regime when $g \rightarrow \infty$ [459]. Therefore, one can tune the network's charge transport properties from the quantum to classical regime by increasing g . The current $I_p(\mathbf{r})$ [461], and the current $I_{r,r'}$ between the sites \mathbf{r} and \mathbf{r}' of the network [462, 463] are both computed using the NEGF formalism. The spatial distributions of $\mu^*(\mathbf{r})$ and $I_{r,r'}$ are shown in Figure 42(c-f) under different g . It has been found that the Ohm's law relates $\mu^*(\mathbf{r})$ to $I_{r,r'}$, $I_{r,r'} = \sigma(\mathbf{r}, \mathbf{r}')[\mu^*(\mathbf{r}) - \mu^*(\mathbf{r}')]$, with $\sigma(\mathbf{r}, \mathbf{r}')$ being the electric conductivity between two neighboring sites [84]. For a small g , the charge transport is in the quantum regime and $\sigma(\mathbf{r}, \mathbf{r}')$ is site-dependent, while for a large g , the charge transport is in the classical regime and $\sigma(\mathbf{r}, \mathbf{r}')$ becomes a constant.

4.2.6. Local chemical potential of non-equilibrium magnons

Magnons, also known as the quanta of spin waves, are the quasi-particles of collective excitations representing electronic spins in a crystal lattice [464–466]. The creation and annihilation operators of a magnon fulfill the boson commutation relations. Being massless bosons, magnons at thermal equilibrium obey the Bose-Einstein distribution and the chemical potential is zero, since the magnon energy and particle number are not conserved [467–469]. In contrast, magnons in a non-equilibrium state can be characterized by a nonzero chemical potential. For instance, in a ferromagnet a magnon may interact with other magnons and with the crystal lattice. The interaction between the magnons and the lattice can conserve [470] or change [471] the number of magnons, depending on the specific form of the interaction. The relaxation times corresponding to different types of interactions are quite different. Take the ferromagnetic yttrium-iron-garnet (YIG) thin films as an example [467]. The thermal relaxation time due to two- or four-magnon scattering mechanisms can be as short as 100-200 ns, while the magnon-lattice relaxation time can be longer than 1 μ s. Consequently, when an external pumping is applied to a sample, the non-equilibrium magnons generated by pumping will thermalize rapidly by magnon-conserving interactions [469], and these thermalized magnons are practically decoupled from the crystal lattice [472]. When the rate of magnon generation balances the magnon decay rate, the number of magnons will eventually reach a constant, and thus a quasi-equilibrium state is established for magnons. Such a quasi-equilibrium state can be described by a Bose-Einstein distribution with a characteristic temperature and a finite chemical potential [467, 468, 473, 474]. Here, the nonzero chemical magnon potential is associated with the frequency of pumped magnons [472].

From all this it is clear that the concept of chemical potential is crucially important for the investigation of the Bose-Einstein condensation (BEC) of magnons [472]. As mentioned above, the population of magnons at a quasi-equilibrium state obeys a Bose-Einstein distribution

$$n(\epsilon_m, \mu_m, \beta_m) = \frac{1}{e^{\beta_m(\epsilon_m - \mu_m)} - 1}, \quad (78)$$

where ϵ_m is the energy of magnons, β_m is the inverse magnon temperature, and μ_m is the magnon chemical potential. The chemical potential μ_m satisfies the following relation with the density of the magnons

$$N(\mu_m, \beta_m) = \int_{\epsilon_{\min}}^{\infty} D(\epsilon_m) n(\epsilon_m, \mu_m, \beta_m) d\epsilon_m. \quad (79)$$

Here, $D(\epsilon_m)$ is the magnon DOS, and ϵ_{\min} is the energy of the lowest state. As n and N increase at a given temperature β_m , the chemical potential μ_m increases as well. It can be seen from Eq. (78) that the magnon chemical potential μ_m cannot be larger than ϵ_{\min} because the magnon number cannot be negative. Thus, Eq. (79) with the condition $\mu_m = \epsilon_{\min}$ defines a critical density N_c . When μ_m reaches the minimal energy state ϵ_{\min} and N is larger than N_c , a large number of magnons occupy the minimal energy state leading to the formation of BEC [472, 473]. Instead, if $\mu_m < \epsilon_{\min}$, N will be smaller than N_c and the condensation does not occur.

In practice, microwave pumping has been employed to generate magnons [467]. The number of magnons generated δN is proportional to the increase of the internal energy δE , i.e., $\delta E = \hbar \nu_p \delta N$, where ν_p is the frequency of the pumped magnons. The increase of μ_m is associated with ν_p [472]. If the elevated μ_m closely approaches to ϵ_{\min} , and N exceeds the critical value N_c , the BEC will reappear [473].

Demidov *et al.* have reported that non-equilibrium magnons can be generated by pure spin current, since the flow of the angular momentum provided by the spin current can be converted into magnons by the spin system of the

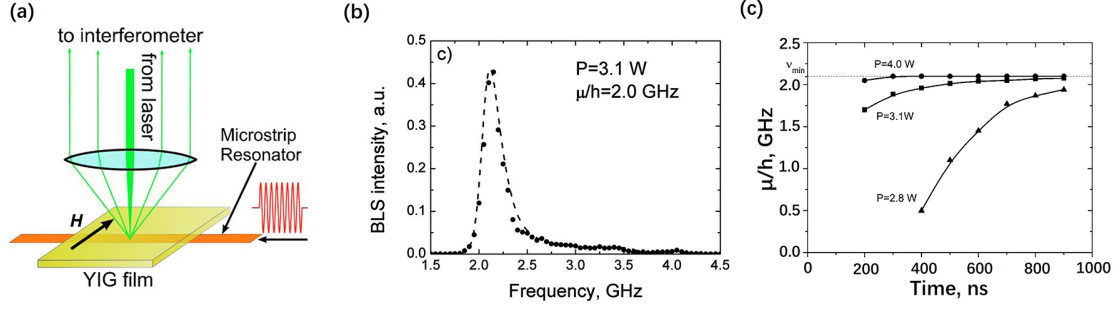


Figure 43: (a) Schematic of the experimental set-up for the measurement of the magnon chemical potential μ_m . The incident laser beam is focused onto the resonator. The beam passing through the YIG film is reflected by the resonator, and passes through the film again. Then the light is collected by a wide-aperture objective lens and sent to the interferometer for analyzing the frequency of photons inelastically scattered by the magnons. A microstrip resonator attached to the YIG film creates a microwave pumping field. (b) Measured BLS spectra of magnons. The circles show data points recorded at the pumping power of 3.1 W. The dash line is the best fit of the spectra based on Eq. (80) with μ_m being a fitting parameter. (c) Measured μ_m versus time at different values of pumping power. Reprinted with permission from [473]. Copyright 2007 American Institute of Physics.

ferromagnet [474, 475]. Their experimental work [474] has shown that a large spin current can drive magnons into a quasi-equilibrium state described by the Bose-Einstein statistics with a nonzero chemical potential.

Using the microwave pumping, Demokritov *et al.* have realized the BEC of quasi-equilibrium magnons at room temperature in YIG thin films [467, 468, 472, 473]. They have applied the Brillouin light scattering (BLS) technique to study the chemical potential of magnons [473]. Figure 43(a) shows the experimental set-up for the measurement of μ_m . An incident laser beam is focused on a local region of the sample, and the reflected light is collected to analysis the frequencies of photons inelastically scattered by the magnons. The measured BLS intensity signal is proportional to the spectral density of magnons [467]

$$\rho(\nu) = D(\nu)n(\nu) = \frac{D(\nu)}{e^{(h\nu - \mu_m)/k_B T_0} - 1}, \quad (80)$$

where ν is the magnon frequency, $n(\nu)$ is the Bose-Einstein distribution function with room temperature T_0 , and $D(\nu)$ is the magnon DOS and can be determined prior to the measurement of μ_m . The dashed line in Figure 43(b) is the best fit of measured signal to Eq. (80) with μ_m being the fitting parameter. Figure 43(c) illustrates the time evolution of μ_m with increasing pumping power. When μ_m reaches the minimal energy level $\mu_m = h\nu_{\min}$ the BEC is formed. Note that the measured BLS intensity carries the information only of a local region, and thus the determined μ_m is, in principle, a local chemical potential of magnons.

The chemical potential of magnons not only can characterize the formation of Bose-Einstein condensation, it also plays an important role in the spin transport of magnetic insulators. For example, Cornelissen *et al.* have reported that the long-range spin and heat transport in YIG films is mainly driven by the magnon chemical potential at room temperature [469].

Du *et al.* have developed a single-spin magnetometry for characterizing the magnon chemical potential [476]. Since the magnon chemical potential is inherently related to spin fluctuations, the μ_m can be quantitatively determined by measuring the magnetic fields generated by these fluctuations. This is realized by using a nitrogen-vacancy center in diamond as a single-spin sensor to measure the vacancy spin relaxation rates Γ_{\pm} to magnetic field fluctuations at the electron-spin resonance frequencies ν_{\pm} . The magnon chemical potential can then be determined as

$$\mu_m = h\nu_{\pm} \left[1 - \frac{\Gamma_{\pm}(0)}{\Gamma_{\pm}(\mu_m)} \right]. \quad (81)$$

Since the local magnetic fields generated by spin fluctuations are so weak, one has to place the magnetic field sensor in nanoscale proximity to the sample. Thus, this approach realizes a local measurement of magnon chemical potential with a nanoscale resolution determined by the distance between the sensor spin and the system under study [476].

5. Summary and perspectives

In this review, we have surveyed recent theoretical and experimental efforts on a topic that is of both fundamental and practical importance for the advancement of nanoscience: the local temperatures of nanoscopic (or mesoscopic) systems out of equilibrium. The contents of this review have focused on physical implications of the notion of local temperature in the following three aspects. (1) The local temperature lays the foundations for the generalization of the thermodynamic laws and relations to non-equilibrium scenarios. (2) It provides an energy scale for local thermal fluctuations and excitations, and (3) it facilitates the characterization of local properties of a given system under external driving conditions.

In Section 2, we have reviewed a variety of theoretical definitions of local temperature based on some of the above physical considerations. In Section 3, we have reviewed the existing experimental strategies for measuring local temperatures, as well as some state-of-the-art techniques and instruments. The reviewed work covers a broad spectrum of non-equilibrium nanosystems, which range from single molecular junctions to two-dimensional nanosheets with sizes of tens or hundreds of nanometers; from near-equilibrium situations to those very far from equilibrium; from stationary states to those undergoing time evolution; and from systems subjected to mechanical forces or thermal gradients to those driven by bias voltage or laser fields. In Section 4, we have finally discussed numerous examples which exemplify the physical implications and practical applications of the concept of local temperature.

Despite all the exciting and encouraging progress, there is still a noticeable gap between theory and experiments. From the theoretical perspective, more attention should be paid to the experimental feasibility of the theoretically proposed definitions or protocols to determine a local temperature. At the same time, it is crucial to go beyond simple models and apply the theoretical definitions or protocols to predict local temperatures in realistic nano-devices under typical experimental conditions. From the experimental perspective, it is appealing, yet rather challenging to break the conventional/classical limits such as the local Boltzmann distribution and the Fourier's law, and to resolve the characteristic quantum effects in nano-sized systems. More work towards increasing the spatial (and temporal) resolution of the instruments and approaches discussed in this review would definitely unravel quantum features of local temperatures out of equilibrium.

Finally, we shall mention several emerging frontiers where the concept of local temperature may play an essential role. First, quantitative predictions of the local temperature distribution based on first-principles simulations are expected to provide useful information in understanding novel phenomena and mechanisms in emerging quantum devices [477]. Second, the accurate determination of such a quantity may offer a new way to understand and characterize the formation and evolution of strongly correlated electronic states, which are at the heart of many exotic or complex materials [448, 450, 451]. Third, the notion of local temperature could also serve as a key quantity in theories of quantum thermodynamics [149–151, 256–258, 260]. The challenge here is to accurately account for the contribution of system-environment entanglement to the thermodynamic energy and entropy, so that a local temperature can be properly defined for an open quantum system. We thus hope this review will stimulate both the theoretical and experimental communities in pursuing these directions of study that are poised to lead to further breakthroughs in these exciting new frontiers and even beyond.

Acknowledgments

The support from the Ministry of Science and Technology of China (Grant Nos. 2016YFA0400900 and 2016YFA0200600) and the National Natural Science Foundation of China (Grant Nos. 21573202 and 21973086) is gratefully acknowledged.

References

References

- [1] M. P. Zeidler, C. Tan, Y. Bellaiche, S. Cherry, S. Häder, U. Gayko, N. Perrimon, Temperature-sensitive control of protein activity by conditionally splicing inteins, *Nat. Biotechnol.* 22 (2004) 871–876. doi:<https://doi.org/10.1038/nbt979>.
- [2] Y.-M. He, B.-G. Ma, Abundance and temperature dependency of protein-protein interaction revealed by interface structure analysis and stability evolution, *Sci. Rep.* 6 (2016) 26737. doi:<https://doi.org/10.1038/srep26737>.

- [3] R. Raccichini, A. Varzi, S. Passerini, B. Scrosati, The role of graphene for electrochemical energy storage, *Nat. Mater.* 14 (2015) 271–279. doi:<https://doi.org/10.1038/nmat4170>.
- [4] J. Sun, H.-W. Lee, M. Pasta, H. Yuan, G. Zheng, Y. Sun, Y. Li, Y. Cu, A phosphorene-graphene hybrid material as a high-capacity anode for sodium-ion batteries, *Nat. Nanotechnol.* 10 (2015) 980–985. doi:<https://doi.org/10.1038/nnano.2015.194>.
- [5] F. H. L. Koppens, T. Mueller, Ph. Avouris, A. C. Ferrari, M. S. Vitiello, M. Polini, Photodetectors based on graphene, other two-dimensional materials and hybrid systems, *Nat. Nanotechnol.* 9 (2014) 780–793. doi:<https://doi.org/10.1038/nnano.2014.215>.
- [6] M. Mader, J. Reichel, T. W. Hänsch, D. Hunger, A scanning cavity microscope, *Nat. Commun.* 6 (2015) 7249. doi:<https://doi.org/10.1038/ncomms8249>.
- [7] T. R. Kelly, M. L. Snapper, A molecular assembler, *Nature* 549 (2017) 336–337. doi:<https://doi.org/10.1038/549336a>.
- [8] R. V. Lapshin, Feature-oriented scanning methodology for probe microscopy and nanotechnology, *Nanotechnology* 15 (2004) 1135. doi:<https://doi.org/10.1088/0957-4484/15/9/006>.
- [9] W. Lee, P. Tseng, D. Di Carlo, *Microtechnology for Cell Manipulation and Sorting*, 1st Edition, Springer International Publishing, 2017.
- [10] M. Di Ventra, S. Evoy, J. R. Hefflin, *Introduction to Nanoscale Science and Technology*, 1st Edition, Springer, New York, 2004.
- [11] Y. N. Patt, S. J. Patel, M. Evers, D. H. Friendly, J. Stark, One billion transistors, one uniprocessor, one chip, *Computer* 30 (1997) 51–57. doi:<https://doi.org/10.1109/2.612249>.
- [12] D. Morr, Scanning tunneling potentiometry, charge transport, and Landauer resistivity dipole from the quantum to the classical transport regime, *Phys. Rev. B.* 95 (2017) 195162. doi:<https://doi.org/10.1103/PhysRevB.95.195162>.
- [13] M. Yamamoto, Y. Azuma, M. Sakamoto, T. Teranishi, H. Ishii, Y. Majima, Y. Noguchi, Molecular floating-gate single-electron transistor, *Sci. Rep.* 7 (2017) 1589. doi:<https://doi.org/10.1038/s41598-017-01578-7>.
- [14] J. Martínez-Blanco, C. Nacci, S. C. Erwin, K. Kanisawa, E. Locane, M. Thomas, F. von Oppen, P. W. Brouwer, S. Fölsch, Gating a single-molecule transistor with individual atoms, *Nat. Phys.* 11 (2015) 640–644. doi:<https://doi.org/10.1038/nphys3385>.
- [15] M. Ratner, A brief history of molecular electronics, *Nat. Nanotechnol.* 8 (2013) 378–381. doi:<https://doi.org/10.1038/nnano.2013.110>.
- [16] A. Aviram, M. A. Ratner, Molecular rectifiers, *Chem. Phys. Lett.* 29 (1974) 277–283. doi:[https://doi.org/10.1016/0009-2614\(74\)85031-1](https://doi.org/10.1016/0009-2614(74)85031-1).
- [17] B. Mann, H. Kuhn, Tunneling through fatty acid salt monolayers, *J. Appl. Phys.* 42 (1971) 4398. doi:<https://doi.org/10.1063/1.1659785>.
- [18] G. Pizzi, M. Gibertini, E. Dib, N. Marzari, G. Iannaccone, G. Fiori, Performance of arsenene and antimonene double-gate MOSFETs from first principles, *Nat. Commun.* 7 (2016) 12585. doi:<https://doi.org/10.1038/ncomms12585>.
- [19] C. Chen, C. Song, J. Yang, D. Chen, W. Zhu, C. Liao, X. Dong, X. Liu, L. Wei, N. Hu, R. He, Y. Zhang, Intramolecular p-i-n junction photovoltaic device based on selectively doped carbon nanotube, *Nano Energy* 32 (2017) 280–286. doi:<https://doi.org/10.1016/j.nanoen.2016.12.048>.
- [20] I. Jo, I.-K. Hsu, Y. J. Lee, M. M. Sadeghi, S. Kim, S. Cronin, E. Tutuc, S. K. Banerjee, Z. Yao, L. Shi, Low-frequency acoustic phonon temperature distribution in electrically biased graphene, *Nano Lett.* 11 (2011) 85–90. doi:<https://doi.org/10.1021/nl102858c>.
- [21] F. Xia, V. Perebeinos, Y. m. Lin, Y. Wu, P. Avouris, The origins and limits of metal-graphene junction resistance, *Nat. Nanotechnol.* 6 (2011) 179–184. doi:<https://doi.org/10.1038/nnano.2011.6>.
- [22] K. L. Grosse, M.-H. Bae, F. Lian, E. Pop, W. P. King, Nanoscale Joule heating, Peltier cooling and current crowding at graphene-metal contacts, *Nat. Nanotechnol.* 6 (2011) 287–290. doi:<https://doi.org/10.1038/nnano.2011.39>.
- [23] M. A. Reed, C. Zhou, C. J. Muller, T. P. Burgin, J. M. Tour, Conductance of a molecular junction, *Science* 278 (1997) 252–254. doi:<https://doi.org/10.1126/science.278.5336.252>.
- [24] N. J. Tao, Electron transport in molecular junctions, *Nat. Nanotechnol.* 1 (2006) 173–181. doi:<https://doi.org/10.1038/nnano.2006.130>.
- [25] S. V. Aradhya, L. Venkataraman, Single-molecule junctions beyond electronic transport, *Nat. Nanotechnol.* 8 (2013) 399–410. doi:<https://doi.org/10.1038/nnano.2013.91>.
- [26] C. Zhou, X. Li, Z. Gong, C. Jia, Y. Lin, C. Gu, G. He, Y. Zhong, J. Yang, X. Guo, Direct observation of single-molecule hydrogen-bond dynamics with single-bond resolution, *Nat. Commun.* 9 (2018) 807. doi:<https://doi.org/10.1038/s41467-018-03203-1>.
- [27] M. Di Ventra, *Electrical transport in nanoscale systems*, 1st Edition, Cambridge University Press, Cambridge, 2008.
- [28] Z. Huang, B. Xu, Y. Chen, M. Di Ventra, N. Tao, Measurement of current-induced local heating in a single molecule junction, *Nano Lett.* 6 (2006) 1240–1244. doi:<https://doi.org/10.1021/nl10608285>.
- [29] E. Evans, Probing the relation between force-lifetime-and chemistry in single molecular bonds, *Annu. Rev. Biophys. Biomol. Struct.* 30 (2001) 105–128. doi:<https://doi.org/10.1146/annurev.biophys.30.1.105>.
- [30] R. H. M. Smit, C. Untiedt, J. M. van Ruitenbeek, The high-bias stability of monatomic chains, *Nanotechnology* 15 (2004) S472–S478. doi:<https://doi.org/10.1088/0957-4484/15/7/055>.
- [31] M. Tsutsui, Y.-k. Taninouchi, S. Kurokawa, A. Sakai, Effective temperature of Au nanocontacts under high biases, *Jpn. J. Appl. Phys.* 44 (2005) 5188–5190. doi:<https://doi.org/10.1143/JJAP.44.5188>.
- [32] J. Varesi, A. Majumdar, Scanning Joule expansion microscopy at nanometer scales, *Appl. Phys. Lett.* 72 (1998) 37. doi:<https://doi.org/10.1063/1.120638>.
- [33] NobelPrize.org, The nobel prize in chemistry, <https://www.nobelprize.org/prizes/chemistry/2016/summary/> (2016).
- [34] S. A. Wolf, D. D. Awschalom, R. A. Buhrman, J. M. Daughton, S. von Molnár, M. L. Roukes, A. Y. Chtchelkanova, D. M. Treger, Spintronics: A spin-based electronics vision for the future, *Science* 294 (2001) 1488–1495. doi:<https://doi.org/10.1126/science.1065389>.
- [35] D. D. Awschalom, L. C. Bassett, A. S. Dzurak, E. L. Hu, J. R. Petta, Quantum spintronics: Engineering and manipulating atom-like spins in semiconductors, *Science* 339 (2013) 1174–1179. doi:<https://doi.org/10.1126/science.1231364>.
- [36] P. Michetti, P. Recher, G. Iannaccone, Electric field control of spin rotation in bilayer graphene, *Nano Lett.* 10 (2010) 4463–4469. doi:<https://doi.org/10.1021/nl102298n>.

- [37] A. Manchon, H. C. Koo, J. Nitta, S. M. Frolov, R. A. Duine, New perspectives for Rashba spin-orbit coupling, *Nat. Mater.* 14 (2015) 871–882. doi:<https://doi.org/10.1038/nmat4360>.
- [38] A. I. Lvovsky, B. C. Sanders, W. Tittel, Optical quantum memory, *Nat. Photonics* 3 (2009) 706–714. doi:<https://doi.org/10.1038/nphoton.2009.231>.
- [39] J. Wolters, G. Buser, A. Horsley, L. Béguin, A. Jöckel, J.-P. Jahn, R. J. Warburton, P. Treutlein, Simple atomic quantum memory suitable for semiconductor quantum dot single photons, *Phys. Rev. Lett.* 119 (2017) 060502. doi:<https://doi.org/10.1103/PhysRevLett.119.060502>.
- [40] L. M. K. Vandersypen, H. Bluhm, J. S. Clarke, A. S. Dzurak, R. Ishihara, A. Morello, D. J. Reilly, L. R. Schreiber, M. Veldhorst, Interfacing spin qubits in quantum dots and donors-hot, dense, and coherent, *npj Quantum Inform.* 3 (2017) 34. doi:<https://doi.org/10.1038/s41534-017-0038-y>.
- [41] R. Maurand, X. Jehl, D. Koteckar-Patil, A. Corna, H. Bohuslavskiy, R. Laviéville, L. Hutin, S. Barraud, M. Vinet, M. Sanquer, S. De Franceschi, A CMOS silicon spin qubit, *Nat. Commun.* 7 (2016) 13575. doi:<https://doi.org/10.1038/ncomms13575>.
- [42] M. Veldhorst, H. G. J. Eenink, C. H. Yang, A. S. Dzurak, Silicon CMOS architecture for a spin-based quantum computer, *Nat. Commun.* 8 (2017) 1766. doi:<https://doi.org/10.1038/s41467-017-01905-6>.
- [43] D.-J. Choi, M. V. Rastei, P. Simon, L. Limot, Conductance-driven change of the Kondo effect in a single cobalt atom, *Phys. Rev. Lett.* 108 (2012) 266803. doi:<https://doi.org/10.1103/PhysRevLett.108.266803>.
- [44] L. Gao, W. Ji, Y. B. Hu, Z. H. Cheng, Z. T. Deng, Q. Liu, N. Jiang, X. Lin, W. Guo, S. X. Du, W. A. Hofer, X. C. Xie, H.-J. Gao, Site-specific Kondo effect at ambient temperatures in iron-based molecules, *Phys. Rev. Lett.* 99 (2007) 106402. doi:<https://doi.org/10.1103/PhysRevLett.99.106402>.
- [45] L. Kouwenhoven, L. Glazman, Revival of the Kondo effect, *Phys. World* 14 (2001) 33. doi:<https://doi.org/10.1088/2058-7058/14/1/28>.
- [46] D. Loss, D. P. DiVincenzo, Quantum computation with quantum dots, *Phys. Rev. A* 57 (1998) 120. doi:<https://doi.org/10.1103/PhysRevA.57.120>.
- [47] J. Park, A. N. Pasupathy, J. I. Goldsmith, C. Chang, Y. Yaish, J. R. Petta, M. Rinkoski, J. P. Sethna, H. D. Abruña, P. L. McEuen, D. C. Ralph, Coulomb blockade and the Kondo effect in single-atom transistors, *Nature* 417 (2002) 722–725. doi:<https://doi.org/10.1038/nature00791>.
- [48] R. Hanson, L. P. Kouwenhoven, J. R. Petta, S. Tarucha, L. M. K. Vandersypen, Spins in few-electron quantum dots, *Rev. Mod. Phys.* 79 (2007) 1217. doi:<https://doi.org/10.1103/RevModPhys.79.1217>.
- [49] Y. V. Pershin, M. Di Ventra, Memory effects in complex materials and nanoscale systems, *Adv. Phys.* 60 (2011) 145–227. doi:<https://doi.org/10.1080/00018732.2010.544961>.
- [50] A. C. Hewson, *The Kondo Problem to Heavy Fermions*, 1st Edition, Cambridge University Press, Cambridge, 1993.
- [51] W. G. van der Wiel, S. De Franceschi, T. Fujisawa, J. M. Elzerman, S. Tarucha, L. P. Kouwenhoven, The Kondo effect in the unitary limit, *Science* 289 (2000) 2105–2108. doi:<https://doi.org/10.1126/science.289.5487.2105>.
- [52] P. W. Anderson, Localized magnetic states in metals, *Phys. Rev.* 124 (1961) 41–53. doi:<https://doi.org/10.1103/PhysRev.124.41>.
- [53] M. Grobis, I. G. Rau, R. M. Potok, H. Shtrikman, D. Goldhaber-Gordon, Universal scaling in nonequilibrium transport through a single channel Kondo dot, *Phys. Rev. Lett.* 100 (2008) 246601. doi:<https://doi.org/10.1103/PhysRevLett.100.246601>.
- [54] D. Goldhaber-Gordon, J. Göres, M. A. Kastner, H. Shtrikman, D. Mahalu, U. Meirav, From the Kondo regime to the mixed-valence regime in a single-electron transistor, *Phys. Rev. Lett.* 81 (1998) 5225. doi:<https://doi.org/10.1103/PhysRevLett.81.5225>.
- [55] S. M. Cronenwett, T. H. Oosterkamp, L. P. Kouwenhoven, A tunable Kondo effect in quantum dots, *Science* 281 (1998) 540–544. doi:<https://doi.org/10.1126/science.281.5376.540>.
- [56] A. Kogan, S. Amasha, D. Goldhaber-Gordon, G. Granger, M. A. Kastner, H. Shtrikman, Measurements of Kondo and spin splitting in single-electron transistors, *Phys. Rev. Lett.* 93 (2004) 166602. doi:<https://doi.org/10.1103/PhysRevLett.93.166602>.
- [57] S. Amasha, I. J. Gelfand, M. A. Kastner, A. Kogan, Kondo temperature dependence of the Kondo splitting in a single-electron transistor, *Phys. Rev. B* 72 (2005) 045308. doi:<https://doi.org/10.1103/PhysRevB.72.045308>.
- [58] S. K. Wang, X. Zheng, J. S. Jin, Y. J. Yan, Hierarchical Liouville-space approach to nonequilibrium dynamical properties of quantum impurity systems, *Phys. Rev. B* 88 (2013) 035129. doi:<http://doi.org/10.1103/PhysRevB.88.035129>.
- [59] A. Rosch, J. Kroha, P. Wölfle, Kondo effect in quantum dots at high voltage: Universality and scaling, *Phys. Rev. Lett.* 87 (2001) 156802. doi:<https://doi.org/10.1103/PhysRevLett.87.156802>.
- [60] X. Wang, L. Yang, L. Ye, X. Zheng, Y. Yan, Precise control of local spin states in an adsorbed magnetic molecule with an STM tip: Theoretical insights from first-principles-based simulation, *J. Phys. Chem. Lett.* 9 (2018) 2418–2425. doi:<https://doi.org/10.1021/acs.jpcllett.8b00808>.
- [61] J. J. Parks, A. R. Champagne, T. A. Costi, W. W. Shum, A. N. Pasupathy, E. Neuscamman, S. Flores-Torres, P. S. Cornaglia, A. A. Aligia, C. A. Balseiro, G. K.-L. Chan, H. D. Abruña, D. C. Ralph, Mechanical control of spin states in spin-1 molecules and the underscreened Kondo effect, *Science* 328 (2010) 1370–1373. doi:<https://doi.org/10.1126/science.1186874>.
- [62] R. Hiraoka, E. Minamitani, R. Arafune, N. Tsukahara, S. Watanabe, M. Kawai, N. Takagi, Single-molecule quantum dot as a Kondo simulator, *Nat. Commun.* 8 (2017) 16012. doi:<https://doi.org/10.1038/ncomms16012>.
- [63] Z. Merali, The new thermodynamics: how quantum physics is bending the rules, *Nature* 551 (2017) 20–22. doi:<https://doi.org/10.1038/551020a>.
- [64] H. Chang, *Inventing Temperature: Measurement and Scientific Progress*, 1st Edition, Oxford University Press, New York, 2004.
- [65] I. Müller, *A History of Thermodynamics*, 1st Edition, Springer-Verlag, New York, 2007.
- [66] R. P. Benedict, *Fundamentals of Temperature, Pressure, and Flow Measurements*, 3rd Edition, John Wiley & Sons, Inc., New York, 1984.
- [67] P. Atkins, J. de Paula, *Atkins' Physical Chemistry*, 8th Edition, W. H. Freeman, New York, 2006.
- [68] M. Stock, R. Davis, E. de Mirandés, M. J. T. Milton, The revision of the SI-the result of three decades of progress in metrology, *Metrologia* 56 (2019) 022001. doi:<https://doi.org/10.1088/1681-7575/ab0013>.
- [69] E. Fowler, R. Guggenheim, *Statistical Thermodynamics. A version of Statistical Mechanics for Students of Physics and Chemistry*, 1st

- Edition, Cambridge University Press, London, 1939.
- [70] Z. Lin, L. V. Zhigilei, V. Celli, Electron-phonon coupling and electron heat capacity of metals under conditions of strong electron-phonon nonequilibrium, *Phys. Rev. B* 77 (2008) 075133. doi:<https://doi.org/10.1103/PhysRevB.77.075133>.
 - [71] D. Halbertal, J. Cuppens, M. B. Shalom, L. Embon, N. Shadmi, Y. Anahory, H. R. Naren, J. Sarkar, A. Uri, Y. Ronen, Y. Myasoedov, L. S. Levitov, E. Joselevich, A. K. Geim, E. Zeldov, Nanoscale thermal imaging of dissipation in quantum systems, *Nature* 539 (2016) 407–410. doi:<https://doi.org/10.1038/nature19843>.
 - [72] G. Hodes, When small is different: Some recent advances in concepts and applications of nanoscale phenomena, *Adv. Mater.* 19 (2007) 639–655. doi:<https://doi.org/10.1002/adma.200601173>.
 - [73] S. N. Khanna, A. W. Jr. Castleman, *Quantum Phenomena in Clusters and Nanostructures*, 1st Edition, Springer-Verlag Berlin Heidelberg, New York, 2003.
 - [74] M. Hartmann, G. Mahler, O. Hess, Local versus global thermal states: Correlations and the existence of local temperatures, *Phys. Rev. E* 70 (2004) 066148. doi:<https://doi.org/10.1103/PhysRevE.70.066148>.
 - [75] M. Hartmann, G. Mahler, O. Hess, Nano-thermodynamics: On the minimal length scale for the existence of temperature, *Physica E* 29 (2005) 66–73. doi:<https://doi.org/10.1016/j.physe.2005.05.002>.
 - [76] M. Hartmann, J. Gemmer, G. Mahler, O. Hess, Scaling behavior of interactions in a modular quantum system and the existence of local temperature, *EPL* 65 (2004) 613. doi:<https://doi.org/10.1209/epl/i2003-10166-3>.
 - [77] M. Hartmann, G. Mahler, O. Hess, Existence of temperature on the nanoscale, *Phys. Rev. Lett.* 93 (2004) 080402. doi:<https://doi.org/10.1103/PhysRevLett.93.080402>.
 - [78] M. Hartmann, G. Mahler, Measurable consequences of the local breakdown of the concept of temperature, *EPL* 70 (2005) 579. doi:<https://doi.org/10.1209/epl/i2004-10518-5>.
 - [79] M. Hartmann, Minimal length scales for the existence of local temperature, *Contemp. Phys.* 47 (2006) 89–102. doi:<https://doi.org/10.1080/00107510600581136>.
 - [80] M. Kliesch, C. Gogolin, M. J. Kastoryano, A. Riera, J. Eisert, Locality of temperature, *Phys. Rev. X* 4 (2014) 031019. doi:<https://doi.org/10.1103/PhysRevX.4.031019>.
 - [81] S. Hernández-Santana, A. Riera, K. V. Hovhannisyan, M. Perarnau-Llobet, L. Tagliacozzo, A. Acín, Locality of temperature in spin chains, *New J. Phys.* 17 (2015) 085007. doi:<https://doi.org/10.1088/1367-2630/17/8/085007>.
 - [82] A. De Pasquale, D. Rossini, R. Fazio, V. Giovannetti, Local quantum thermal susceptibility, *Nat. Commun.* 7 (2016) 12782. doi:<https://doi.org/10.1038/ncomms12782>.
 - [83] G. De Palma, A. De Pasquale, V. Giovannetti, Universal locality of quantum thermal susceptibility, *Phys. Rev. A* 95 (2017) 052115. doi:<https://doi.org/10.1103/PhysRevA.95.052115>.
 - [84] D. J. Griffiths, *Introduction to Electrodynamics*, 3rd Edition, Prentice Hall, New Jersey, 1999.
 - [85] J. H. Lienhard IV, J. H. Lienhard V, *A Heat Transfer Textbook*, 4th Edition, Phlogiston Press, Cambridge, MA, 2011.
 - [86] R. Landauer, Spatial variation of currents and fields due to localized scatterers in metallic conduction, *IBM J. Res. Dev.* 1 (1957) 223–231. doi:<https://doi.org/10.1147/rd.13.0223>.
 - [87] M. Büttiker, Four-terminal phase-coherent conductance, *Phys. Rev. Lett.* 57 (1986) 1761. doi:<https://doi.org/10.1103/PhysRevLett.57.1761>.
 - [88] Y. Dubi, M. Di Ventra, Reconstructing Fourier’s law from disorder in quantum wires, *Phys. Rev. B* 79 (2009) 115415. doi:<https://doi.org/10.1103/PhysRevB.79.115415>.
 - [89] Y. Dubi, M. Di Ventra, Fourier’s law: Insight from a simple derivation, *Phys. Rev. E* 79 (2009) 042101. doi:<https://doi.org/10.1103/PhysRevE.79.042101>.
 - [90] R. Kubo, The fluctuation-dissipation theorem, *Rep. Prog. Phys.* 29 (1966) 255. doi:<https://doi.org/10.1088/0034-4885/29/1/306>.
 - [91] A. Einstein, Über die von der molekularkinetischen theorie der Wärme geforderte bewegung von in ruhenden Flüssigkeiten suspendierten teilchen, *Ann. Phys.* 7 (1905) 549–60. doi:<https://doi.org/10.1002/andp.19053220806>.
 - [92] H. Grabert, P. Schramm, G.-L. Ingold, Quantum Brownian motion: The functional integral approach, *Phys. Rep.* 168 (1988) 115–207. doi:[https://doi.org/10.1016/0370-1573\(88\)90023-3](https://doi.org/10.1016/0370-1573(88)90023-3).
 - [93] U. Weiss, *Quantum Dissipative Systems*, 3rd Edition, World Scientific, Singapore, 2008. doi:<https://doi.org/10.1142/6738>.
 - [94] S. Nakajima, On quantum theory of transport phenomena: Steady diffusion, *Prog. Theor. Phys.* 20 (1958) 948–959. doi:<https://doi.org/10.1143/PTP.20.948>.
 - [95] R. Zwanzig, Ensemble method in the theory of irreversibility, *J. Chem. Phys.* 33 (1960) 1338–1341. doi:<https://doi.org/10.1063/1.1731409>.
 - [96] R. Zwanzig, On the identity of three generalized master equations, *Physica* 30 (1964) 1109–1123. doi:[https://doi.org/10.1016/0031-8914\(64\)90102-8](https://doi.org/10.1016/0031-8914(64)90102-8).
 - [97] Y. J. Yan, R. X. Xu, Quantum mechanics of dissipative systems, *Annu. Rev. Phys. Chem.* 56 (2005) 187–219. doi:<https://doi.org/10.1146/annurev.physchem.55.091602.094425>.
 - [98] H. Spohn, Kinetic equations from Hamiltonian dynamics: Markovian limits, *Rev. Mod. Phys.* 52 (1980) 569. doi:<https://doi.org/10.1103/RevModPhys.52.569>.
 - [99] H.-P. Breuer, E.-M. Laine, J. Piilo, B. Vacchini, Colloquium: Non-Markovian dynamics in open quantum systems, *Rev. Mod. Phys.* 88 (2016) 021002. doi:<https://doi.org/10.1103/RevModPhys.88.021002>.
 - [100] A. G. Redfield, On the theory of relaxation processes, *IBM J. Res. Dev.* 1 (1957) 19–31. doi:<https://doi.org/10.1147/rd.11.0019>.
 - [101] A. G. Redfield, The theory of relaxation processes, *Adv. Magn. Reson.* 1 (1965) 1–32. doi:<https://doi.org/10.1016/B978-1-4832-3114-3.50007-6>.
 - [102] G. Lindblad, On the generators of quantum dynamical semigroups, *Commun. Math. Phys.* 48 (1976) 119–130. doi:<https://doi.org/10.1007/BF01608499>.
 - [103] V. Gorini, A. Kossakowski, E. C. G. Sudarshan, Completely positive dynamical semigroups of N-level systems, *J. Math. Phys.* 17 (1976)

821. doi:<https://doi.org/10.1063/1.522979>.
- [104] R. Alicki, K. Lendi, *Quantum Dynamical Semigroups and Applications*, Springer, New York, 1987. doi:<https://doi.org/10.1007/3-540-18276-4>.
 - [105] Y. Tanimura, R. Kubo, Time evolution of a quantum system in contact with a nearly Gaussian-Markovian noise bath, *J. Phys. Soc. Jpn.* 58 (1989) 101–114. doi:<https://doi.org/10.1143/JPSJ.58.101>.
 - [106] Y. Tanimura, Nonperturbative expansion method for a quantum system coupled to a harmonic-oscillator bath, *Phys. Rev. A* 41 (1990) 6676. doi:<https://doi.org/10.1103/PhysRevA.41.6676>.
 - [107] Y. A. Yan, F. Yang, Y. Liu, J. S. Shao, Hierarchical approach based on stochastic decoupling to dissipative systems, *Chem. Phys. Lett.* 395 (2004) 216–221. doi:<https://doi.org/10.1016/j.cpllett.2004.07.036>.
 - [108] R. X. Xu, P. Cui, X.-Q. Li, Y. Mo, Y. J. Yan, Exact quantum master equation via the calculus on path integrals, *J. Chem. Phys.* 122 (2005) 041103. doi:<https://doi.org/10.1063/1.1850899>.
 - [109] L. Z. Ye, X. L. Wang, D. Hou, R. X. Xu, X. Zheng, Y. J. Yan, HEOM-QUICK: a program for accurate, efficient, and universal characterization of strongly correlated quantum impurity systems, *WIREs Comput. Mol. Sci.* 6 (2016) 608, <https://doi.org/10.1002/wcms.1269>.
 - [110] L. Diósi, Quantum stochastic processes as models for state vector reduction, *J. Phys. A: Math. Gen.* 21 (1988) 2885. doi:<https://doi.org/10.1088/0305-4470/21/13/013>.
 - [111] L. Diósi, W. T. Strunz, The non-Markovian stochastic Schrödinger equation for open systems, *Phys. Lett. A* 235 (1997) 569–573. doi:[https://doi.org/10.1016/S0375-9601\(97\)00717-2](https://doi.org/10.1016/S0375-9601(97)00717-2).
 - [112] N. Gisin, I. C. Percival, The quantum-state diffusion model applied to open systems, *J. Phys. A: Math. Gen.* 25 (1992) 5677. doi:<https://doi.org/10.1088/0305-4470/25/21/023>.
 - [113] I. Percival, *Quantum State Diffusion*, 1st Edition, Cambridge University Press, Cambridge, England, 1999.
 - [114] J. T. Stockburger, H. Grabert, Exact c -number representation of non-Markovian quantum dissipation, *Phys. Rev. Lett.* 88 (2002) 170407. doi:<https://doi.org/10.1103/PhysRevLett.88.170407>.
 - [115] J. S. Shao, Decoupling quantum dissipation interaction via stochastic fields, *J. Chem. Phys.* 120 (2004) 5053. doi:<https://doi.org/10.1063/1.1647528>.
 - [116] J. M. Moix, J. S. Cao, A hybrid stochastic hierarchy equations of motion approach to treat the low temperature dynamics of non-Markovian open quantum systems, *J. Chem. Phys.* 139 (2013) 134106. doi:<https://doi.org/10.1063/1.4822043>.
 - [117] L. Han, V. Chernyak, Y.-A. Yan, X. Zheng, Y. Yan, Stochastic representation of Non-Markovian fermionic quantum dissipation (2019). doi:<https://doi.org/10.1103/PhysRevLett.123.050601>.
 - [118] I. de Vega, D. Alonso, Dynamics of non-Markovian open quantum systems, *Rev. Mod. Phys.* 89 (2017) 015001. doi:<https://doi.org/10.1103/RevModPhys.89.015001>.
 - [119] J. T. Stockburger, C. H. Mak, Dynamical simulation of current fluctuations in a dissipative two-state system, *Phys. Rev. Lett.* 80 (1998) 2657. doi:<https://doi.org/10.1103/PhysRevLett.80.2657>.
 - [120] L. Cui, H.-D. Zhang, X. Zheng, R.-X. Xu, Y. Yan, Highly efficient and accurate sum-overpoles expansion of Fermi and Bose functions at near zero temperatures: Fano spectrum decomposition scheme, *J. Chem. Phys.* 151 (2019) 024110. doi:<https://doi.org/10.1063/1.5096945>.
 - [121] H.-L. Engquist, P. W. Anderson, Definition and measurement of the electrical and thermal resistances, *Phys. Rev. B* 24 (1981) 1151(R). doi:<https://doi.org/10.1103/PhysRevB.24.1151>.
 - [122] A. Horn, *Ultra-fast Material Metrology*, 1st Edition, Wiley-VCH, 2009.
 - [123] J. Keizer, *Statistical Thermodynamics of Nonequilibrium Processes*, 1st Edition, Springer-Verlag, New York, 1987.
 - [124] Y. Demirel, *Nonequilibrium Thermodynamics Transport and Rate Processes in Physical, Chemical and Biological Systems*, 3rd Edition, Elsevier Science, 2014.
 - [125] R. F. O’Connell, Does the third law of thermodynamics hold in the quantum regime?, *J. Stat. Phys.* 124 (2006) 15–23. doi:<https://doi.org/10.1007/s10955-006-9151-6>.
 - [126] J. M. Moix, Y. Zhao, J. Cao, Equilibrium-reduced density matrix formulation: Influence of noise, disorder, and temperature on localization in excitonic systems, *Phys. Rev. B* 85 (2012) 115412. doi:<https://doi.org/10.1103/PhysRevB.85.115412>.
 - [127] A. Verbeure, Detailed balance and equilibrium, *Commun. Math. Phys.* 95 (1984) 301–305. doi:<https://doi.org/10.1007/BF01212400>.
 - [128] M. H. Alexander, G. E. Hall, P. J. Dagdigian, The approach to equilibrium: Detailed balance and the master equation, *J. Chem. Educ.* 88 (2011) 1538–1543. doi:<https://doi.org/10.1021/ed2001329>.
 - [129] D. A. Egolf, Equilibrium regained: From nonequilibrium chaos to statistical mechanics, *Science* 287 (2000) 101–104. doi:<https://doi.org/10.1126/science.287.5450.101>.
 - [130] R. H. Fowler, *Statistical Mechanics: The Theory of the Properties of Matter in Equilibrium*, 2nd Edition, Cambridge University Press, Cambridge, 1966.
 - [131] T. Döppner, O. L. Landen, H. J. Lee, P. Neumayer, S. P. Regan, S. H. Glenzer, Temperature measurement through detailed balance in x-ray Thomson scattering, *High Energy Dens. Phys.* 5 (2009) 182–186. doi:<https://doi.org/10.1016/j.hedp.2009.05.012>.
 - [132] J. C. Valenzuela, C. Krauland, D. Mariscal, I. Krashenninnikov, C. Niemann, T. Ma, P. Mabey, G. Gregori, P. Wiewior, A. M. Covington, F. N. Beg, Measurement of temperature and density using non-collective X-ray Thomson scattering in pulsed power produced warm dense plasmas, *Sci. Rep.* 8 (2018) 8432. doi:<https://doi.org/10.1038/s41598-018-26608-w>.
 - [133] S. Mukamel, *The Principles of Nonlinear Optical Spectroscopy*, 1st Edition, Oxford University Press, New York, 1995.
 - [134] G. D. Mahan, *Many-Particle Physics*, 3rd Edition, Vol. 1, Plenum, New York, 2000.
 - [135] P. Yan, G. E. W. Bauer, H. Zhang, Energy repartition in the nonequilibrium steady state, *Phys. Rev. B* 95 (2017) 024417. doi:<https://doi.org/10.1103/PhysRevB.95.024417>.
 - [136] W.-M. Zhang, P.-Y. Lo, H.-N. Xiong, M. W.-Y. Tu, F. Nori, General non-Markovian dynamics of open quantum systems, *Phys. Rev. Lett.* 109 (2012) 170402. doi:<https://doi.org/10.1103/PhysRevLett.109.170402>.
 - [137] U. Seifert, T. Speck, Fluctuation-dissipation theorem in nonequilibrium steady states, *EPL* 89 (2009) 10007. doi:<https://doi.org/10.1088/0305-4470/89/10/10007>.

- 1209/0295-5075/89/10007.
- [138] J. Casas-Vázquez, D. Jou, Temperature in non-equilibrium states: a review of open problems and current proposals, *Rep. Prog. Phys.* 66 (2003) 1937–2023. doi:<https://doi.org/10.1088/0034-4885/66/11/R03>.
 - [139] A. Puglisi, A. Sarracino, A. Vulpiani, Temperature in and out of equilibrium: A review of concepts, tools and attempts, *Phys. Rep.* 709-710 (2017) 1–60. doi:<https://doi.org/10.1016/j.physrep.2017.09.001>.
 - [140] Y. Dubi, M. Di Ventra, Thermoelectric effects in nanoscale junctions, *Nano Lett.* 9 (2009) 97–101. doi:<https://doi.org/10.1021/nl8025407>.
 - [141] A. Caso, L. Arrachea, G. S. Lozano, Local and effective temperatures of quantum driven systems, *Phys. Rev. B* 81 (2010) 041301. doi:<https://doi.org/10.1103/PhysRevB.81.041301>.
 - [142] A. Caso, L. Arrachea, G. S. Lozano, Local temperatures and heat flow in quantum driven systems, *Phys. Rev. B* 83 (2011) 165419. doi:<https://doi.org/10.1103/PhysRevB.83.165419>.
 - [143] J. Meair, J. P. Bergfield, C. A. Stafford, Ph. Jacquod, Local temperature of out-of-equilibrium quantum electron systems, *Phys. Rev. B* 90 (2014) 035407. doi:<https://doi.org/10.1103/PhysRevB.90.035407>.
 - [144] Y. Dubi, M. Di Ventra, Colloquium: Heat flow and thermoelectricity in atomic and molecular junctions, *Rev. Mod. Phys.* 83 (2011) 131. doi:<https://doi.org/10.1103/RevModPhys.83.131>.
 - [145] J. P. Bergfield, M. A. Ratner, C. A. Stafford, M. Di Ventra, Tunable quantum temperature oscillations in graphene nanostructures, *Phys. Rev. B* 91 (2015) 125407. doi:<https://doi.org/10.1103/PhysRevB.91.125407>.
 - [146] C. Bustamante, J. Liphardt, F. Ritort, The nonequilibrium thermodynamics of small systems, *Phys. Today* 58 (2005) 43. doi:<https://doi.org/10.1063/1.2012462>.
 - [147] C. Hörhammer, H. Büttner, Information and entropy in quantum Brownian motion thermodynamic entropy versus von Neumann entropy, *J. Stat. Phys.* 133 (2008) 1161. doi:<https://doi.org/10.1007/s10955-008-9640-x>.
 - [148] A. E. Allahverdyan, Th. M. Nieuwenhuizen, Breakdown of the Landauer bound for information erasure in the quantum regime, *Phys. Rev. E* 64 (2001) 056117. doi:<https://doi.org/10.1103/PhysRevE.64.056117>.
 - [149] J. Aliaga, D. Otero, A. Plastino, A. N. Proto, Quantum thermodynamics and information theory, *Phys. Rev. A* 38 (1988) 918. doi:<https://doi.org/10.1103/PhysRevA.38.918>.
 - [150] R. S. Johal, Quantum heat engines and nonequilibrium temperature, *Phys. Rev. E* 80 (2009) 041119. doi:<https://doi.org/10.1103/PhysRevE.80.041119>.
 - [151] S. Alipour, F. Benatti, F. Bakhshinezhad, M. Afsary, S. Marcantoni, A. T. Rezakhani, Correlations in quantum thermodynamics: Heat, work, and entropy production, *Sci. Rep.* 6 (2016) 35568. doi:<https://doi.org/10.1038/srep35568>.
 - [152] M. Horodecki, J. Oppenheim, Fundamental limitations for quantum and nanoscale thermodynamics, *Nat. Commun.* 9 (2013) 2059. doi:<https://doi.org/10.1038/ncomms3059>.
 - [153] P. Skrzypczyk, A. J. Short, S. Popescu, Work extraction and thermodynamics for individual quantum systems, *Nat. Commun.* 5 (2014) 4185. doi:<https://doi.org/10.1038/ncomms5185>.
 - [154] R. Uzdin, A. Levy, R. Kosloff, Equivalence of quantum heat machines, and quantum-thermodynamic signatures, *Phys. Rev. X* 5 (2015) 031044. doi:<https://doi.org/10.1103/PhysRevX.5.031044>.
 - [155] K. Esfarjani, G. A. Mansoori, Statistical mechanical modeling and its application to nanosystems, *Handbook Theor. Comput. Nanotechnol.* 1 (2005) 1–45. doi:<https://doi.org/10.1002/9783527627929>.
 - [156] P. Bialas, J. Spiechowicz, J. Łuczka, Quantum analogue of energy equipartition theorem, *J. Phys. A: Math. Theor.* 52 (2019) 15LT01. doi:<https://doi.org/10.1088/1751-8121/ab03f2>.
 - [157] N. J. Peacock, D. C. Robinson, M. J. Forrest, P. D. Wilcock, V. V. Sannikov, Measurement of the electron temperature by Thomson scattering in Tokamak T3, *Nature* 224 (1969) 488–490. doi:<https://doi.org/10.1038/224488a0>.
 - [158] S. G. Belostotskiy, R. Khandelwal, Q. Wang, V. M. Donnelly, D. J. Economou, N. Sadeghi, Measurement of electron temperature and density in an argon microdischarge by laser Thomson scattering, *Appl. Phys. Lett.* 92 (2008) 221507. doi:<https://doi.org/10.1063/1.2939437>.
 - [159] J. P. Bergfield, C. A. Stafford, Many-body theory of electronic transport in single-molecule heterojunctions, *Phys. Rev. B* 79 (2009) 245125. doi:<https://doi.org/10.1103/PhysRevB.79.245125>.
 - [160] R. Alicki, Quantum open systems as a model of a heat engine, *J. Phys. A: Math. Gen.* 12 (1979) L103. doi:<https://doi.org/10.1088/0305-4470/12/5/007>.
 - [161] R. Kosloff, A quantum mechanical open system as a model of a heat engine, *J. Chem. Phys.* 80 (1984) 1625. doi:<https://doi.org/10.1063/1.446862>.
 - [162] E. H. Lieb, J. Yngvason, The physics and mathematics of the second law of thermodynamics, *Phys. Rep.* 310 (1999) 1–96. doi:[https://doi.org/10.1016/S0370-1573\(98\)00082-9](https://doi.org/10.1016/S0370-1573(98)00082-9).
 - [163] T. D. Kieu, The second law, Maxwell’s demon, and work derivable from quantum heat engines, *Phys. Rev. Lett.* 93 (2004) 140403. doi:<https://doi.org/10.1103/PhysRevLett.93.140403>.
 - [164] A. Levy, R. Alicki, R. Kosloff, Quantum refrigerators and the third law of thermodynamics, *Phys. Rev. E* 85 (2012) 061126. doi:<https://doi.org/10.1103/PhysRevE.85.061126>.
 - [165] R. Kosloff, Quantum thermodynamics: A dynamical viewpoint, *Entropy* 15 (2013) 2100–2128. doi:<https://doi.org/10.3390/e15062100>.
 - [166] H. E. D. Scovil, E. O. Schulz-DuBois, Three-level masers as heat engines, *Phys. Rev. Lett.* 2 (1959) 262. doi:<https://doi.org/10.1103/PhysRevLett.2.262>.
 - [167] J. E. Geusic, E. O. Schulz-DuBios, H. E. D. Scovil, Quantum equivalence of the Carnot cycle, *Phys. Rev.* 156 (1967) 343. doi:<https://doi.org/10.1103/PhysRev.156.343>.
 - [168] F. L. Curzon, B. Ahlborn, Efficiency of a Carnot engine at maximum power output, *Am. J. Phys.* 43 (1975) 22. doi:<https://doi.org/10.1119/1.10023>.
 - [169] S. Marcantoni, S. Alipour, F. Benatti, R. Floreanini, A. T. Rezakhani, Entropy production and non-Markovian dynamical maps, *Sci. Rep.* 7

- (2017) 12447. doi:<https://doi.org/10.1038/s41598-017-12595-x>.
- [170] G. Clos, D. Porras, U. Warring, T. Schaetz, Time-resolved observation of thermalization in an isolated quantum system, *Phys. Rev. Lett.* 117 (2016) 170401. doi:<https://doi.org/10.1103/PhysRevLett.117.170401>.
- [171] J. Monsel, C. Elouard, A. Auffèves, An autonomous quantum machine to measure the thermodynamic arrow of time, *npj Quantum Inform.* 4 (2018) 59. doi:<https://doi.org/10.1038/s41534-018-0109-8>.
- [172] A. Ü. C. Hardal, Ö. E. Müstecaplıoğlu, Superradiant quantum heat engine, *Sci. Rep.* 5 (2015) 12953. doi:<https://doi.org/10.1038/srep12953>.
- [173] J. P. Pekola, T. T. Heikkilä, A. M. Savin, J. T. Flyktman, F. Giazotto, F. W. J. Hekking, Limitations in cooling electrons using normal-metal-superconductor tunnel junctions, *Phys. Rev. Lett.* 92 (2004) 056804. doi:<https://doi.org/10.1103/PhysRevLett.92.056804>.
- [174] A. Caso, L. Arrachea, G. S. Lozano, Defining the effective temperature of a quantum driven system from current-current correlation functions, *Eur. Phys. J. B* 85 (2012) 266. doi:<https://doi.org/10.1140/epjb/e2012-30303-0>.
- [175] Z. Huang, F. Chen, R. D’agosta, P. A. Bennett, M. Di Ventra, N. Tao, Local ionic and electron heating in single-molecule junctions, *Nat. Nanotechnol.* 2 (2007) 698–703. doi:<https://doi.org/10.1038/nnano.2007.345>.
- [176] D. R. Ward, D. A. Corley, J. M. Tour, D. Natelson, Vibrational and electronic heating in nanoscale junctions, *Nat. Nanotechnol.* 6 (2011) 33–38. doi:<https://doi.org/10.1038/nnano.2010.240>.
- [177] B. C. Hsu, Y.-S. Liu, S. H. Lin, Y.-C. Chen, Seebeck coefficients in nanoscale junctions: Effects of electron-vibration scattering and local heating, *Phys. Rev. B* 83 (2011) 041404(R). doi:<https://doi.org/10.1103/PhysRevB.83.041404>.
- [178] H. R. Krishna-murthy, K. G. Wilson, J. W. Wilkins, Temperature-dependent susceptibility of the symmetric Anderson model: Connection to the Kondo model, *Phys. Rev. Lett.* 35 (1975) 1101. doi:<https://doi.org/10.1103/PhysRevLett.35.1101>.
- [179] I. Paul, C. Pépin, M. R. Norman, Kondo breakdown and hybridization fluctuations in the Kondo-Heisenberg lattice, *Phys. Rev. Lett.* 98 (2007) 026402. doi:<https://doi.org/10.1103/PhysRevLett.98.026402>.
- [180] H. Hessling, On the local equilibrium condition, <https://arxiv.org/abs/hep-th/9411094> (1994).
- [181] Y.-C. Chen, M. Zwolak, M. Di Ventra, Local heating in nanoscale conductors, *Nano Lett.* 3 (2003) 1691–1694. doi:<https://doi.org/10.1021/nl0348544>.
- [182] L. Ye, D. Hou, X. Zheng, Y. Yan, M. Di Ventra, Local temperatures of strongly-correlated quantum dots out of equilibrium, *Phys. Rev. B* 91 (2015) 205106. doi:<https://doi.org/10.1103/PhysRevB.91.205106>.
- [183] L. Ye, X. Zheng, Y. Yan, M. Di Ventra, Thermodynamic meaning of local temperature of nonequilibrium open quantum systems, *Phys. Rev. B* 94 (2016) 245105. doi:<https://doi.org/10.1103/PhysRevB.94.245105>.
- [184] A. Schiller, S. Hershfield, Toulouse limit for the nonequilibrium Kondo impurity: Currents, noise spectra, and magnetic properties, *Phys. Rev. B* 58 (1998) 14978. doi:<https://doi.org/10.1103/PhysRevB.58.14978>.
- [185] S. Hershfield, J. H. Davies, J. W. Wilkins, Probing the Kondo resonance by resonant tunneling through an Anderson impurity, *Phys. Rev. Lett.* 67 (1991) 3720. doi:<https://doi.org/10.1103/PhysRevLett.67.3720>.
- [186] H. Ness, Nonequilibrium density matrix for quantum transport: Hershfield approach as a McLennan-Zubarev form of the statistical operator, *Phys. Rev. E* 88 (2013) 022121. doi:<https://doi.org/10.1103/PhysRevE.88.022121>.
- [187] L. F. Cugliandolo, J. Kurchan, L. Peliti, Energy flow, partial equilibration, and effective temperatures in systems with slow dynamics, *Phys. Rev. E* 55 (1997) 3898. doi:<https://doi.org/10.1103/PhysRevE.55.3898>.
- [188] L. F. Cugliandolo, G. Lozano, Quantum aging in mean-field models, *Phys. Rev. Lett.* 80 (1998) 4979. doi:<https://doi.org/10.1103/PhysRevLett.80.4979>.
- [189] L. Foini, L. F. Cugliandolo, A. Gambassi, Dynamic correlations, fluctuation-dissipation relations, and effective temperatures after a quantum quench of the transverse field Ising chain, *J. Stat. Mech.* (2012) P09011. doi:<https://doi.org/10.1088/1742-5468/2012/09/P09011>.
- [190] M. Galperin, A. Nitzan, M. A. Ratner, Resonant inelastic tunneling in molecular junctions, *Phys. Rev. B* 73 (2006) 045314. doi:<https://doi.org/10.1103/PhysRevB.73.045314>.
- [191] H. Ness, Nonequilibrium distribution functions for quantum transport: Universality and approximation for the steady state regime, *Phys. Rev. B* 89 (2014) 045409. doi:<https://doi.org/10.1103/PhysRevB.89.045409>.
- [192] F. Intravaia, R. O. Behunin, D. A. R. Dalvit, Quantum friction and fluctuation theorems, *Phys. Rev. A* 89 (2014) 050101(R). doi:<https://doi.org/10.1103/PhysRevA.89.050101>.
- [193] L. Foini, A. Gambassi, R. Konik, L. F. Cugliandolo, Measuring effective temperatures in a generalized Gibbs ensemble, *Phys. Rev. E* 95 (2017) 052116. doi:<https://doi.org/10.1103/PhysRevE.95.052116>.
- [194] L. F. Cugliandolo, The effective temperature, *J. Phys. A: Math. Theor.* 44 (2011) 483001. doi:<https://doi.org/10.1088/1751-8113/44/48/483001>.
- [195] Y. Meir, N. S. Wingreen, Landauer formula for the current through an interacting electron region, *Phys. Rev. Lett.* 68 (1992) 2512. doi:<https://doi.org/10.1103/PhysRevLett.68.2512>.
- [196] J. P. Bergfield, C. A. Stafford, Thermoelectric signatures of coherent transport in single-molecule heterojunctions, *Nano Lett.* 9 (2009) 3072–3076. doi:<https://doi.org/10.1021/nl901554s>.
- [197] D. A. Ryndyk, *Theory of Quantum Transport at Nanoscale*, 1st Edition, Springer International Publishing, New York, 2016.
- [198] B. Dong, X. L. Lei, Effect of the Kondo correlation on the thermopower in a quantum dot, *J. Phys.: Condens. Matter* 14 (2002) 11747–11756. doi:<https://doi.org/10.1088/0953-8984/14/45/316>.
- [199] P. N. Butcher, Thermal and electrical transport formalism for electronic microstructures with many terminals, *J. Phys.: Condens. Matter* 2 (1990) 4869. doi:<https://doi.org/10.1088/0953-8984/2/22/008>.
- [200] M. Turek, K. A. Matveev, Cotunneling thermopower of single electron transistors, *Phys. Rev. B* 65 (2002) 115332. doi:<https://doi.org/10.1103/PhysRevB.65.115332>.
- [201] C. Kittel, *Introduction to Solid State Physics*, 8th Edition, John Wiley & Sons, New York, 2004.
- [202] X.-Q. Li, J. Luo, Y.-G. Yang, P. Cui, Y. Yan, Quantum master-equation approach to quantum transport through mesoscopic systems, *Phys. Rev. B* 71 (2005) 205304. doi:<https://doi.org/10.1103/PhysRevB.71.205304>.

- [203] U. Harbola, M. Esposito, S. Mukamel, Quantum master equation for electron transport through quantum dots and single molecules, *Phys. Rev. B* 74 (2007) 235309. doi:<https://doi.org/10.1103/PhysRevB.74.235309>.
- [204] J. S. Jin, X. Zheng, Y. J. Yan, Exact dynamics of dissipative electronic systems and quantum transport: Hierarchical equations of motion approach, *J. Chem. Phys.* 128 (2008) 234703. doi:<https://doi.org/10.1063/1.2938087>.
- [205] J. Hu, M. Luo, F. Jiang, R. X. Xu, Y. J. Yan, Padé spectrum decompositions of quantum distribution functions and optimal hierarchical equations of motion construction for quantum open systems, *J. Chem. Phys.* 134 (2011) 244106. doi:<https://doi.org/10.1063/1.3602466>.
- [206] J.-S. Wang, B. K. Agarwalla, H. Li, J. Thingna, Nonequilibrium Green's function method for quantum thermal transport, *Front. Phys.* 9 (2014) 673–697. doi:<https://doi.org/10.1007/s11467-013-0340-x>.
- [207] M. Thoss, F. Evers, Perspective: Theory of quantum transport in molecular junctions, *J. Chem. Phys.* 148 (2018) 030901. doi:<https://doi.org/10.1063/1.5003306>.
- [208] S. Y. Quek, K. H. Khoo, Predictive DFT-based approaches to charge and spin transport in single-molecule junctions and two-dimensional materials: Successes and challenges, *Acc. Chem. Res.* 47 (2014) 3250–3257. doi:<https://doi.org/10.1021/ar4002526>.
- [209] S. Liu, A. Nurbawono, C. Zhang, Density functional theory for steady-state nonequilibrium molecular junctions, *Sci. Rep.* 5 (2015) 15386. doi:<https://doi.org/10.1038/srep15386>.
- [210] M. Di Ventra, S. T. Pantelides, N. D. Lang, First-principles calculation of transport properties of a molecular device, *Phys. Rev. Lett.* 84 (2000) 979. doi:<https://doi.org/10.1103/PhysRevLett.84.979>.
- [211] Y. Ni, X. Wang, S.-C. Z. W. Tao, K.-L. Yao, The spin-dependent transport properties of zigzag α -graphyne nanoribbons and new device design, *Sci. Rep.* 6 (2016) 25914. doi:<https://doi.org/10.1038/srep25914>.
- [212] J. Tescht, P. Leicht, F. Blumenschein, L. Gragnaniello, M. Fonin, L. E. M. Steinkasserer, B. Paulus, E. Voloshina, Y. Dedkov, Structural and electronic properties of graphene nanoflakes on Au(111) and Ag(111), *Sci. Rep.* 6 (2016) 23439. doi:<https://doi.org/10.1038/srep23439>.
- [213] X. Ji, J. Zhang, Y. Wang, H. Qian, Z. Yu, A theoretical model for metalgraphene contact resistance using a DFT-NEGF method, *Phys. Chem. Chem. Phys.* 15 (2013) 17883–17886. doi:<https://doi.org/10.1039/C3CP52589A>.
- [214] D. Perera, J. Rohrer, Structure sensitivity of electronic transport across graphene grain boundaries, *Phys. Rev. B* 98 (2018) 155432. doi:<https://doi.org/10.1103/PhysRevB.98.155432>.
- [215] W. Kohn, L. J. Sham, Self-consistent equations including exchange and correlation effects, *Phys. Rev.* 140 (1965) A1133. doi:<https://doi.org/10.1103/PhysRev.140.A1133>.
- [216] R. Parr, W. Yang, *Density-Functional Theory of Atoms and Molecules*, Oxford University Press, New York, 1989.
- [217] J. Taylor, H. Guo, J. Wang, *Ab initio* modeling of quantum transport properties of molecular electronic devices, *Phys. Rev. B* 63 (2001) 245407. doi:<https://doi.org/10.1103/PhysRevB.63.245407>.
- [218] J. Heurich, J. C. Cuevas, W. Wenzel, G. Schön, Electrical transport through single-molecule junctions: From molecular orbitals to conduction channels, *Phys. Rev. Lett.* 88 (2002) 256803. doi:<https://doi.org/10.1103/PhysRevLett.88.256803>.
- [219] S. Y. Quek, L. Venkataraman, H. J. Choi, S. G. Louie, M. S. Hybertsen, J. B. Neaton, Amine-gold linked single-molecule circuits: Experiment and theory, *Nano Lett.* 7 (2007) 3477–3482. doi:<https://doi.org/10.1021/nl072058i>.
- [220] Y. Kim, A. Garcia-Lekue, D. Sysoiev, T. Frederiksen, U. Groth, E. Scheer, Charge transport in azobenzene-based single-molecule junctions, *Phys. Rev. Lett.* 109 (2012) 226801. doi:<https://doi.org/10.1103/PhysRevLett.109.226801>.
- [221] N. Sai, M. Zwolak, G. Vignale, M. Di Ventra, Dynamical corrections to the DFT-LDA electron conductance in nanoscale systems, *Phys. Rev. Lett.* 94 (2005) 186810. doi:<https://doi.org/10.1103/PhysRevLett.94.186810>.
- [222] Y. Xue, S. Datta, M. A. Ratner, First-principles based matrix Green's function approach to molecular electronic devices: general formalism, *Chem. Phys.* 281 (2002) 151–170. doi:[https://doi.org/10.1016/S0301-0104\(02\)00446-9](https://doi.org/10.1016/S0301-0104(02)00446-9).
- [223] S. Kurth, G. Stefanucci, C.-O. Almbladh, A. Rubio, E. K. U. Gross, Time-dependent quantum transport: A practical scheme using density functional theory, *Phys. Rev. B* 72 (2005) 035308. doi:<https://doi.org/10.1103/PhysRevB.72.035308>.
- [224] E. Runge, E. K. U. Gross, Density-functional theory for time-dependent systems, *Phys. Rev. Lett.* 52 (1984) 997–1000. doi:<https://doi.org/10.1103/PhysRevLett.52.997>.
- [225] M. Di Ventra, T. N. Todorov, Transport in nanoscale systems: the microcanonical versus grand-canonical picture, *J. Phys.: Condens. Matter* 16 (2004) 8025. doi:<https://doi.org/10.1088/0953-8984/16/45/024>.
- [226] K. Burke, R. Car, R. Gebauer, Density functional theory of the electrical conductivity of molecular devices, *Phys. Rev. Lett.* 94 (2005) 146803. doi:<https://doi.org/10.1103/PhysRevLett.94.146803>.
- [227] M. Di Ventra, R. D'Agosta, Stochastic time-dependent current-density-functional theory, *Phys. Rev. Lett.* 98 (2007) 226403. doi:<https://doi.org/10.1103/PhysRevLett.98.226403>.
- [228] R. D'Agosta, M. Di Ventra, Stochastic time-dependent current-density-functional theory: A functional theory of open quantum systems, *Phys. Rev. B* 78 (2008) 165105. doi:<https://doi.org/10.1103/PhysRevB.78.165105>.
- [229] X. Zheng, C. Yam, F. Wang, G. Chen, Existence of time-dependent density-functional theory for open electronic systems: Time-dependent holographic electron density theorem, *Phys. Chem. Chem. Phys.* 13 (2011) 14358–14364. doi:<https://doi.org/10.1039/C1CP20777F>.
- [230] C. Yam, X. Zheng, G. Chen, Y. Wang, T. Frauenheim, T. A. Niehaus, Time-dependent versus static quantum transport simulations beyond linear response, *Phys. Rev. B* 83 (2011) 245448. doi:<https://doi.org/10.1103/PhysRevB.83.245448>.
- [231] X. Zheng, R. Wang, Time-dependent density-functional theory for open electronic systems, *Sci. China Chem.* 57 (2014) 26–35. doi:<https://doi.org/10.1007/s11426-013-5020-8>.
- [232] R. Wang, X. Zheng, Y. Kwok, H. Xie, G. Chen, C. Yam, Time-dependent density functional theory for open systems with a positivity-preserving decomposition scheme for environment spectral functions, *J. Chem. Phys.* 142 (2015) 144112. doi:<https://doi.org/10.1063/1.4917172>.
- [233] R. L. Wang, D. Hou, X. Zheng, Time-dependent density-functional theory for real-time electronic dynamics on material surfaces, *Phys. Rev. B* 88 (2013) 205126. doi:<https://doi.org/10.1103/PhysRevB.88.205126>.

- [234] M. Elstner, D. Porezag, G. Jungnickel, J. Elsner, M. Haugk, Th. Frauenheim, S. Suhai, G. Seifert, Self-consistent-charge density-functional tight-binding method for simulations of complex materials properties, *Phys. Rev. B* 58 (1998) 7260. doi:<https://doi.org/10.1103/PhysRevB.58.7260>.
- [235] C. Yam, L. Meng, Y. Zhang, G. Chen, A multiscale quantum mechanics/electromagnetics method for device simulations, *Chem. Soc. Rev.* 44 (2015) 1763–1776. doi:<https://doi.org/10.1039/C4CS00348A>.
- [236] C. Yam, J. Peng, Q. Chen, S. Markov, J. Z. Huang, N. Wong, W. C. Chew, G. Chen, A multi-scale modeling of junctionless field-effect transistors, *Appl. Phys. Lett.* 103 (2013) 062109. doi:<https://doi.org/10.1063/1.4817911>.
- [237] L. Arrachea, E. Fradkin, Chiral heat transport in driven quantum Hall and quantum spin Hall edge states, *Phys. Rev. B* 84 (2011) 235436. doi:<https://doi.org/10.1103/PhysRevB.84.235436>.
- [238] L. Arrachea, N. Bode, F. von Oppen, Vibrational cooling and thermoelectric response of nanoelectromechanical systems, *Phys. Rev. B* 90 (2014) 125450. doi:<https://doi.org/10.1103/PhysRevB.90.125450>.
- [239] H. Aita, L. Arrachea, C. Naón, E. Fradkin, Heat transport through quantum Hall edge states: Tunneling versus capacitive coupling to reservoirs, *Phys. Rev. B* 88 (2013) 085122. doi:<https://doi.org/10.1103/PhysRevB.88.085122>.
- [240] D. Venturelli, R. Fazio, V. Giovannetti, Minimal self-contained quantum refrigeration machine based on four quantum dots, *Phys. Rev. Lett.* 110 (2013) 256801. doi:<https://doi.org/10.1103/PhysRevLett.110.256801>.
- [241] F. Foieri, L. Arrachea, ac-dc voltage profile and four point impedance of a quantum driven system, *Phys. Rev. B* 82 (2010) 125434. doi:<https://doi.org/10.1103/PhysRevB.82.125434>.
- [242] F. Foieri, L. Arrachea, M. J. Sánchez, dc four-point resistance of a double-barrier quantum pump, *Phys. Rev. B* 79 (2009) 085430. doi:<https://doi.org/10.1103/PhysRevB.79.085430>.
- [243] A. Shastry, C. A. Stafford, Temperature and voltage measurement in quantum systems far from equilibrium, *Phys. Rev. B* 94 (2016) 155433. doi:<https://doi.org/10.1103/PhysRevB.94.155433>.
- [244] Y.-C. Chen, M. Zwolak, M. Di Ventra, Inelastic effects on the transport properties of alkanethiols, *Nano Lett.* 5 (2005) 621–624. doi:<https://doi.org/10.1021/nl047899t>.
- [245] Z. Yang, A. Tackett, M. Di Ventra, Variational and nonvariational principles in quantum transport calculations, *Phys. Rev. B* 66 (2002) 041405(R). doi:<https://doi.org/10.1103/PhysRevB.66.041405>.
- [246] M. Di Ventra, S. T. Pantelides, N. D. Lang, First-principles calculation of transport properties of a molecular device, *Phys. Rev. Lett.* 84 (2000) 979–982. doi:<https://doi.org/10.1103/PhysRevLett.84.979>.
- [247] N. W. Ashcroft, N. D. Mermin, *Solid State Physics*, 1st Edition, Holt, Rinehart and Winston, New York, 1976.
- [248] D. J. Wold, C. D. Frisbie, Fabrication and characterization of metal-molecule-metal junctions by conducting probe atomic force microscopy, *J. Am. Chem. Soc.* 123 (2001) 5549–5556. doi:<https://doi.org/10.1021/ja0101532>.
- [249] T. N. Todorov, Local heating in ballistic atomic-scale contacts, *Philos. Mag. B* 77 (1998) 965–973. doi:<https://doi.org/10.1080/13642819808206398>.
- [250] R. D’Agosta, N. Sai, M. Di Ventra, Local electron heating in nanoscale conductors, *Nano Lett.* 6 (2006) 2935–2938. doi:<https://doi.org/10.1021/nl062316w>.
- [251] D. R. Schmidt, R. J. Schoelkopf, A. N. Cleland, Photon-mediated thermal relaxation of electrons in nanostructures, *Phys. Rev. Lett.* 2004 (2004) 045901. doi:<https://doi.org/10.1103/PhysRevLett.93.045901>.
- [252] T. Soddemann, B. Dünweg, K. Kremer, Dissipative particle dynamics: A useful thermostat for equilibrium and nonequilibrium molecular dynamics simulations, *Phys. Rev. E* 68 (2003) 046702. doi:<https://doi.org/10.1103/PhysRevE.68.046702>.
- [253] Z.-Y. Ong, E. Pop, Molecular dynamics simulation of thermal boundary conductance between carbon nanotubes and SiO₂, *Phys. Rev. B* 81 (2010) 155408. doi:<https://doi.org/10.1103/PhysRevB.81.155408>.
- [254] J. Hickman, Y. Mishin, Temperature fluctuations in canonical systems: Insights from molecular dynamics simulations, *Phys. Rev. Lett.* 84 (2016) 184311. doi:<https://doi.org/10.1103/PhysRevB.94.184311>.
- [255] P. W. Ayers, R. G. Parr, A. Nagy, Local kinetic energy and local temperature in the density-functional theory of electronic structure, *Int. J. Quantum Chem.* 90 (2002) 309–326. doi:<https://doi.org/10.1002/qua.989>.
- [256] A. Bartana, R. Kosloff, D. J. Tannor, Laser cooling of molecular internal degrees of freedom by a series of shaped pulses, *J. Chem. Phys.* 99 (1993) 196. doi:<https://doi.org/10.1063/1.465797>.
- [257] T. Feldmann, R. Kosloff, Quantum four-stroke heat engine: Thermodynamic observables in a model with intrinsic friction, *Phys. Rev. E* 68 (2003) 016101. doi:<https://doi.org/10.1103/PhysRevE.68.016101>.
- [258] H. Weimer, M. J. Henrich, F. Rempp, H. Schröder, G. Mahler, Local effective dynamics of quantum systems: A generalized approach to work and heat, *EPL* 83 (2008) 30008. doi:<https://doi.org/10.1209/0295-5075/83/30008>.
- [259] M. Di Ventra, Y. Dubi, Information compressibility, entropy variation and approach to steady state in open systems, *EPL* 85 (2009) 40004. doi:<https://doi.org/10.1209/0295-5075/85/40004>.
- [260] M. M. Ali, W.-M. Huang, W.-M. Zhang, Quantum thermodynamics of a single particle system, <https://arxiv.org/abs/1803.04658v3> (2018).
- [261] P. A. Camati, J. P. S. Peterson, T. B. Batalhão, K. Micadei, A. M. Souza, R. S. Sarthour, I. S. Oliveira, R. M. Serra, Experimental rectification of entropy production by Maxwell’s demon in a quantum system, *Phys. Rev. Lett.* 117 (2016) 240502. doi:<https://doi.org/10.1103/PhysRevLett.117.240502>.
- [262] R. Islam, R. Ma, P. M. Preiss, M. E. Tai, A. Lukin, M. Rispoli, M. Greiner, Measuring entanglement entropy in a quantum many-body system, *Nature* 528 (2015) 77–83. doi:<https://doi.org/10.1038/nature15750>.
- [263] C.-F. Li, J.-S. Xu, X.-Y. Xu, K. Li, G.-C. Guo, Experimental investigation of the entanglement-assisted entropic uncertainty principle, *Nat. Phys.* 7 (2011) 752–756. doi:<https://doi.org/10.1038/nphys2047>.
- [264] D. A. Abanin, E. Demler, Measuring entanglement entropy of a generic many-body system with a quantum switch, *Phys. Rev. Lett.* 109 (2012) 020504. doi:<https://doi.org/10.1103/PhysRevLett.109.020504>.
- [265] F. Giazotto, F. Taddei, P. D’Amico, R. Fazio, F. Beltram, Nonequilibrium spin-dependent phenomena in mesoscopic superconductor-normal metal tunnel structures, *Phys. Rev. B* 76 (2007) 184518. doi:<https://doi.org/10.1103/PhysRevB.76.184518>.
- [266] T. T. Heikkilä, M. Hatami, G. E. W. Bauer, Spin heat accumulation and its relaxation in spin valves, *Phys. Rev. B* 81 (2010) 100408(R).

- doi:<https://doi.org/10.1103/PhysRevB.81.100408>.
- [267] M. Galperin, M. A. Ratner, A. Nitzan, Molecular transport junctions: vibrational effects, *J. Phys.: Condens. Matter* 19 (2007) 103201. doi:<https://doi.org/10.1088/0953-8984/19/10/103201>.
 - [268] F. Giazotto, T. T. Heikkilä, A. Luukanen, A. M. Savin, J. P. Pekola, Opportunities for mesoscopies in thermometry and refrigeration: Physics and applications, *Rev. Mod. Phys.* 78 (2006) 217. doi:<https://doi.org/10.1103/RevModPhys.78.217>.
 - [269] H. Pothier, S. Guéron, N. O. Birge, D. Esteve, M. H. Devoret, Energy distribution function of quasiparticles in mesoscopic wires, *Phys. Rev. Lett.* 79 (1997) 3490. doi:<https://doi.org/10.1103/PhysRevLett.79.3490>.
 - [270] M. Galperin, A. Nitzan, M. A. Ratner, Heat conduction in molecular transport junctions, *Phys. Rev. B* 75 (2007) 155312. doi:<https://doi.org/10.1103/PhysRevB.75.155312>.
 - [271] J. Koch, M. Semmelhack, F. von Oppen, A. Nitzan, Current-induced nonequilibrium vibrations in single-molecule devices, *Phys. Rev. B* 73 (2006) 155306. doi:<https://doi.org/10.1103/PhysRevB.73.155306>.
 - [272] F. Pierre, H. Pothier, D. Esteve, M. H. Devoret, Energy redistribution between quasiparticles in mesoscopic silver wires, *J. Low Temp. Phys.* 118 (2000) 437–445. doi:<https://doi.org/10.1023/A:1004606420464>.
 - [273] F. Pierre, A. Anthore, H. Pothier, C. Urbina, D. Esteve, Multiple Andreev reflections revealed by the energy distribution of quasiparticles, *Phys. Rev. Lett.* 86 (2001) 1078. doi:<https://doi.org/10.1103/PhysRevLett.86.1078>.
 - [274] B. Huard, A. Anthore, F. Pierre, H. Pothier, N. O. Birge, D. Esteve, Intensity of Coulomb interaction between quasiparticles in diffusive metallic wires, *Solid State Commun.* 131 (2004) 599–607. doi:<https://doi.org/10.1016/j.ssc.2004.05.020>.
 - [275] Y.-F. Chen, T. Dirks, G. Al-Zoubi, N. O. Birge, N. Mason, Nonequilibrium tunneling spectroscopy in carbon nanotubes, *Phys. Rev. Lett.* 102 (2009) 036804. doi:<https://doi.org/10.1103/PhysRevLett.102.036804>.
 - [276] N. Bronn, N. Mason, Spatial dependence of electron interactions in carbon nanotubes, *Phys. Rev. B* 88 (2013) 161409(R). doi:<https://doi.org/10.1103/PhysRevB.88.161409>.
 - [277] A. Anthore, F. Pierre, H. Pothier, D. Esteve, Magnetic-field-dependent quasiparticle energy relaxation in mesoscopic wires, *Phys. Rev. Lett.* 90 (2003) 076806. doi:<https://doi.org/10.1103/PhysRevLett.90.076806>.
 - [278] C. Altimiras, H. le Sueur, U. Gennser, A. Cavanna, D. Mailly, F. Pierre, Non-equilibrium edge-channel spectroscopy in the integer quantum Hall regime, *Nat. Phys.* 6 (2010) 34–39. doi:<https://doi.org/10.1038/nphys1429>.
 - [279] D. Chandler, *Introduction to Modern Statistical Mechanics*, 1st Edition, Oxford University Press, New York, 1987.
 - [280] N. Andrenacci, F. Corberi, E. Lippiello, Fluctuation-dissipation relation in an ising model without detailed balance, *Phys. Rev. E* 73 (2006) 046124. doi:<https://doi.org/10.1103/PhysRevE.73.046124>.
 - [281] C. Battle, C. P. Broedersz, N. Fakhri, V. F. Geyer, J. Howard, C. F. Schmidt, F. C. MacKintosh, Broken detailed balance at mesoscopic scales in active biological systems, *Science* 352 (2016) 604–607. doi:<https://doi.org/10.1126/science.aac8167>.
 - [282] F. S. Gnesotto, F. Mura, J. Gladrow, C. P. Broedersz, Broken detailed balance and non-equilibrium dynamics in living systems: a review, *Rep. Prog. Phys.* 81 (2018) 066601. doi:<https://doi.org/10.1088/1361-6633/aab3ed>.
 - [283] Z. Zhang, W. Wu, J. Wang, Fluctuation-dissipation theorem for nonequilibrium quantum systems, *EPL* 115 (2016) 20004. doi:<https://doi.org/10.1209/0295-5075/115/20004>.
 - [284] T. Speck, U. Seifert, Restoring a fluctuation-dissipation theorem in a nonequilibrium steady state, *EPL* 74 (2006) 391. doi:<https://doi.org/10.1209/epl/i2005-10549-4>.
 - [285] L. Arrachea, L. F. Cugliandolo, Study of a fluctuation-dissipation relation of a dissipative driven mesoscopic system, *EPL* 70 (2005) 642. doi:<https://doi.org/10.1209/epl/i2004-10515-8>.
 - [286] Y. M. Blanter, M. Büttiker, Shot noise in mesoscopic conductors, *Phys. Rep.* 336 (2000) 1–166. doi:[https://doi.org/10.1016/S0370-1573\(99\)00123-4](https://doi.org/10.1016/S0370-1573(99)00123-4).
 - [287] C. de C. Chamon, D. E. Freed, X. G. Wen, Tunneling and quantum noise in one-dimensional Luttinger liquids, *Phys. Rev. B* 51 (1995) 2363. doi:<https://doi.org/10.1103/PhysRevB.51.2363>.
 - [288] P. Ripka, Electric current sensors: a review, *Meas. Sci. Technol.* 21 (2010) 112001. doi:<https://doi.org/10.1088/0957-0233/21/11/112001>.
 - [289] P. Dutta, P. M. Horn, Low-frequency fluctuations in solids: $\frac{1}{f}$ noise, *Rev. Mod. Phys.* 53 (1981) 497. doi:<https://doi.org/10.1103/RevModPhys.53.497>.
 - [290] A. A. Clerk, M. H. Devoret, S. M. Girvin, F. Marquardt, R. J. Schoelkopf, Introduction to quantum noise, measurement, and amplification, *Rev. Mod. Phys.* 82 (2010) 1155. doi:<https://doi.org/10.1103/RevModPhys.82.1155>.
 - [291] G. Mills, H. Zhou, A. Midha, L. Donaldson, J. M. R. Weaver, Scanning thermal microscopy using batch fabricated thermocouple probes, *Appl. Phys. Lett.* 72 (1998) 2900. doi:<https://doi.org/10.1063/1.121453>.
 - [292] K. Kim, J. Chung, G. Hwang, O. Kwon, J. S. Lee, Quantitative measurement with scanning thermal microscope by preventing the distortion due to the heat transfer through the air, *ACS Nano* 5 (2011) 8700–8709. doi:<https://doi.org/10.1021/nn2026325>.
 - [293] A. Hammiche, M. Reading, H. M. Pollock, M. Song, D. J. Hourston, Localized thermal analysis using a miniaturized resistive probe, *Rev. Sci. Instrum.* 67 (1996) 4268. doi:<https://doi.org/10.1063/1.1147525>.
 - [294] P. Tovee, M. Pumarol, D. Zeze, K. Kjoller, O. Kolosov, Nanoscale spatial resolution probes for scanning thermal microscopy of solid state materials, *J. Appl. Phys.* 112 (2012) 114317. doi:<https://doi.org/10.1063/1.4767923>.
 - [295] F. Menges, H. Riel, A. Stemmer, B. Gotsmann, Quantitative thermometry of nanoscale hot spots, *Nano Lett.* 12 (2012) 596–601. doi:<https://doi.org/10.1021/nl203169t>.
 - [296] F. Menges, P. Mensch, H. Schmid, H. Riel, A. Stemmer, B. Gotsmann, Temperature mapping of operating nanoscale devices by scanning probe thermometry, *Nat. Commun.* 7 (2016) 10874. doi:<https://doi.org/10.1038/ncomms10874>.
 - [297] J. K. Gimzewski, Ch. Gerber, E. Meyer, R. R. Schlittler, Observation of a chemical reaction using a micromechanical sensor, *Chem. Phys. Lett.* 217 (1994) 589–594. doi:[https://doi.org/10.1016/0009-2614\(93\)E1419-H](https://doi.org/10.1016/0009-2614(93)E1419-H).
 - [298] J. Varesi, J. Lai, T. Perazzo, Z. Shi, A. Majumdar, Photothermal measurements at picowatt resolution using uncooled micro-optomechanical sensors, *Appl. Phys. Lett.* 71 (1997) 306. doi:<https://doi.org/10.1063/1.120440>.
 - [299] S. Sadat, E. Meyhofer, P. Reddy, High resolution resistive thermometry for micro/nanoscale measurements, *Rev. Sci. Instrum.* 83 (2012)

084902. doi:<https://doi.org/10.1063/1.4744963>.
- [300] S. Sadat, E. Meyhofer, P. Reddy, Resistance thermometry-based picowatt-resolution heat-flow calorimeter, *Appl. Phys. Lett.* 102 (2013) 163110. doi:<https://doi.org/10.1063/1.4802239>.
- [301] E. Dechaumphai, R. Chen, Sub-picowatt resolution calorimetry with niobium nitride thin-film thermometer, *Rev. Sci. Instrum.* 85 (2014) 094903. doi:<https://doi.org/10.1063/1.4895678>.
- [302] B. Song, Y. Ganjeh, S. Sadat, D. Thompson, A. Fiorino, V. Fernández-Hurtado, J. Feist, F. J. Garcia-Vidal, J. C. Cuevas, P. Reddy, E. Meyhofer, Enhancement of near-field radiative heat transfer using polar dielectric thin films, *Nat. Nanotechnol.* 10 (2015) 253–258. doi:<https://doi.org/10.1038/nnano.2015.6>.
- [303] W. Lee, W. Fon, B. W. Axelrod, M. L. Roukes, High-sensitivity microfluidic calorimeters for biological and chemical applications, *PNAS* 106 (2009) 15225. doi:<https://doi.org/10.1073/pnas.0901447106>.
- [304] S. Wang, S. Yu, M. S. Siedler, P. M. Ihnat, D. I. Filoti, M. Lu, L. Zuo, Micro-differential scanning calorimeter for liquid biological samples, *Rev. Sci. Instrum.* 87 (2016) 105005. doi:<https://doi.org/10.1063/1.4965443>.
- [305] L. Zhu, A. Fiorino, D. Thompson, R. Mittapally, E. Meyhofer, P. Reddy, Near-field photonic cooling through control of the chemical potential of photons, *Nature* 566 (2019) 239–244. doi:<https://doi.org/10.1038/s41586-019-0918-8>.
- [306] D. Thompson, L. Zhu, R. Mittapally, S. Sadat, Z. Xing, P. McArdle, M. M. Qazilbash, P. Reddy, E. Meyhofer, Hundred-fold enhancement in far-field radiative heat transfer over the blackbody limit, *Nature* 561 (2018) 216–221. doi:<https://doi.org/10.1038/s41586-018-0480-9>.
- [307] A. Fiorino, L. Zhu, D. Thompson, R. Mittapally, P. Reddy, E. Meyhofer, Nanogap near-field thermophotovoltaics, *Nat. Nanotechnol.* 13 (2018) 806–811. doi:<https://doi.org/10.1038/s41565-018-0172-5>.
- [308] L. Cui, W. Jeong, V. Fernández-Hurtado, J. Feist, F. J. García-Vidal, J. C. Cuevas, E. Meyhofer, P. Reddy, Study of radiative heat transfer in Ångström- and nanometre-sized gaps, *Nat. Commun.* 8 (2017) 14479. doi:<https://doi.org/10.1038/ncomms14479>.
- [309] K. Kim, B. Song, V. Fernández-Hurtado, W. Lee, W. Jeong, L. Cui, D. Thompson, J. Feist, M. T. Homer Reid, F. J. García-Vidal, J. C. Cuevas, E. Meyhofer, P. Reddy, Radiative heat transfer in the extreme near field, *Nature* 528 (2015) 387–391. doi:<https://doi.org/10.1038/nature16070>.
- [310] B. Song, D. Thompson, A. Fiorino, Y. Ganjeh, P. Reddy, E. Meyhofer, Radiative heat conductances between dielectric and metallic parallel plates with nanoscale gaps, *Nat. Nanotechnol.* 11 (2016) 509–514. doi:<https://doi.org/10.1038/nnano.2016.17>.
- [311] S. Lee, K. Hippalgaonkar, F. Yang, J. Hong, C. Ko, J. Suh, K. Liu, K. Wang, J. J. Urban, X. Zhang, C. Dames, S. A. Hartnoll, O. Delaire, J. Wu, Anomalous low electronic thermal conductivity in metallic vanadium dioxide, *Science* 355 (2017) 371–374. doi:<https://doi.org/10.1126/science.aag0410>.
- [312] S. Lee, F. Yang, J. Suh, S. Yang, Y. Lee, G. Li, H. S. Choe, A. Suslu, Y. Chen, C. Ko, J. Park, K. Liu, J. Li, K. Hippalgaonkar, J. J. Urban, S. Tongay, J. Wu, Anisotropic in-plane thermal conductivity of black phosphorus nanoribbons at temperatures higher than 100K, *Nat. Commun.* 6 (2015) 8573. doi:<https://doi.org/10.1038/ncomms9573>.
- [313] L. Shi, D. Li, C. Yu, W. Jang, D. Kim, Z. Yao, P. Kim, A. Majumdar, Measuring thermal and thermoelectric properties of one-dimensional nanostructures using a microfabricated device, *J. Heat Transfer* 125 (2003) 881–888. doi:<https://doi.org/10.1115/1.1597619>.
- [314] C. Canetta, A. Narayanaswamy, Measurement of optical coupling between adjacent bi-material microcantilevers, *Rev. Sci. Instrum.* 84 (2013) 105002. doi:<https://doi.org/10.1063/1.4824430>.
- [315] K. Kim, W. Jeong, W. Lee, S. Sadat, D. Thompson, E. Meyhofer, P. Reddy, Quantification of thermal and contact resistances of scanning thermal probes, *Appl. Phys. Lett.* 105 (2014) 203107. doi:<https://doi.org/10.1063/1.4902075>.
- [316] Y. Gao, B. Zhao, J. J. Vlassak, C. Schick, Nanocalorimetry: Door opened for *in situ* material characterization under extreme non-equilibrium conditions, *Prog. Mater. Sci.* 104 (2019) 53–137. doi:<https://doi.org/10.1016/j.pmatsci.2019.04.001>.
- [317] C. W. Chang, A. M. Fennimore, A. Afanasiev, D. Okawa, T. Ikuno, H. Garcia, D. Li, A. Majumdar, A. Zettl, Isotope effect on the thermal conductivity of boron nitride nanotubes, *Phys. Rev. Lett.* 97 (2006) 085901. doi:<https://doi.org/10.1103/PhysRevLett.97.085901>.
- [318] M. Y. Efremov, E. A. Olson, M. Zhang, F. Schiettekatte, Z. Zhang, L. H. Allen, Ultrasensitive, fast, thin-film differential scanning calorimeter, *Rev. Sci. Instrum.* 75 (2004) 179. doi:<https://doi.org/10.1063/1.1633000>.
- [319] K. Willa, Z. Diao, D. Campanini, U. Welp, R. Divan, M. Hudl, Z. Islam, W.-K. Kwok, A. Rydh, Nanocalorimeter platform for *in situ* specific heat measurements and x-ray diffraction at low temperature, *Rev. Sci. Instrum.* 88 (2017) 125108. doi:<https://doi.org/10.1063/1.5016592>.
- [320] J. K. Gimzewski, C. Gerber, E. Meyer, R. R. Schlittler, *Forces in Scanning Probe Methods*, Springer Netherlands, Dordrecht, 1995.
- [321] J. R. Barnes, S. J. Stephenson, M. E. Welland, Ch. Gerber, J. K. Gimzewski, Photothermal spectroscopy with femtojoule sensitive using a micromechanical device, *Nature* 372 (1994) 79–81. doi:<https://doi.org/10.1038/372079a0>.
- [322] J. R. Barnes, R. J. Stephenson, C. N. Woodburn, S. J. O'Shea, M. E. Welland, T. Rayment, J. K. Gimzewski, Ch. Gerber, A femtojoule calorimeter using micromechanical sensors, *Rev. Sci. Instrum.* 65 (1994) 3793. doi:<https://doi.org/10.1063/1.1144509>.
- [323] W. C. Young, R. G. Budynas, *Roark's Formulas for Stress and Strain*, 7th Edition, McGraw-Hill Professional, 2001.
- [324] J. Lai, T. Perazzo, Z. Shi, A. Majumdar, Optimization and performance of high-resolution micro-optomechanical thermal sensors, *Sens. Actuators A* 58 (1997) 113–119. doi:[https://doi.org/10.1016/S0924-6427\(96\)01401-X](https://doi.org/10.1016/S0924-6427(96)01401-X).
- [325] S. Shen, A. Henry, J. Tong, R. Zheng, G. Chen, Polyethylene nanofibres with very high thermal conductivities, *Nat. Nanotechnol.* 5 (2010) 251–255. doi:<https://doi.org/10.1038/nnano.2010.27>.
- [326] P. Kim, L. Shi, A. Majumdar, P. L. McEuen, Thermal transport measurements of individual multiwalled nanotubes, *Phys. Rev. Lett.* 87 (2001) 215502. doi:<https://doi.org/10.1103/PhysRevLett.87.215502>.
- [327] C. Yu, L. Shi, Z. Yao, D. Li, A. Majumdar, Thermal conductance and thermopower of an individual single-wall carbon nanotube, *Nano Lett.* 5 (2005) 1842–1846. doi:<https://doi.org/10.1021/nl051044e>.
- [328] D. Li, Y. Wu, P. Kim, L. Shi, P. Yang, A. Majumdar, Thermal conductivity of individual silicon nanowires, *Appl. Phys. Lett.* 83 (2003) 2934. doi:<https://doi.org/10.1063/1.1616981>.
- [329] L. Cui, W. Jeong, S. Hur, M. Matt, J. C. Klöckner, F. Pauly, P. Nielaba, J. C. Cuevas, E. Meyhofer, P. Reddy, Quantized thermal transport in single-atom junctions, *Science* 355 (2017) 1192–1195. doi:<https://doi.org/10.1126/science.aam6622>.

- [330] L. Cui, R. Miao, K. Wang, D. Thompson, L. A. Zotti, J. C. Cuevas, E. Meyhofer, P. Reddy, Peltier cooling in molecular junctions, *Nat. Nanotechnol.* 13 (2018) 122–127. doi:<https://doi.org/10.1038/s41565-017-0020-z>.
- [331] D. Segal, Probing the limits of heat flow, *Science* 355 (2017) 1125–1126. doi:<https://doi.org/10.1126/science.aam9362>.
- [332] C. Canetta, A. Narayanaswamy, Sub-picowatt resolution calorimetry with a bi-material microcantilever sensor, *Appl. Phys. Lett.* 102 (2013) 103112. doi:<https://doi.org/10.1063/1.4795625>.
- [333] M. V. Salapaka, H. S. Bergh, J. Lai, A. Majumdar, E. McFarland, Multi-mode noise analysis of cantilevers for scanning probe microscopy, *J. Appl. Phys.* 81 (1997) 2480. doi:<https://doi.org/10.1063/1.363955>.
- [334] J. P. Bergfield, C. A. Stafford, Thermoelectric corrections to quantum voltage measurement, *Phys. Rev. B* 90 (2014) 235438. doi:<https://doi.org/10.1103/PhysRevB.90.235438>.
- [335] C. Canetta, S. Guo, A. Narayanaswamy, Measuring thermal conductivity of polystyrene nanowires using the dual-cantilever technique, *Rev. Sci. Instrum.* 85 (2014) 104901. doi:<https://doi.org/10.1063/1.4896330>.
- [336] C. W. Chang, D. Okawa, H. Garcia, A. Majumdar, A. Zettl, Breakdown of Fourier's law in nanotube thermal conductors, *Phys. Rev. Lett.* 101 (2008) 075903. doi:<https://doi.org/10.1103/PhysRevLett.101.075903>.
- [337] D. Roy, Crossover from ballistic to diffusive thermal transport in quantum langevin dynamics study of a harmonic chain connected to self-consistent reservoirs, *Phys. Rev. E* 77 (2008) 062102. doi:<https://doi.org/10.1103/PhysRevE.77.062102>.
- [338] N. Yang, G. Zhang, B. Li, Violation of Fourier's law and anomalous heat diffusion in silicon nanowires, *Nano Today* 5 (2010) 85–90. doi:<https://doi.org/10.1016/j.nantod.2010.02.002>.
- [339] J. A. Johnson, A. A. Maznev, J. Cuffe, J. K. Eliason, A. J. Minnich, T. Kehoe, C. M. S. Torres, G. Chen, K. A. Nelson, Direct measurement of room-temperature nondiffusive thermal transport over micron distances in a silicon membrane, *Phys. Rev. Lett.* 110 (2013) 025901. doi:<https://doi.org/10.1103/PhysRevLett.110.025901>.
- [340] S. Liu, G. H. Clever, Y. Takezawa, M. Kaneko, K. Tanaka, X. Guo, M. Shionoya, Direct conductance measurement of individual metallo-DNA duplexes within single-molecule break junctions, *Angew. Chem. Int. Ed.* 50 (2011) 8886–8890. doi:<https://doi.org/10.1002/anie.201102980>.
- [341] M. L. Perrin, R. Frisenda, M. Koole, J. S. Seldenthuis, J. A. Celis Gil, H. Valkenier, J. C. Hummelen, N. Renaud, F. C. Grozema, J. M. Thijssen, D. Dulić, H. S. J. van der Zant, Large negative differential conductance in single-molecule break junctions, *Nat. Nanotechnol.* 9 (2014) 830–834. doi:<https://doi.org/10.1038/nnano.2014.177>.
- [342] J. M. Beebe, B. Kim, J. W. Gadzuk, C. D. Frisbie, J. G. Kushmerick, Transition from direct tunneling to field emission in metal-molecule-metal junctions, *Phys. Rev. Lett.* 97 (2006) 026801. doi:<https://doi.org/10.1103/PhysRevLett.97.026801>.
- [343] E. H. Huisman, C. M. Guédon, B. J. van Wees, S. J. van der Molen, Interpretation of transition voltage spectroscopy, *Nano Lett.* 9 (2009) 3909–3913. doi:<https://doi.org/10.1021/nl9021094>.
- [344] C. Bruot, J. Hihath, N. J. Tao, Mechanically controlled molecular orbital alignment in single molecule junctions, *Nat. Nanotechnol.* 7 (2012) 35–40. doi:<https://doi.org/10.1038/nnano.2011.212>.
- [345] N. Agrait, A. L. Yeyati, J. M. van Ruitenbeek, Quantum properties of atomic-sized conductors, *Phys. Rep.* 377 (2003) 81–279. doi:[https://doi.org/10.1016/S0370-1573\(02\)00633-6](https://doi.org/10.1016/S0370-1573(02)00633-6).
- [346] D. Xiang, H. Jeong, T. Lee, D. Mayer, Mechanically controllable break junctions for molecular electronics, *Adv. Mater.* 25 (2013) 4845. doi:<https://doi.org/10.1002/adma.201301589>.
- [347] C. Huang, A. V. Rudnev, W. Hong, T. Wandlowski, Break junction under electrochemical gating: testbed for single-molecule electronics, *Chem. Soc. Rev.* 44 (2015) 889–901. doi:<https://doi.org/10.1039/C4CS00242C>.
- [348] L. Wang, L. Wang, L. Zhang, D. Xiang, Advance of mechanically controllable break junction for molecular electronics, *Top. Curr. Chem.* 375 (2017) 61. doi:<https://doi.org/10.1007/s41061-017-0149-0>.
- [349] W. Zhang, H. Liu, J. Lu, L. Ni, H. Liu, Q. Li, M. Qiu, B. Xu, T. Lee, Z. Zhao, X. Wang, M. Wang, T. Wang, A. Offenhäusser, D. Mayer, W.-T. Hwang, D. Xiang, Atomic switches of metallic point contacts by plasmonic heating, *Light: Sci. Appl.* 8 (2019) 34. doi:<https://doi.org/10.1038/s41377-019-0144-z>.
- [350] H. Yasuda, A. Sakai, Conductance of atomic-scale gold contacts under high-bias voltages, *Phys. Rev. B* 56 (1997) 1069. doi:<https://doi.org/10.1103/PhysRevB.56.1069>.
- [351] K. Itakura, K. Yuki, S. Kurokawa, H. Yasuda, A. Sakai, Bias dependence of the conductance of Au nanocontacts, *Phys. Rev. B* 60 (1999) 11163. doi:<https://doi.org/10.1103/PhysRevB.60.11163>.
- [352] J. M. Kras, J. M. van Ruitenbeek, L. J. de Jongh, Atomic structure and quantized conductance in metal point contacts, *Physica B* 218 (1996) 228–233. doi:[https://doi.org/10.1016/0921-4526\(95\)00601-X](https://doi.org/10.1016/0921-4526(95)00601-X).
- [353] K. S. Rails, D. C. Ralph, R. A. Buhrman, Individual-defect electromigration in metal nanobridges, *Phys. Rev. B* 40 (1989) 11561. doi:<https://doi.org/10.1103/PhysRevB.40.11561>.
- [354] N. Neél, J. Kröger, R. Berndt, Two-level conductance fluctuations of a single-molecule junction, *Nano Lett.* 11 (2011) 3593–3596. doi:<https://doi.org/10.1021/nl201327c>.
- [355] T. N. Todorov, J. Hoekstra, A. P. Sutton, Current-induced embrittlement of atomic wires, *Phys. Rev. Lett.* 86 (2001) 3606. doi:<https://doi.org/10.1103/PhysRevLett.86.3606>.
- [356] M. Tsutsui, S. Kurokawa, A. Sakai, Bias-induced local heating in Au atom-sized contacts, *Nanotechnology* 17 (2006) 5334. doi:<https://doi.org/10.1088/0957-4484/17/21/008>.
- [357] M. Tsutsui, S. Kurokawa, A. Sakai, Bias-induced local heating in atom-sized metal contacts at 77 K, *Appl. Phys. Lett.* 90 (2007) 133121. doi:<https://doi.org/10.1063/1.2719682>.
- [358] Z. Yang, M. Chshiev, M. Zwolak, Y.-C. Chen, M. Di Ventra, Role of heating and current-induced forces in the stability of atomic wires, *Phys. Rev. B* 71 (2005) 041402(R). doi:<https://doi.org/10.1103/PhysRevB.71.041402>.
- [359] M. Asheghi, Y. Yang, *Micro- and Nano-Scale Diagnostic Techniques for Thermometry and Thermal Imaging of Microelectronic and Data Storage Devices*, 1st Edition, Springer Berlin Heidelberg, Berlin, Heidelberg, 2005, pp. 155–196.
- [360] F. Haupt, A. Imamoglu, M. Kroner, Single quantum dot as an optical thermometer for millikelvin temperatures, *Phys. Rev. Appl.* 2 (2014) 024001. doi:<https://doi.org/10.1103/PhysRevApplied.2.024001>.

- [361] J.-U. Lee, D. Yoon, H. Kim, S. W. Lee, H. Cheong, Thermal conductivity of suspended pristine graphene measured by Raman spectroscopy, *Phys. Rev. B* 83 (2011) 081419(R). doi:<https://doi.org/10.1103/PhysRevB.83.081419>.
- [362] H. Liu, Y. Fan, J. Wang, Z. Song, H. Shi, R. Han, Y. Sha, Y. Jiang, Intracellular temperature sensing: An ultra-bright luminescent nanothermometer with non-sensitivity to pH and ionic strength, *Sci. Rep.* 5 (2015) 14879. doi:<https://doi.org/10.1038/srep14879>.
- [363] K. Okabe, N. Inada, C. Gota, Y. Harada, T. Funatsu, S. Uchiyama, Intracellular temperature mapping with a fluorescent polymeric thermometer and fluorescence lifetime imaging microscopy, *Nat. Commun.* 3 (2012) 705. doi:<https://doi.org/10.1038/ncomms1714>.
- [364] D. Evanko, A thermometer for cells, *Nat. Methods* 9 (2012) 328. doi:<https://doi.org/10.1038/nmeth.1966>.
- [365] G. Kucsko, P. C. Maurer, N. Y. Yao, M. Kubo, H. J. Noh, P. K. Lo, H. Park, M. D. Lukin, Nanometre-scale thermometry in a living cell, *Nature* 500 (2013) 54–58. doi:<https://doi.org/10.1038/nature12373>.
- [366] R. Tanimoto, T. Hiraiwa, Y. Nakai, Y. Shindo, K. Oka, N. Hiroi, A. Funahashi, Detection of temperature difference in neuronal cells, *Sci. Rep.* 6 (2016) 22071. doi:<https://doi.org/10.1038/srep22071>.
- [367] C. D. S. Brites, P. P. Lima, N. J. O. Silva, A. Millán, V. S. Amaral, F. Palacio, L. D. Carlos, Thermometry at the nanoscale, *Nanoscale* 12 (2012) 4799–4829. doi:<https://doi.org/10.1039/C2NR30663H>.
- [368] D. Jaque, F. Vetrone, Luminescence nanothermometry, *Nanoscale* 4 (2012) 4301–4326. doi:<https://doi.org/10.1039/C2NR30764B>.
- [369] M. M. Kim, A. Giry, M. Mastiani, G. O. Rodrigues, A. Reisa, P. Mandin, Microscale thermometry: A review, *Microelectron. Eng.* 148 (2015) 129–142. doi:<https://doi.org/10.1016/j.mee.2015.11.002>.
- [370] M. Farzaneh, K. Maize, D. Lüerßen, J. A. Summers, P. M. Mayer, P. E. Raad, K. P. Pipe, A. Shakouri, R. J. Ram, J. A. Hudgings, CCD-based thermoreflectance microscopy: principles and applications, *J. Phys. D: Appl. Phys.* 42 (2009) 143001. doi:<https://doi.org/10.1088/0022-3727/42/14/143001>.
- [371] A. W. Bushmaker, V. V. Deshpande, M. W. Bockrath, S. B. Cronin, Direct observation of mode selective electron-phonon coupling in suspended carbon nanotubes, *Nano Lett.* 7 (2007) 3618–3622. doi:<https://doi.org/10.1021/nl071840f>.
- [372] V. V. Deshpande, S. Hsieh, A. W. Bushmaker, M. Bockrath, S. B. Cronin, Spatially resolved temperature measurements of electrically heated carbon nanotubes, *Phys. Rev. Lett.* 102 (2009) 105501. doi:<https://doi.org/10.1103/PhysRevLett.102.105501>.
- [373] L. M. Malard, M. A. Pimenta, G. Dresselhaus, M. S. Dresselhaus, Raman spectroscopy in graphene, *Phys. Rep.* 473 (2009) 51–87. doi:<https://doi.org/10.1016/j.physrep.2009.02.003>.
- [374] M. S. Dresselhaus, G. Dresselhaus, R. Saito, A. Jorio, Raman spectroscopy of carbon nanotubes, *Phys. Rep.* 409 (2005) 47–99. doi:<https://doi.org/10.1016/j.physrep.2004.10.006>.
- [375] Y. Wu, J. Maultzsch, E. Knoesel, B. Chandra, M. Huang, M. Y. Sfeir, L. E. Brus, J. Hone, T. F. Heinz, Variable electron-phonon coupling in isolated metallic carbon nanotubes observed by Raman scattering, *Phys. Rev. Lett.* 99 (2007) 027402. doi:<https://doi.org/10.1103/PhysRevLett.99.027402>.
- [376] Z. Ioffe, T. Shamai, A. Ophir, G. Noy, I. Yutsis, K. Kfir, O. Cheshnovsky, Y. Selzer, Detection of heating in current-carrying molecular junctions by Raman scattering, *Nat. Nanotechnol.* 3 (2008) 727–732. doi:<https://doi.org/10.1038/nnano.2008.304>.
- [377] M. Oron-Carl, R. Krupke, Raman spectroscopic evidence for hot-phonon generation in electrically biased carbon nanotubes, *Phys. Rev. Lett.* 100 (2008) 127401. doi:<https://doi.org/10.1103/PhysRevLett.100.127401>.
- [378] A. Otto, W. Akemann, A. Pucci, Normal bands in surface-enhanced Raman scattering (SERS) and their relation to the electron-hole pair excitation background in SERS, *Isr. J. Chem.* 46 (2006) 307. doi:https://doi.org/10.1560/IJC_46_3_307.
- [379] M. Mecklenburg, W. A. Hubbard, E. R. White, R. Dhall, S. B. Cronin, S. Aloni, B. C. Regan, Nanoscale temperature mapping in operating microelectronic devices, *Science* 347 (2015) 629–632. doi:<https://doi.org/10.1126/science.aaa2433>.
- [380] C. Colliex, Taking temperature at the nanoscale, *Science* 347 (2015) 611–612. doi:<https://doi.org/10.1126/science.aaa5311>.
- [381] M. J. Lagos, P. E. Batson, Thermometry with subnanometer resolution in the electron microscope using the principle of detailed balancing, *Nano Lett.* 18 (2018) 4556–4563. doi:<https://doi.org/10.1021/acs.nanolett.8b01791>.
- [382] J. C. Idrobo, A. R. Lupini, T. Feng, R. R. Unocic, F. S. Walden, D. S. Gardiner, T. C. Lovejoy, N. Dellby, S. T. Pantelides, O. L. Krivanek, Temperature measurement by a nanoscale electron probe using energy gain and loss spectroscopy, *Phys. Rev. Lett.* 120 (2018) 095901. doi:<https://doi.org/10.1103/PhysRevLett.120.095901>.
- [383] M. J. Lagos, A. Trügler, U. Hohenester, P. E. Batson, Mapping vibrational surface and bulk modes in a single nanocube, *Nature* 543 (2017) 529–532. doi:<https://doi.org/10.1038/nature21699>.
- [384] L. Aigouy, G. Tessier, M. Mortier, B. Charlot, Scanning thermal imaging of microelectronic circuits with a fluorescent nanoprobe, *Appl. Phys. Lett.* 87 (2005) 184105. doi:<https://doi.org/10.1063/1.2123384>.
- [385] M. A. R. C. Alencar, G. S. Maciel, C. B. de Araújo, A. Patra, Er³⁺-doped BaTiO₃ nanocrystals for thermometry: Influence of nanoenvironment on the sensitivity of a fluorescence based temperature sensor, *Appl. Phys. Lett.* 84 (2004) 4753. doi:<https://doi.org/10.1063/1.1760882>.
- [386] B. Samson, L. Aigouy, P. Löw, C. Bergaud, B. J. Kim, M. Mortier, ac thermal imaging of nanoheaters using a scanning fluorescent probe, *Appl. Phys. Lett.* 92 (2008) 023101. doi:<https://doi.org/10.1063/1.2832673>.
- [387] H. Berthou, C. K. Jörgensen, Optical-fiber temperature sensor based on upconversion-excited fluorescence, *Opt. Lett.* 15 (1990) 1100–1102. doi:<https://doi.org/10.1364/OL.15.001100>.
- [388] E. Maurice, G. Monnom, B. Dussardier, A. Saïssy, D. B. Ostrowsky, G. W. Baxter, Erbium-doped silica fibers for intrinsic fiber-optic temperature sensors, *Appl. Opt.* 34 (1995) 8019–8025. doi:<https://doi.org/10.1364/AO.34.008019>.
- [389] S. Pailhès, H. Euchner, V. M. Giordano, R. Debord, A. Assy, S. Gomès, A. Bosak, D. Machon, S. Paschen, M. de Boissieu, Localization of propagative phonons in a perfectly crystalline solid, *Phys. Rev. Lett.* 113 (2014) 025506. doi:<https://doi.org/10.1103/PhysRevLett.113.025506>.
- [390] Y.-J. Yu, M. Y. Han, S. Berciaud, A. B. Georgescu, T. F. Heinz, L. E. Brus, K. S. Kim, P. Kim, High-resolution spatial mapping of the temperature distribution of a Joule self-heated graphene nanoribbon, *Appl. Phys. Lett.* 99 (2011) 183105. doi:<https://doi.org/10.1063/1.3657515>.
- [391] F. Menges, H. Riel, A. Stemmer, C. Dimitrakopoulos, B. Gotsmann, Thermal transport into graphene through nanoscopic contacts, *Phys. Rev. Lett.* 111 (2013) 205901. doi:<https://doi.org/10.1103/PhysRevLett.111.205901>.

- [392] G. Mills, H. Zhou, A. Midha, L. Donaldson, J. M. R. Weaver, Scanning thermal microscopy using batch fabricated thermocouple probes, *Appl. Phys. Lett.* 72 (1998) 2900. doi:<https://doi.org/10.1063/1.121453>.
- [393] K. Luo, Z. Shi, J. Lai, A. Majumdar, Nanofabrication of sensors on cantilever probe tips for scanning multiprobe microscopy, *Appl. Phys. Lett.* 68 (1996) 325. doi:<https://doi.org/10.1063/1.116074>.
- [394] Y. Zhang, P. S. Dobson, J. M. R. Weaver, Batch fabricated dual cantilever resistive probe for scanning thermal microscopy, *Microelectron. Eng.* 88 (2011) 2435–2438. doi:<https://doi.org/10.1016/j.mee.2011.02.040>.
- [395] R. J. Pylkki, P. J. Moyer, P. E. West, Scanning near-field optical microscopy and scanning thermal microscopy, *Jpn. J. Appl. Phys.* 33 (1994) 3785. doi:<https://doi.org/10.1143/JJAP.33.3785>.
- [396] O. Nakabeppu, M. Chandrachood, Y. Wu, J. Lai, A. Majumdar, Scanning thermal imaging microscopy using composite cantilever probes, *Appl. Phys. Lett.* 66 (1995) 694. doi:<https://doi.org/10.1063/1.114102>.
- [397] E. Saïdi, B. Samson, L. Aigouy, S. Volz, P. Löw, C. Bergaud, M. Mortier, Scanning thermal imaging by near-field fluorescence spectroscopy, *Nanotechnology* 20 (2009) 115703. doi:<https://doi.org/10.1088/0957-4484/20/11/115703>.
- [398] S. Gomès, A. Assy, P.-O. Chapuis, Scanning thermal microscopy: A review, *Phys. Status Solidi A* 212 (2015) 477–494. doi:<https://doi.org/10.1002/pssa.201400360>.
- [399] P. D. Tovee, M. Pumarol, D. Zeze, K. Kjoller, O. Kolosov, Nanoscale spatial resolution probes for scanning thermal microscopy of solid state materials, *J. App. Phys.* 112 (2012) 114317. doi:<https://doi.org/10.1063/1.4767923>.
- [400] J. Hirotsu, J. Amano, T. Ikuta, T. Nishiyama, K. Takahashi, Carbon nanotube thermal probe for quantitative temperature sensing, *Sens. Actuators, A* 199 (2013) 1–8. doi:<https://doi.org/10.1016/j.sna.2013.04.038>.
- [401] P. D. Tovee, M. E. Pumarol, M. C. Rosamond, R. Jones, M. C. Petty, D. A. Zeze, O. V. Kolosov, Nanoscale resolution scanning thermal microscopy using carbon nanotube tipped thermal probes, *Phys. Chem. Chem. Phys.* 16 (2014) 1174–1181. doi:<https://doi.org/10.1039/C3CP53047G>.
- [402] W. Lee, K. Kim, W. Jeong, L. A. Zotti, F. Pauly, J. C. Cuevas, P. Reddy, Heat dissipation in atomic-scale junctions, *Nature* 498 (2013) 209–212. doi:<https://doi.org/10.1038/nature12183>.
- [403] S. Sadat, A. Tan, Y. J. Chua, P. Reddy, Nanoscale thermometry using point contact thermocouples, *Nano Lett.* 10 (2010) 2613–2617. doi:<https://doi.org/10.1021/nl101354e>.
- [404] K. Kim, W. Jeong, W. Lee, P. Reddy, Ultra-high vacuum scanning thermal microscopy for nanometer resolution quantitative thermometry, *ACS Nano* 6 (2012) 4248–4257. doi:<https://doi.org/10.1021/nn300774n>.
- [405] A. Majumdar, J. Varesi, Nanoscale temperature distributions measured by scanning Joule expansion microscopy, *J. Heat Transfer* 120 (1998) 297–305. doi:<https://doi.org/10.1115/1.2824245>.
- [406] M. Cannaeerts, D. Buntinx, A. Volodin, C. Van Haesendonck, Calibration of a scanning Joule expansion microscope (SJEM), *Appl. Phys. A* 72 (2001) S67–S70. doi:<https://doi.org/10.1007/s003390100648>.
- [407] S. P. Gurrum, Y. K. Joshi, W. P. King, K. Ramakrishna, Scanning Joule expansion microscopy of a constriction in thin metallic film, *J. Heat Transfer* 127 (2005) 809. doi:<https://doi.org/10.1115/1.2033315>.
- [408] X. Xie, K. L. Grosse, J. Song, C. Lu, S. Dunham, F. Du, A. E. Islam, Y. Li, Y. Zhang, E. Pop, Y. Huang, W. P. King, J. A. Rogers, Quantitative thermal imaging of single-walled carbon nanotube devices by scanning Joule expansion microscopy, *ACS Nano* 6 (2012) 10267–10275. doi:<https://doi.org/10.1021/nn304083a>.
- [409] L. Aigouy, E. Saïdi, L. Lalouat, J. Labéguerie-Eg  a, M. Mortier, P. L  w, C. Bergaud, AC thermal imaging of a microwire with a fluorescent nanocrystal: Influence of the near field on the thermal contrast, *J. Appl. Phys.* 106 (2009) 074301. doi:<https://doi.org/10.1063/1.3233940>.
- [410] C. A. Stafford, Local temperature of an interacting quantum system far from equilibrium, *Phys. Rev. B* 93 (2016) 245403. doi:<https://doi.org/10.1103/PhysRevB.93.245403>.
- [411] P. A. Jacquet, Thermoelectric transport properties of a chain of quantum dots with self-consistent reservoirs, *J. Stat. Phys.* 134 (2009) 709–748. doi:<https://doi.org/10.1007/s10955-009-9697-1>.
- [412] A. Shastry, C. A. Stafford, Cold spots in quantum systems far from equilibrium: Local entropies and temperatures near absolute zero, *Phys. Rev. B* 92 (2015) 245417. doi:<https://doi.org/10.1103/PhysRevB.92.245417>.
- [413] C. A. Stafford, A. Shastry, Local entropy of a nonequilibrium fermion system, *J. Chem. Phys.* 146 (2017) 092324. doi:<https://doi.org/10.1063/1.4975810>.
- [414] A. Shastry, Y. Xu, C. A. Stafford, The third law of thermodynamics in open quantum systems, *J. Chem. Phys.* 151 (2019) 064115. doi:<https://doi.org/10.1063/1.5100182>.
- [415] W. Jost, *Physical Chemistry An Advanced Treatise*, 1st Edition, Vol. 1, Academic Press, New York, 1971.
- [416] J. Prost, J.-F. Joanny, J. M. R. Parrondo, Generalized fluctuation-dissipation theorem for steady-state systems, *Phys. Rev. Lett.* 103 (2009) 090601. doi:<https://doi.org/10.1103/PhysRevLett.103.090601>.
- [417] M. Mehboudi, A. Sanpera, J. M. R. Parrondo, Fluctuation-dissipation theorem for non-equilibrium quantum systems, *Quantum* 2 (2018) 66. doi:<https://doi.org/10.22331/q-2018-05-24-66>.
- [418] W.-M. Zhang, Exact master equation and general non-Markovian dynamics in open quantum systems, *Eur. Phys. J. Special Topics* 227 (2019) 1849–1867. doi:<https://doi.org/10.1140/epjst/e2018-800047-4>.
- [419] M. M. Ali, W.-M. Zhang, Nonequilibrium transient dynamics of photon statistics, *Phys. Rev. A* 95 (2017) 033830. doi:<https://doi.org/10.1103/PhysRevA.95.033830>.
- [420] P.-Y. Lo, H.-N. Xiong, W.-M. Zhang, Breakdown of Bose-Einstein distribution in photonic crystals, *Sci. Rep.* 5 (2015) 9423. doi:<https://doi.org/10.1038/srep09423>.
- [421] H.-N. Xiong, P.-Y. Lo, W.-M. Zhang, D. H. Feng, F. Nori, Non-Markovian complexity in the quantum-to-classical transition, *Sci. Rep.* 5 (2015) 13353. doi:<https://doi.org/10.1038/srep13353>.
- [422] A. Dhar, Heat transport in low-dimensional systems, *Adv. Phys.* 57 (2008) 457–537. doi:<https://doi.org/10.1080/00018730802538522>.
- [423] M. Michel, M. Hartmann, J. Gemmer, G. Mahler, Fourier’s law confirmed for a class of small quantum systems, *Eur. Phys. J. B* 34 (2003)

- 325–330. doi:<https://doi.org/10.1140/epjb/e2003-00228-x>.
- [424] P. L. Garrido, P. I. Hurtado, B. Nadrowski, Simple one-dimensional model of heat conduction which obeys Fourier’s law, *Phys. Rev. Lett.* 86 (2001) 5486. doi:<https://doi.org/10.1103/PhysRevLett.86.5486>.
- [425] J. P. Bergfield, S. M. Story, R. C. Stafford, C. A. Stafford, Probing Maxwell’s demon with a nanoscale thermometer, *ACS Nano* 7 (2013) 4429. doi:<https://doi.org/10.1021/nn401027u>.
- [426] J. P. Bergfield, M. A. Ratner, C. A. Stafford, M. Di Ventra, Tunable quantum temperature oscillations in graphene and carbon nanoribbons, <https://arxiv.org/abs/1305.6602> (2013).
- [427] Y.-J. Yu, Y. Zhao, S. Ryu, L. E. Brus, K. S. Kim, P. Kim, Tuning the graphene work function by electric field effect, *Nano Lett.* 9 (2009) 3430–3434. doi:<https://doi.org/10.1021/nl901572a>.
- [428] M. F. Craciun, S. Russo, M. Yamamoto, S. Tarucha, Tuneable electronic properties in graphene, *Nano Today* 6 (2011) 42–60. doi:<https://doi.org/10.1016/j.nantod.2010.12.001>.
- [429] H. Hermann, Localization of electron wave functions in one-dimensional disordered systems, *Phys. Stat. Sol. B* 66 (1974) 117–122. doi:<https://doi.org/10.1002/pssb.2220660112>.
- [430] V. M. Pereira, F. Guinea, J. M. B. Lopes dos Santos, N. M. R. Peres, A. H. C. Neto, Disorder induced localized states in graphene, *Phys. Rev. Lett.* 96 (2006) 036801. doi:<https://doi.org/10.1103/PhysRevLett.96.036801>.
- [431] J. Billy, V. Josse, Z. Zuo, A. Bernard, B. Hambrecht, P. Lugan, D. Clément, L. Sanchez-Palencia, P. Bouyer, A. Aspect, Direct observation of Anderson localization of matter waves in a controlled disorder, *Nature* 453 (2008) 891–894. doi:<https://doi.org/10.1038/nature07000>.
- [432] L. Berthier, J. Kurchan, Non-equilibrium glass transitions in driven and active matter, *Nat. Phys.* 9 (2013) 310–314. doi:<https://doi.org/10.1038/nphys2592>.
- [433] S. Inui, C. A. Stafford, J. P. Bergfield, Emergence of Fourier’s law of heat transport in quantum electron systems, *ACS Nano* 12 (2018) 4304–4311. doi:<https://doi.org/10.1021/acsnano.7b08816>.
- [434] E. Roduner, Understanding catalysis, *Chem. Soc. Rev.* 43 (2014) 8226–8239. doi:<https://doi.org/10.1039/C4CS00210E>.
- [435] M. Bonn, C. Hess, S. Funk, J. H. Miners, B. N. J. Persson, M. Wolf, G. Ertl, Femtosecond surface vibrational spectroscopy of CO adsorbed on Ru(001) during desorption, *Phys. Rev. Lett.* 84 (2000) 4653. doi:<https://doi.org/10.1103/PhysRevLett.84.4653>.
- [436] K. Stépán, J. Güdde, U. Höfer, Time-resolved measurement of surface diffusion induced by femtosecond laser pulses, *Phys. Rev. Lett.* 94 (2005) 236103. doi:<https://doi.org/10.1103/PhysRevLett.94.236103>.
- [437] E. H. G. Backus, A. Eichler, A. W. Kleyn, M. Bonn, Real-time observation of molecular motion on a surface, *Science* 310 (2005) 1790–1793. doi:<https://doi.org/10.1126/science.1120693>.
- [438] I. M. Lane, D. A. King, Z.-P. Liu, H. Arnolds, Real-time observation of nonadiabatic surface dynamics: The first picosecond in the dissociation of NO on iridium, *Phys. Rev. Lett.* 97 (2006) 186105. doi:<https://doi.org/10.1103/PhysRevLett.97.186105>.
- [439] K. Watanabe, K. Inoue, I. F. Nakai, Y. Matsumoto, Nonadiabatic coupling between C-O stretching and Pt substrate electrons enhanced by frustrated mode excitations, *Phys. Rev. B* 81 (2010) 241408(R). doi:<https://doi.org/10.1103/PhysRevB.81.241408>.
- [440] K. Inoue, K. Watanabe, T. Sugimoto, Y. Matsumoto, T. Yasuike, Disentangling multidimensional nonequilibrium dynamics of adsorbates: CO desorption from Cu(100), *Phys. Rev. Lett.* 117 (2016) 186101. doi:<https://doi.org/10.1103/PhysRevLett.117.186101>.
- [441] I. Anisimov, B. L. Kapeliovich, T. L. Perel’man, Electron emission from metal surfaces exposed to ultrashort laser pulses, *Sov. Phys. JETP* 39 (1974) 375.
- [442] P. B. Allen, Theory of thermal relaxation of electrons in metals, *Phys. Rev. Lett.* 59 (1987) 1460. doi:<https://doi.org/10.1103/PhysRevLett.59.1460>.
- [443] I. Lončarić, M. Alducin, P. Saalfrank, J. I. Juaristi, Femtosecond-laser-driven molecular dynamics on surfaces: Photodesorption of molecular oxygen from Ag(110), *Phys. Rev. B* 93 (2016) 014301. doi:<https://doi.org/10.1103/PhysRevB.93.014301>.
- [444] C. Springer, M. Head-Gordon, J. C. Tully, Simulations of femtosecond laser-induced desorption of CO from Cu(100), *Surf. Sci.* 320 (1994) L57–L62. doi:[https://doi.org/10.1016/0039-6028\(94\)00569-9](https://doi.org/10.1016/0039-6028(94)00569-9).
- [445] C. Springer, M. Head-Gordon, Simulations of the femtosecond laser-induced desorption of CO from Cu(100) at 0.5 ML coverage, *Chem. Phys.* 205 (1996) 73–89. doi:[https://doi.org/10.1016/0301-0104\(95\)00316-9](https://doi.org/10.1016/0301-0104(95)00316-9).
- [446] D. Novko, J. C. Tremblay, M. Alducin, J. I. Juaristi, Ultrafast transient dynamics of adsorbates on surfaces deciphered: The case of CO on Cu(100), *Phys. Rev. Lett.* 122 (2019) 016806. doi:<https://doi.org/10.1103/PhysRevLett.122.016806>.
- [447] D. Novko, M. Alducin, J. I. Juaristi, Electron-mediated phonon-phonon coupling drives the vibrational relaxation of CO on Cu(100), *Phys. Rev. Lett.* 120 (2018) 156804. doi:<https://doi.org/10.1103/PhysRevLett.120.156804>.
- [448] D. Lobaskin, S. Kehrein, Violation of the fluctuation-dissipation theorem and heating effects in the time-dependent Kondo model, *J. Stat. Phys.* 123 (2006) 301–313. doi:<https://doi.org/10.1007/s10955-006-9055-5>.
- [449] A. Mitra, A. J. Millis, Spin dynamics and violation of the fluctuation dissipation theorem in a nonequilibrium ohmic spin-boson model, *Phys. Rev. B* 72 (2005) 121102(R). doi:<https://doi.org/10.1103/PhysRevB.72.121102>.
- [450] S. Kirchner, Q. Si, On the concept of effective temperature in current carrying quantum critical states, *Phys. Status Solidi B* 247 (2010) 631–634. doi:<https://doi.org/10.1002/pssb.200983073>.
- [451] P. Ribeiro, Q. Si, S. Kirchner, Local quantum criticality out of equilibrium: Effective temperatures and scaling in the steady-state regime, *EPL* 102 (2013) 50001. doi:<https://doi.org/10.1209/0295-5075/102/50001>.
- [452] P. Murali, D. W. Pohl, Scanning tunneling potentiometry, *Appl. Phys. Lett.* 48 (1986) 514. doi:<https://doi.org/10.1063/1.96491>.
- [453] B. G. Briner, R. M. Feenstra, T. P. Chin, J. M. Woodall, Local transport properties of thin bismuth films studied by scanning tunneling potentiometry, *Phys. Rev. B* 54 (1996) R5283(R). doi:<https://doi.org/10.1103/PhysRevB.54.R5283>.
- [454] B. Voigtländer, V. Cherepanov, S. Korte, A. Leis, D. Cuma, S. Just, F. Lüpke, Invited review article: Multi-tip scanning tunneling microscopy: Experimental techniques and data analysis, *Rev. Sci. Instrum.* 89 (2018) 101101. doi:<https://doi.org/10.1063/1.5042346>.
- [455] K. W. Clark, X.-G. Zhang, I. V. Vlassiuk, G. He, R. M. Feenstra, A.-P. Li, Spatially resolved mapping of electrical conductivity across individual domain (grain) boundaries in graphene, *ACS Nano* 7 (2013) 7956–7966. doi:<https://doi.org/10.1021/nn403056k>.
- [456] P. Willke, T. Druga, R. G. Ulbrich, M. A. Schneider, M. Wenderoth, Spatial extent of a Landauer residual-resistivity dipole in graphene

- quantified by scanning tunnelling potentiometry, *Nat. Commun.* 6 (2015) 6399. doi:<https://doi.org/10.1038/ncomms7399>.
- [457] W. Wang, K. Munakata, M. Rozler, M. R. Beasley, Local transport measurements at mesoscopic length scales using scanning tunneling potentiometry, *Phys. Rev. Lett.* 110 (2013) 236802. doi:<https://doi.org/10.1103/PhysRevLett.110.236802>.
 - [458] S.-H. Ji, J. B. Hannon, R. M. Tromp, V. Perebeinos, J. Tersoff, F. M. Ross, Atomic-scale transport in epitaxial graphene, *Nat. Mater.* 11 (2012) 114–119. doi:<https://doi.org/10.1038/nmat3170>.
 - [459] D. K. Morr, Crossover from quantum to classical transport, *Contemp. Phys.* 57 (2016) 19–45. doi:<http://doi.org/10.1080/00107514.2015.1075728>.
 - [460] W. Wang, M. R. Beasley, Theoretical description of scanning tunneling potentiometry, <https://arxiv.org/abs/1007.1512> (2011).
 - [461] K. H. Bevan, A first principles scanning tunneling potentiometry study of an opaque graphene grain boundary in the ballistic transport regime, *Nanotechnology* 25 (2014) 415701. doi:<https://doi.org/10.1088/0957-4484/25/41/415701>.
 - [462] J. Rammer, H. Smith, Quantum field-theoretical methods in transport theory of metals, *Rev. Mod. Phys.* 58 (1986) 323. doi:<https://doi.org/10.1103/RevModPhys.58.323>.
 - [463] C. Caroli, R. Combescot, P. Nozieres, D. Saint-James, Direct calculation of the tunneling current, *J. Phys. C: Solid State Phys.* 4 (1971) 916–929. doi:<https://doi.org/10.1088/0022-3719/4/8/018>.
 - [464] A. A. Serga, A. V. Chumak, B. Hillebrands, YIG magnonics, *J. Phys. D: Appl. Phys.* 43 (2010) 264002. doi:<https://doi.org/10.1088/0022-3727/43/26/264002>.
 - [465] G. E. W. Bauer, E. Saitoh, B. J. van Wees, Spin caloritronics, *Nat. Mater.* 11 (2012) 391–399. doi:<https://doi.org/10.1038/nmat3301>.
 - [466] A. V. Chumak, V. I. Vasyuchka, A. A. Serga, B. Hillebrands, Magnon spintronics, *Nat. Phys.* 11 (2015) 453–461. doi:<https://doi.org/10.1038/nphys3347>.
 - [467] S. O. Demokritov, V. E. Demidov, O. Dzyapko, G. A. Melkov, A. A. Serga, B. Hillebrands, A. N. Slavin, Bose-Einstein condensation of quasi-equilibrium magnons at room temperature under pumping, *Nature* 443 (2006) 430–433. doi:<https://doi.org/10.1038/nature05117>.
 - [468] S. O. Demokritov, V. E. Demidov, O. Dzyapko, G. A. Melkov, A. N. Slavin, Quantum coherence due to Bose-Einstein condensation of parametrically driven magnons, *New J. Phys.* 10 (2008) 045029. doi:<https://doi.org/10.1088/1367-2630/10/4/045029>.
 - [469] L. J. Cornelissen, K. J. H. Peters, G. E. W. Bauer, R. A. Duine, B. J. van Wees, Magnon spin transport driven by the magnon chemical potential in a magnetic insulator, *Phys. Rev. B* 94 (2016) 014412. doi:<https://doi.org/10.1103/PhysRevB.94.014412>.
 - [470] M. Sparks, *Ferromagnetic Relaxation Theory*, 1st Edition, McGraw-Hill, New York, 1964.
 - [471] S. Streib, N. Vidal-Silva, K. Shen, G. E. W. Bauer, Magnon-phonon interactions in magnetic insulators, *Phys. Rev. B* 99 (2019) 184442. doi:<https://doi.org/10.1103/PhysRevB.99.184442>.
 - [472] O. Dzyapko, V. E. Demidov, S. O. Demokritov, G. A. Melkov, A. N. Slavin, Direct observation of Bose-Einstein condensation in a parametrically driven gas of magnons, *New J. Phys.* 9 (2007) 64. doi:<https://doi.org/10.1088/1367-2630/9/3/064>.
 - [473] O. Dzyapko, V. E. Demidov, S. O. Demokritov, G. A. Melkov, A. N. Slavin, Quasiequilibrium gas of magnons with a nonzero chemical potential: A way to Bose-Einstein condensation, *J. Appl. Phys.* 101 (2007) 09C103. doi:<https://doi.org/10.1063/1.2693891>.
 - [474] V. E. Demidov, S. Urazhdin, B. Divinskiy, V. D. Bessonov, A. B. Rinkevich, V. V. Ustinov, S. O. Demokritov, Chemical potential of quasi-equilibrium magnon gas driven by pure spin current, *Nat. Commun.* 8 (2017) 1579. doi:<https://doi.org/10.1038/s41467-017-01937-y>.
 - [475] V. E. Demidov, S. Urazhdin, E. R. J. Edwards, M. D. Stiles, R. D. McMichael, S. O. Demokritov, Control of magnetic fluctuations by spin current, *Phys. Rev. Lett.* 107 (2011) 107204. doi:<https://doi.org/10.1103/PhysRevLett.107.107204>.
 - [476] C. Du, T. van der Sar, T. X. Zhou, P. Upadhyaya, F. Casola, H. Zhang, M. C. Onbasli, C. A. Ross, R. L. Walsworth, Y. Tserkovnyak, A. Yacoby, Control and local measurement of the spin chemical potential in a magnetic insulator, *Science* 357 (2017) 195–198. doi:<https://doi.org/10.1126/science.aak9611>.
 - [477] F. G. Eich, M. Di Ventra, G. Vignale, Functional theories of thermoelectric phenomena, *J. Phys.: Condens. Matter* 29 (2017) 063001. doi:<https://doi.org/10.1088/1361-648X/29/6/063001>.